Imperial College London

Development of Improved Cultivation Methods for Environmental Microorganisms

- by -

Andrew Gordon Morrison

Imperial College London

Department of Infectious Disease

Thesis submitted to Imperial College London for the degree of

Doctor of Philosophy

January, 2024

Dedication

To my grandparents, parents, sister, and family.

Abstract

Cultivation of bacteria remains an essential prerequisite for numerous research and biotechnological applications. Despite their ubiquity, only a minority of environmental bacteria are cultivable using standard techniques. Therefore, a vast microbial 'dark matter' awaits exploration for valuable therapeutics or research potential. Despite innovations in enhanced cultivation techniques, limitations remain including throughput, dependencies on environmental factors or abrupt transitions of microorganisms from native to laboratory conditions. This thesis addresses these challenges with the development, optimisation, and experimental assessment of two novel cultivation methodologies. The first methodology allows for the gradual transition and acclimatisation of microorganisms from native environments to culture media using the novel Enhanced Domestication (EDEN) device. Compared to the instantaneous transition, acclimatisation of pond water bacteria to R2A culture media significantly enhanced cultivation diversity, colony yield and greater taxonomic range of isolates including those previously reported to be recalcitrant to cultivation. Moreover, likely novel taxa cultivated with EDEN exhibited antimicrobial activity against methicillin-resistant *Staphylococcus aureus*. The second methodology involves the development of a cell encapsulation apparatus, termed Bacterial Encapsulation and Containment (BEAD), enabling microinjection and cultivation of bacteria within alginate hydrogel beads using an automated pneumatic pump system. The performance of *in situ* cultivation with BEAD-encapsulated bacteria were assessed using the newly developed cultivation cassettes growth chambers. The findings propose enhanced cultivation strategies to unlock the biosynthetic potential of uncultured environmental bacteria.

Declaration of Originality

I, Andrew Gordon Morrison, declare that the work presented in this doctoral thesis titled, Development of Improved Cultivation Methods for Environmental Microorganisms, is entirely my own and performed whilst under the supervision of Dr Harry Low and Professor Martin Buck while a PhD candidate at Imperial College London. I confirm that, where work published by others is discussed, that it is clearly and appropriately referenced and any work presented which was done in collaboration with others, I clearly acknowledge the contributions of myself and others.

Andrew Gordon Morrison

January 2024

Copyright Declaration

The copyright of this thesis rests with the author. Unless otherwise indicated, its contents are licensed under a Creative Commons Attribution-Non-Commercial 4.0 International Licence (CC BY-NC). Under this licence, you may copy and redistribute the material in any medium or format. You may also create and distribute modified versions of the work. This is on the condition that: you credit the author and do not use it, or any derivative works, for a commercial purpose. When reusing or sharing this work, ensure you make the licence terms clear to others by naming the licence and linking to the licence text. Where a work has been adapted, you should indicate that the work has been changed and describe those changes. Please seek permission from the copyright holder for uses of this work that are not included in this licence or permitted under UK copyright law.

Acknowledgement of Collaboration

- Execution of pipelines and coding for R analysis of Illumina reads was performed by Dr Raphaella Jackson (Imperial College London).
- Optimisation of EDEN device was aided by Yovita Hendra.
- Screening of EDEN isolates for antimicrobial activity was aided by Caitlin McShane.

Publications

- Morrison, G. A., Jackson, R., Freemont, P., Low, H. H., Acclimatisation of bacteria to culture media facilitates cultivation of previously uncultivated bacteria (in preparation).
- Morrison, G. A., Low, H. H., Contained encapsulation and cultivation of bacteria within alginate beads (in preparation).

Acknowledgements

First and foremost, I would like to thank Dr Harry Low for the opportunity to undertake such an incredible project. With his continued dedication, mentorship, and support during my time as a PhD student, I have been fortunate to have learnt so much. Thank you to the philanthropic sponsors of this PhD, you have provided me a life-changing opportunity to devote myself to such a fascinating subject. I extend my appreciation to Professor Martin Buck for offering help and advice whenever needed. Thank you Dr Tiago Costa and Dr Andrew Edwards, for your support and helpful advice.

Thank you to the master's and undergraduate students who helped me on my journey; Maria Donde, Maria Loizou, Oliver and Yovita your help and dedication are noticed and appreciated. Thank to members of Imperial College Hackspace particularly David Miller and Harry Barnett for help and advice. Thank you to Professor Paul Freemont and lab members for 3D printer usage and advice when needed. Particularly thanks to Dr Raphaella Jackson; firstly, for looking out for my well-being and moral support, and secondly for providing an exceptional data analysis that was vital for both this thesis and beyond. Thank you to work experience student Caitlin for dedicating her free time to help set up assays. Thanks to Professor Zoltan Takats and lab members Toma and Alvaro for helping in projects, especially Toma for helping in 3D printing, sharing consumables, support, and friendship.

Thank you to Low lab members old and new. Thank you Max, Souvik, Ioanna, Michael, Jayanti, Alasdair and Matteo for continued advice, support and friendship. Thank you to members of 5th floor Life Sciences, particularly Emma, for continued support and friendship. Thank you also to Dr David Riglar and lab members Clare, Nina, David, and Silvia for providing advice, support, and friendship throughout. Thank you to section staff Soo Mei, Liz, and Edina for keeping lab operations running smoothly and friendly support. Thank you Mum, Dad and Charlotte for leading me to where I am now and being there for me whenever needed.

List of Figures

Figure 1.1: Diffusion chamber microbial cultivation methods. 21
Figure 1.2: Combining microfluidics and cell encapsulation for high-throughput cell cultivation. 23
Figure 1.3: Microcapsule coating examples 30
Figure 1.4: Comparison of FFF and VPP 3D printer technologies. 39
Figure 1.5. 3D printed microfluidics. 45
Figure 2.1: Overview of cultivation experiments. 54
Figure 2.2: Community cultivation experiment for NGS Illumina sequencing. 56
Figure 2.3: Cultivability of pond water microorganisms with dilution mixtures of R2A and SFPW. ..60
Figure 2.4: Acclimatisation to culture media for enhancing microbial cultivation. 61
Figure 2.5: EDEN development. 63
Figure 2.6: Single plate EDEN with biofilm. 63
Figure 2.7: Biocompatibility of adhesives with *B. subtilis* and *E. coli*. 64
Figure 2.8: Demonstration of EDEN fabrication by direct membrane printing. 65
Figure 2.9: EDEN fabrication by print-pause-print technique with direct membrane integration. 68
Figure 2.10: Biocompatibility of PLA plastic with *B. subtilis* and pond water microorganisms. 68
Figure 2.11: Automated EDEN media delivery system and variables. 70
Figure 2.12: Validation of automated media delivery system and diffusibility of EDEN. 71
Figure 2.13: Cell densities of EDEN wells and rarefaction curve of samples. 72
Figure 2.14: MetaNMDS plot of communities cultivated by different cultivation methods. 73
Figure 2.15: EDEN acclimatisation cultivates significantly greater community diversity. 74
Figure 2.16: Heatmap of order-level bacterial taxonomy of cultivated communities. 75
Figure 2.17: EDEN acclimatisation cultivates greater unique and likely uncultivated ASVs. 77
Figure 2.18: Acclimatisation to R2A with EDEN enhances microcolony cultivation probability. 78
Figure 2.19: EDEN acclimatisation enhances greater diversity and likely uncultivated isolates. 80
Figure 2.20: Microbial inhibition assay for detection of antimicrobial compounds from EDEN isolates. 81
Figure 3.1: Cultivation cassette components. 97
Figure 3.2: Microfluidic encapsulation and cultivation of *B. subtilis* within agarose microdroplets. 99
Figure 3.3: Evaluation of capsule coatings for cultivation and containment of *B. subtilis*. 100
Figure 3.4: Interfacial polymerisation of Fe(III)-tannic acid restores but does not contain microcolony growth. 101
Figure 3.5: Colony growth of randomly dispersed *B. subtilis* within alginate beads. 102
Figure 3.6: Capillary mount for microinjection of inner-phase within outer-phase droplets. 103
Figure 3.7: ATPS to maintain phase-separation and localisation of IP within beads. 104
Figure 3.8: Automated phase synchronisation for microinjection of IP into OP droplets. 105
Figure 3.9: Apparatus with automated phase synchronisation and microinjection system. 106
Figure 3.10: Positioning of IP within alginate beads. 107
Figure 3.11: Diffusion of fluorescein into alginate beads. 108
Figure 3.12: Biocompatibility of crosslinking buffers and media. 109
Figure 3.13: Biocompatibility of crosslinking buffers and media on viable pond community cells. ...110
Figure 3.14: Contained cultivation of microcolonies within alginate beads. 111
Figure 3.15: Loading of beads into cultivation cassettes. 114
Figure 3.16: Isolate cultivation comparison of plate R2A and BEAD *in situ* methods. 115

List of Tables

Table 1.1: Comparison of hydrogels for cell encapsulation and cultivation. 27
Table 1.2: 3D printing materials for applications in cell encapsulation and cultivation. 43
Table 2.1: Silva classification and antimicrobial activity of EDEN acclimatised isolates.....82
Table 3.1: Optimal conditions for digesting alginate beads on agar petri dishes with alginate lyase. 112
Table 3.2: Digestion time of alginate beads within 96 deep well blocks with alginate lyase. 113

List of Abbreviations

16S rRNA	16S ribosomal RNA
2PP	Two-photon polymerization
3MF	3d manufacturing format
AAAS	American Association for the Advancement of Science
ABS	Acrylonitrile butadiene styrene
ACS	American chemical society
ASM	American Society for Microbiology
ASV	Amplicon sequence variant
ATCC	American type culture collection
ATPS	Aqueous two-phase systems
BEAD	Bacterial encapsulation and containment
BEDA	Bisphenol a diglyceryl ether
BF	Brightfield
BGCs	Biosynthetic gene clusters
CAD	Computer-aided design
CC BY	Creative commons attribution
CFDA SE	Carboxyfluorescein diacetate, succinimidyl ester
CNC	Computer numerical control
CV	Coefficient of Variation
DC	Direct current
DLP	Digital light processing
DMD	Digital micromirror device
DNA	Deoxyribonucleic acid
EDTA	Ethylenediaminetetraacetic acid
ESBL	Extended spectrum beta-lactamase
FACS	Fluorescence-activated cell sorting
FDM	Fused deposition modelling
FEMS	Federation of European Microbiological Societies
FFF	Fused filament fabrication
GelMA	Gelatin methacryloyl
GFP	Green fluorescent protein
HA-MA	Hyaluronic acid methacrylate
HCl	Hydrochloric acid
HDDA	1,6-hexanediol diacrylate
HFE	Hydrofluoroether
Hz	Hertz
iChip	Isolation chip
ID	Inner diameter
IP	Inner-phase
ISO	International Organization for Standardization
kDa	Kilodalton

LbL	Layer-by-Layer
LED	Light-emitting diode
LMPA	Ultra-low melting point agarose
MD Pod	Microbial domestication pod
MDPI	Multidisciplinary digital publishing institute
MIC	Minimum inhibitory concentration
MOC	Metal-organic complex
MOPS	3-(N-morpholino)propanesulfonic acid
MRSA	Methicillin-resistant *Staphylococcus aureus*
NAS	National Academy of Sciences
NEMA	National electrical manufacturers association
NGS	Next-generation sequencing
NMDS	Nonmetric multidimensional scaling
OD	Optical density
OP	Outer phase
PA	Nylon/polyamide
PAA	Poly(allylamine)
PC	Polycarbonate
PCR	Polymerase chain reaction
PDADMAC	Polydiallyldimethylammonium chloride
PDMS	Poly (dimethylsiloxane)
PDMS	Polydimethylsiloxane
PEG	Poly(ethylene glycol)
PEG-DA	Poly(ethylene glycol) diacrylate
PEGNB	Poly(ethylene glycol) norbornene
PEI	Polyetherimide
PET	Polyethylene terephthalate
PETG	Polyethylene terephthalate glycol
PLA	Polylactic acid
PLL	Poly-l-lysine
PLO	Poly-ornithine
PMA	Poly(methacrylate)
PNIPAAm	Poly(N-isopropyl acrylamide)
PP	Polypropylene
PTEG	Polyethylene terephthalate glycol
PTFE	Polytetrafluoroethylene
PVA	Poly(vinyl alcohol)
PVC	Poly(vinyl Chloride)
PU	Polyurethane
R2A	Reasoner’s 2A media
RNA	Ribonucleic acid
rpm	Revolutions per minute
RT	Room temperature

SCARA	Selective compliance articulated robot arm
SD	Standard deviation
sfGFP	Superfolder green fluorescent protein
SFPW	Sterile-filtered pond water
Si	Silica
SINA	Silva incremental aligner
SLA	Stereolithography
STL	Standard tessellation language
TMOS	Tetramethoxysilane
TPO	Lithium phenyl(2,4,6-trimethylbenzoyl)phosphinate
TPU	Thermoplastic polyurethanes
UCST	Upper critical solution temperature
UV	Ultraviolet
v/w	Volume/weight
VBNC	Viable but not cultivable
VPP	Vat photopolymerisation
ZIF-8	Zeolitic imidazolate framework-8

Table of Contents

DEDICATION **2**

ABSTRACT **3**

DECLARATION OF ORIGINALITY **4**

COPYRIGHT DECLARATION **5**

ACKNOWLEDGEMENT OF COLLABORATION **6**

PUBLICATIONS **7**

ACKNOWLEDGEMENTS **8**

LIST OF FIGURES **9**

LIST OF TABLES **10**

LIST OF ABBREVIATIONS **11**

TABLE OF CONTENTS **14**

CHAPTER 1. INTRODUCTION AND LITERATURE REVIEW **17**

1.1 Summary **17**

1.2 Methods and applications for cultivating previously uncultivable bacteria **17**
1.2.1 Evidence for uncultivable bacteria 17
1.2.2 Optimisation of growth conditions 19
1.2.3 Single cell isolation 19
1.2.4 Diffusion chamber cultivation 20
1.2.5 Applications for cultivating previously uncultivated bacteria 23

1.3 Cell encapsulation materials and methods **25**
1.3.1 Thermoresponsive encapsulation polymers 28
1.3.2 Ionic-gelating encapsulation polymers 28
1.3.3 Photo-crosslinking encapsulation polymers 28
1.3.4 Capsule surface coatings 29
1.3.5 Enclosed channel microencapsulation devices 31
1.3.6 Gravity-assisted microencapsulation devices 32

1.4 3D Printing Techniques and Applications in Cell Encapsulation and Cultivation **34**
1.4.1 Material extrusion 3D printers 34
1.4.2 Material extrusion polymers 35
1.4.3 Vat photopolymerisation 3D printers 36
1.4.4 Vat photopolymerisation polymers 37
1.4.5 Applications of 3D printing in cell encapsulation and microfluidics 44
1.4.6 Applications of 3D printing in cell culture 45

1.5 Conclusion **46**

1.6 Thesis Aims **48**

CHAPTER 2. ENHANCED CULTIVATION OF BACTERIA BY ACCLIMATISATION TO CULTIVATION MEDIA **49**

2.1 Introduction **49**
2.1.1 Limitations of standard cultivation methods for environmental bacteria 49
2.1.2 Chapter aims and objectives 50

2.2 Methods and Materials **51**
2.2.1 Cells and media 51
2.2.2 Cell extraction and quantification 51
2.2.3 Fabrication of Enhanced Domestication platform (EDEN) 51
2.2.4 Biocompatibility assessment 52
2.2.5 Automated pump system and validation 52
2.2.6 EDEN acclimatisation and cultivation experiments 52
2.2.7 Illumina community sequencing and analysis 56
2.2.8 Isolate sequencing and analysis 57
2.2.9 Antimicrobial detection assay 58

2.3 Results **59**
2.3.1 Cultivability of pond water microorganisms 59
2.3.2 EDEN design and optimisation 60
2.3.3 EDEN optimisation and fabrication using direct membrane 3D printing 64
2.3.4 Construction of an automated EDEN liquid media delivery system 68
2.3.5 EDEN acclimatisation enhances community cultivation diversity and novelty 71
2.3.6 EDEN acclimatisation cultivates unique and likely uncultivated taxa 76
2.3.7 EDEN acclimatisation significantly increases cultivation yield 77
2.3.8 EDEN acclimatisation enhances isolate cultivation diversity and novelty 78
2.3.9 Antimicrobial activity of acclimatised bacteria 80

2.4 Discussion **82**
2.4.1 Cultivability of pond water bacteria 82
2.4.2 EDEN fabrication 84
2.4.3 Effectiveness of R2A acclimatisation on bacterial community cultivation 85
2.4.4 Effectiveness of R2A acclimatisation on bacterial microcolony cultivation 86
2.4.5 Effectiveness of R2A acclimatisation on bacterial isolate cultivation 87
2.4.6 Potential mechanisms for enhanced cultivability with EDEN acclimatisation 88
2.4.7 Methodological utility in natural product discovery 89
2.4.8 Conclusion 90

CHAPTER 3. ENCAPSULATION OF ENVIRONMENTAL BACTERIA FOR CONTAINED *IN SITU* CULTIVATION **91**

3.1 Introduction **91**
3.1.1 Challenges of a microfluidic approach for *in situ* cultivation of environmental bacteria 91
3.1.2 Chapter aims and objectives 92

3.2 Materials and methods **93**
3.2.1 Cells and media 93
3.2.2 Modification of *B. subtilis* for constitutive sfGFP expression 93
3.2.3 PDMS chip microfluidic encapsulation and cultivation of bacteria 93
3.2.4 Surface modifications of agarose droplets 94
3.2.5 Fabrication of non-3D printed alginate encapsulation device 94
3.2.6 Fabrication of 3D printed capillary mount 95

3.2.7 Pneumatic oscillating pressure apparatus for centralised alginate bead encapsulation 95
3.2.8 Environmental cell extraction and quantification 96
3.2.9 Fabrication of cultivation cassettes 96
3.2.10 Alginate cell encapsulation and *in situ* cultivation 97
3.2.11 Recovery of cells from alginate beads 98
3.2.12 16S rDNA amplification and analysis for isolate identification 98

3.3 Results 99
3.3.1 Microfluidic encapsulation of bacteria within agarose microdroplets 99
3.3.2 Agarose encapsulation method modifications 99
3.3.3 Spatial containment of cells within alginate capsules 101
3.3.4 Development of the BEAD method 102
3.3.5 Development of automated pneumatic pump and ATPS for microinjection of bacteria 103
3.3.6 Biocompatibility of alginate encapsulation 108
3.3.7 Alginate encapsulation cell containment 110
3.3.8 Optimisation of cell decapsulation 111
3.3.9 Development of cultivation cassettes for *in situ* cultivation of encapsulated bacteria 113
3.3.10 *In situ* cultivation of encapsulated bacteria within cultivation cassettes 114

3.4 Discussion 116
3.4.1 Microfluidic approaches for encapsulation and *in situ cultivation* of microorganisms 116
3.4.2 BEAD method performance 116
3.4.3 BEAD method applications 118

3.5 Conclusion 119

REFERENCES 120

Chapter 1. Introduction and Literature Review

1.1 Summary

Obtaining pure, isolated growth of microorganisms remains fundamental for most applications in biotechnology and research. However, a microorganism's propensity to replicate under standard laboratory conditions is only observed in a minority of the total environmental population. Therefore, there remains a large discrepancy between the diversity of microorganisms cultivated in the laboratory and that in the environment. Indeed, of the estimated 0.8–1.6 million bacterial species, only ~20,000 have cultivated representatives to date (1,2). Understanding optimal microbial growth conditions will enhance the phylogenetic diversity available for research applications such as drug discovery for new antibiotics. Much remains unknown about uncultivated microorganisms, including what conditions and techniques should be utilised for successful cultivation. This chapter reviews strategies for improved cultivation of environmental microorganisms, with particular emphasis on 'uncultured' species. As bacteria are most frequently explored in environmental samples, this thesis and chapter will focus on bacteria. Furthermore, relevant advances in high-throughput cell cultivation and rapid prototyping are discussed.

1.2 Methods and applications for cultivating previously uncultivable bacteria

1.2.1 Evidence for uncultivable bacteria

Cultivation of bacteria is facilitated proliferation typically in a defined environment using a solid or liquid culture medium. Despite advances in cultivation-independent methods within bioinformatics and high-throughput sequencing, laboratory cultivation of bacteria remains essential in many applications within molecular biology, industrial processes, and natural product discovery. As early as 1898, it was observed that counts of bacteria under direct microscopy were greatly disproportionate to subsequently cultivated colonies, later described as the 'great plate count anomaly' (3–5). Indeed, the diversity of bacteria that remain uncultured was only truly appreciated with the advent of environmental 16S rRNA sequencing, revealing large phylogenies of microorganisms recalcitrant to current cultivation techniques (6,7).

The definition of 'uncultivable' bacteria remains subject to debate. Such cells can be considered readily dividing but inhibited due to a lack of necessary growth factors or the presence of antagonistic substances, or alternatively, non-dividing cells in a viable but not cultivable (VBNC) or otherwise dormant state (8). The alternative definition, 'uncultured', has been recently proposed by Steen et al. highlighting it is unknown if a species is truly uncultivable unless sufficient information has been acquired, or until it has been successfully cultivated (9). Experimentally, previously uncultivable bacteria have been defined as taxa with significant genetic divergence from cultivated representatives, typically as isolates with <97% 16S rRNA sequence similarity to a described cultivated species (9–11). However, this definition can be criticised for not acknowledging that unexplored environments may contain yet unidentified cultivable species, and that genetic divergence does not necessarily correlate to cultivation proficiency (9).

The number of bacteria predicted to be uncultivable also remains under debate. A commonly used statistic is >99% of environmental bacteria, citing sources of Staley & Konopka, as well as Amann et al. that compared microscopy counts of bacteria with subsequently cultivated colonies from a variety of environmental sources (5,12–15). However, cultivation rates vary greatly depending on environmental sources, cell quantification techniques and culturing methods chosen. Cultivation efficiency is typically higher in nutrient-rich environments such as faeces compared to nutrient-poor environments such as deserts. (8,16,17).

In bioinformatic approaches, the abundances of uncultivated bacteria can be estimated by quantifying environmental 16S rRNA sequences below the given cultivated bacterium identity threshold of 97% (9,11,18). Estimates vary greatly depending on sample source, choice of next-generation sequencing (NGS) technology and analysis tools. For example, in an analysis by Martiny in 2019, human-associated microbiomes comprised the highest average sequence similarities to cultivated species (>99%), while marine sediments had the lowest (~93%) (18). Here, differences in cultivated species between environments may highlight biases from location accessibility, research interest and biome complexity. The median environmental 16S rRNA sequence similarity to cultivated representatives was 97.3 (SD± 2.3%) (18). However, such analysis was derived from amplicon datasets containing sequences derived from primers biased to cultivated bacteria (18). In a follow-up analysis by Steen et al. using unbiased PCR-free shotgun sequences, the median sequence similarity was ~88%, with only 6% of sequences over the 97% identity threshold (9). Similar results were found by Schloss et al., observing 18.9% of bacterial sequences and 6.8% of archaeal sequences

to be from isolated organisms, with 24 of 65 bacterial and 14 of 20 archaeal phyla lacking cultivated representatives, respectively (19). Although subject to debate, overall these analyses indicate that the majority of known environmental microorganisms remain uncultivated.

1.2.2 Optimisation of growth conditions

Media and cultivation conditions have traditionally been directed towards the selective cultivation of human pathogens or industrial microbes of interest. This is typically achieved using nutrient-rich conditions and mammalian temperature (37˚C), which are likely inappropriate for most other environmental species (20–22). Thus, efforts have been made to optimise culture conditions for broader taxa (21,22). In selective media, specific nutrient sources can be altered to favour species growth of interest, such as carbon and nitrogen sources, pH, temperature, native growth factors or the addition of antibiotics (23–26). Although success has been found in enhancing cultivation through the identification of specific growth factors, defining selective media for uncultivated bacteria is challenging due to a lack of knowledge of required conditions (24,25,27). Thus, in contrast to selective media, a non-selective medium incorporates a diverse source of metabolites and co-factors capable of utilisation in diverse heterotrophic metabolic pathways. For example, Reasoner's 2A (R2A) is an effective but relatively low-nutrient cultivation medium comprising yeast extract, amino acids, glucose, and pyruvate compatible for broad non-selective cultivation of water-borne contaminants (21). Additional optimisations are to measure and emulate environmental variables and incorporate these with non-selective growth media. For example, reducing nutrient concentrations and temperature with extended incubation time has yielded high proportions of previously uncultivated bacteria (10,21,28). Native media, incorporated in the form of soil extracts, may additionally enhance cultivation efficiencies (29,30). Other variables to consider include gas composition and the choice of solid or liquid culture formats (31,32). However, given the complexities of environments, there is unlikely to be a single approach optimal for the cultivation of all microorganisms.

1.2.3 Single cell isolation

As complex biomes may contain thousands of species, obtaining isogenic growth requires physical isolation from communities (33). Samples can be therefore diluted to smaller, subsampled communities or near and below single-cell concentrations to mitigate competition from fast or aggressively growing species that may dominate cultivation vessels. The latter is

known as the dilution-to-extinction technique, whereby cultures permit a greater yield of slow-growing or nutrient averse species (34,35).

Single cell isolation approaches complement microfluidics or cell microencapsulation techniques. Here, single cells can be encapsulated or compartmentalised and cultivated in high-throughput chambers or chip arrays (28,34,36,37). Microencapsulated cells are furthermore analysable with flow cytometry, allowing for sorting of cells by growth rate, phylogeny, or bioactivity (37,38).

However, a limitation of single-cell isolation is the removal of community context or cell-cell communication that may facilitate cultivation (39,40). However, while examples are known for obligatory co-cultivational relationships, competition between microorganisms appears to be more prevalent than cooperation in examined environmental communities (24,27,41–45). This is further reflected in negative correlations found between inoculation density and cultivation efficiencies (26). Nonetheless, cultivation in both single-cell and co-cultivation formats shows promise for cultivating previously uncultivated bacteria.

1.2.4 Diffusion chamber cultivation

Diffusion growth chambers feature a hollow structure sealed with a diffusible membrane (pore size 0.01-4 µm), allowing permeation of nutrients and growth factors while preventing cell migration. In this format, isolated cells can be grown *in situ* at the source environment thereby receiving native nutrients and restoring partial cell-cell communication. Exemplified by Kaeberlein et al., diffusion growth chambers submerged in a marine aquarium were used to cultivate previously uncultivated Bacteroides (Figure 1.1A) (46). Later innovations in diffusion chamber techniques led to the high-throughput isolation chip (iChip) capable of growing 192 isolates simultaneously with up to 10-fold greater cultivation yields (Figure 1.1B-C) (11,47). In a similar format, comprising an inverted tissue culture insert lined with soil slurry, was used to obtain uncultured isolates of the poorly cultivated phylum Saccharibacteria (previously candidate division TM7) (Figure 1.1D) (14). Chamber membranes, comprising hollow-fibre polyvinylidene fluoride (PVDF), have additionally been used to enhance cultivation of novel isolates, increasing from 2 to 31% (Figure 1.1E) (48).

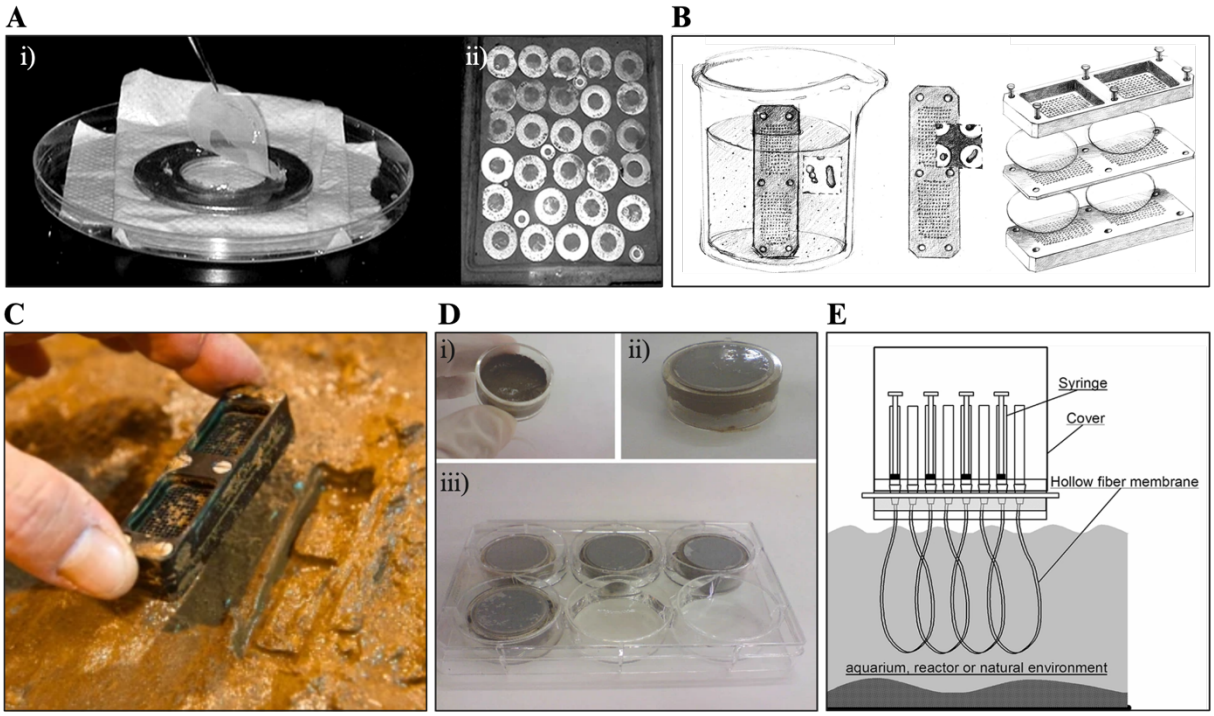

Figure 1.1: Diffusion chamber microbial cultivation methods.
(**A**) Cultivation of bacteria within metal washer-based diffusion chamber. Bacteria are immobilised within the washer with agarose and sandwiched with porous membrane enabling diffusion of native nutrients and growth factors. i) Displaying porous membrane with forceps and ii) sealed diffusion chambers ready for *in situ* incubation within marine sediment. Reprinted from (46) with permission from AAAS, copyright (2002). (**B**) Drawing of iChip inoculation and assembly. The iChip comprises a 192 growth well chip that is submerged in a molten agarose solution containing environmental cells at a concentration resulting in approximately single cells occupying each well. The growth well chip is then pressure-sealed with porous membrane and support plates. Reprinted from (11) with permission from ASM under CC BY 4.0 license http://creativecommons.org/licenses/by/4.0/. (**C**) Incubation of iChip *in situ* of native environment. Reproduced from (47) with permission from Springer Nature, copyright (2015). (**D**) Cultivation of soil microorganisms on a soil matrix substrate using tissue culture inserts. i) Tissue culture insert compacted with a soil substrate. ii) The insert is inverted with inoculation of extracted soil microbes on top of the membrane which may receive diffused nutrients from soil substrate. iii) Inoculated inserts are placed into 6 well plates with water to prevent evaporation. Reprinted from (14) with permission from Springer Nature, Nature Protocols, copyright (2005). (**E**) Hollow-fiber membrane chamber for *in situ* cultivation. The porous membrane fiber is infused with diluted environmental cells and retrieved with a syringe. The fibers are then submerged in a simulated native environments for *in situ* cultivation. Reprinted from (48) with permission from ASM under CC BY 4.0 license, copyright (2009).

Recently, diffusion chamber cultivation has been combined with microfluidics for ultra-high throughput *in situ* cultivation (49,50). Using agarose-microencapsulated bacteria contained within a diffusion chamber termed microbial domestication pod (MD Pod), several millions of cells can be cultivated *in situ* simultaneously (Figure 1.2A) (49,50). However, a current limitation of this approach is the lack of containment of cells within hydrogel capsules, leading to the rapid outgrowth and contamination of the surrounding medium (28,51). While the

implementation of filtration columns may aid removal of free cells from microdroplets, others have attempted structurally robust capsules for improved cell containment (Figure 1.2B-C) (28,38,52). For example, contained *in situ* cultivation using porous polysulfone-coated agar spheres have been used to obtain novel proteobacteria (Figure 1.2D) (53). Poly (dimethylsiloxane) (PDMS) nanoculture systems have recently been demonstrated for contained cultivation of *Pseudomonas* (Figure 1.2E-F) (54,55). However, such approaches currently lack throughput or biocompatible encapsulation or recovery processes for effective use (56,57).

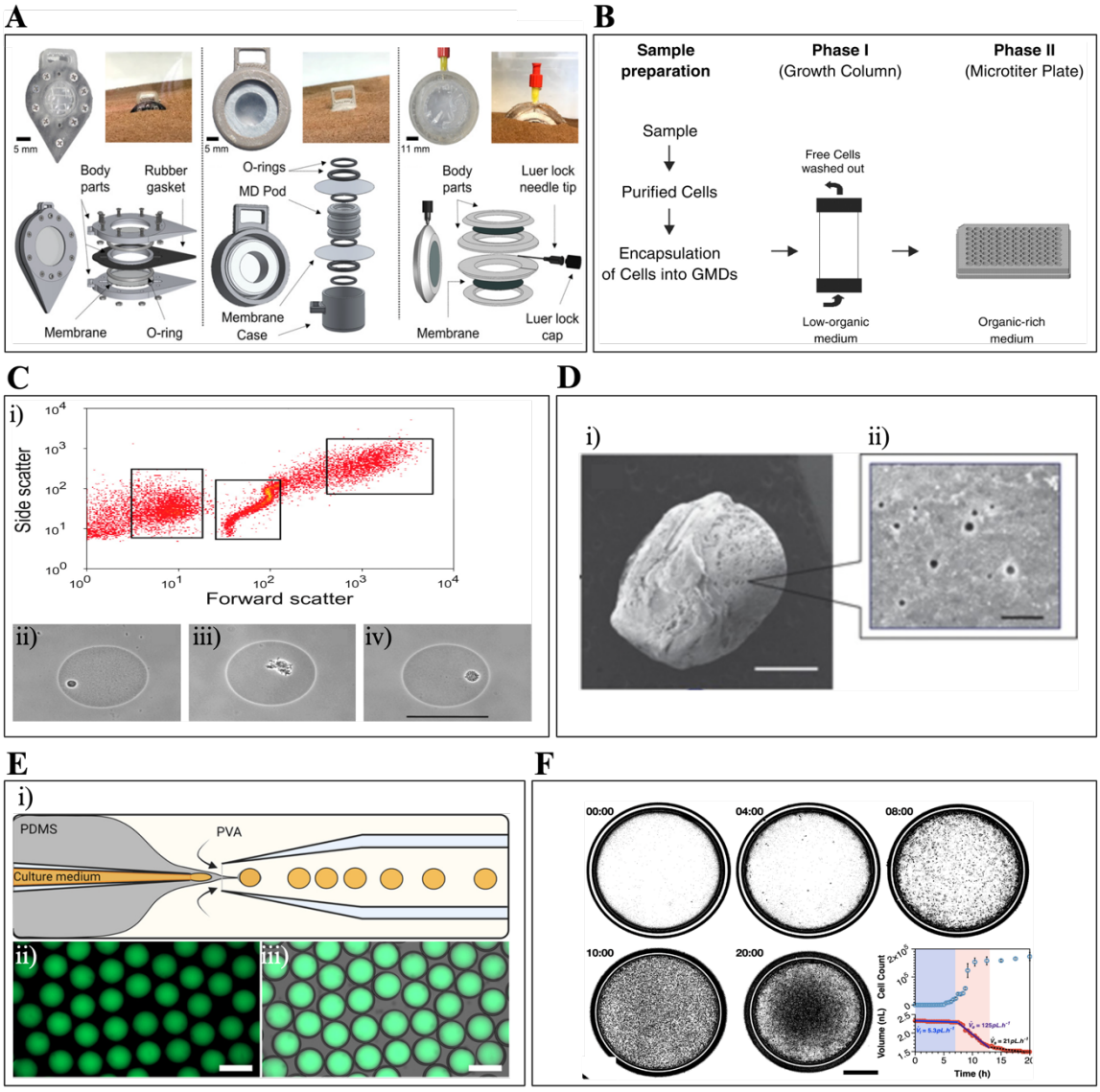

Figure 1.2: Combining microfluidics and cell encapsulation for high-throughput cell cultivation. (**A**) MD pods designs for *in situ* cultivation of agarose-microencapsulated bacteria. The MD Pods comprise a diffusion growth chamber sealed with diffusible membrane and support structures. Marine microorganisms, encapsulated in agarose microbeads via a microfluidic device, are loaded into the MD Pods for high-throughput *in situ* cultivation. Reproduced from (49) with permission from Wiley copyright (2022). (**B**) Experimental procedure for encapsulation and cultivation of microorganisms within gel microdroplets (GMD) and continuous culture vessels maintaining constant nutrient exchange while removing waste and free cells. Microcolonies within droplets can be transferred to a nutrient-rich medium for further cultivation. Reprinted from (52) copyright (2002) NAS. (**C**) i) Using flow cytometry, microcolonies can additionally be sorted by growth rate. ii-iv) Example microcolonies cultivated within GMDs. Scale bar 50 µm. Reprinted from (52) copyright (2002) NAS (**D**) i) Encapsulation of bacteria within polysulfone-coated agarose spheres. Scale bar 1 mm. ii) Zoom of the porous capsule surface that enables application with *in situ* cultivation. Scale bar 5 µm. Reprinted from (53) with permission from FEMS Microbiology Ecology under CC BY 4.0 license. (**E**) i) Generation of porous PDMS nanoculture capsules using triple emulsion microfluidics. ii) Fluorescent tagged confluent *E. coli* nanocultures and iii) brightfield overlay. Scale bar 200 µm. Reprinted from (55), copyright (2022) ACS. (**F**) 20 h timelapse of PDMS *P. aeruginosa* nanoculture grown in hypertonic solution (154 mM NaCl). Graph details the volumetric flow rates of fluid leaving the capsules alongside cell counts. Scale bar: 50 µm. Reprinted from (54) with permission from Elsevier, Materials Today Communications, copyright (2021).

1.2.5 Applications for cultivating previously uncultivated bacteria

Approximately 1.27 million people died as a direct cause of antimicrobial resistant infection in 2019 and is expected to reach 10 million by 2050 (58). The majority of clinically used antibiotics are derived from microorganisms, however, the rate of discovering new antimicrobial classes has been insufficient to keep pace with the increases of antimicrobial resistance (59). Although partly attributable to socioeconomic factors, the lack of diversity in microbial cultivations restricts the range of natural products available for drug discovery efforts (59). Consequently, there is a depletion of screenable compounds and an escalation in hit replication, further discouraging pharmaceutical drug discovery endeavours. However, it is predicted uncultivated bacteria harbour a diverse unexplored array of genes for secondary metabolite biosynthesis (60). Thus, enhancing microbial cultivation diversity may lead to the discovery of potentially important novel therapeutics and reinvigoration of drug discovery pipelines (60,61).

Recent work has demonstrated the potential for discovering novel compounds from uncultivated species. For example, a previously uncultivated Betaproteobacterium *Eleftheria terrae* isolated from an iChip was found to produce the novel depsipeptide teixobactin active against gram-positive pathogens including MRSA (13). Additionally, using a cultivation-independent approach involving biosynthetic gene cluster (BGC) clone libraries obtained from environmental DNA, a novel calcium-dependant antibiotic was isolated from an unknown

microorganism (62). Such examples, alongside BGC predictions from metagenomic data, indicate the uncultured majority offers a promising source of discovery for new natural products including antibiotics (60,61).

1.3 Cell encapsulation materials and methods

Encapsulating cells in 3D environments presents numerous benefits for cell culture, including shielding from mechanical stress, enhanced visualisation, increased throughput, and maintained diffusibility for nutrients, signalling compounds, and gases. Cell encapsulation has seen applications within high-throughput cultivation of environmental microorganisms, protection of transplanted cells from immune recognition and increases of efficiency in bioreactors (63–65). Numerous methods and materials are available for cell encapsulation depending on required application. Polymers used for cell encapsulation and cultivation can be categorised by their mechanism of cross-linking, being thermal, ionic, photocovalent (Table 1.1) (66).

Gelation Mechanism	Polymer Examples and Properties	Advantages	Disadvantages	Examples in cell encapsulation
Thermoresponsive	– Polymers miscible when heated, gelate when cooled (67). – Natural polymers of agarose, carrageenan, collagen and gelatine (67). – Synthetic polymers of poly(ethylene glycol) diacrylate (PEG-DA) and poly(N-isopropyl acrylamide) homo-polymer (PNIPAAm) (66,68).	– Transition temperature can closely match the physiological temperature of cells (69). – Rapid gelation in aqueous environments (69). – Easy gelation achieved without the need for ions or gel stabilization additives (66).	– Requirement for temperature control of fluid delivery and microfluidic devices (49,69). – Mechanical strength may be inadequate for cell containment (22,49,50). – Inappropriate for cells intolerable to heat-shock (69). – Fewer options for cell release or decapsulation (66).	– High encapsulation viability of gram-positive and negative bacteria using ultra-low gelling temperature agarose (69). – *In situ* cultivation of bacteria (11,49,50,53). – Cultivation and enrichment of slow-growing microorganisms by FACS (38). – Encapsulation of *E. coli* for high-throughput sorting of phenotypic traits and synthetic constructs (70). – Encapsulation of biosensors for detection of environmental contaminants (71).
Ionic gelation	– Crosslinked in the presence of divalent cations such as $CaCl_2$, $SrCl_2$ or $BaCl_2$ (72). – Polyelectrolytes of alginate, k-carrageenan and chitosan (66).	– Rapid and tuneable gelation under mild aqueous and biocompatible conditions (73,74). – Controllable release and decapsulation by adjusting	– Imprecise gelation occurs when highly soluble divalent cations are utilised (74,76). – Gelation and the mechanical characteristics of the hydrogel are	– All aqueous phase encapsulation and 3-D cultivation of mammalian cells within alginate core-shell capsules (77). – Cytoprotective polydopamine-coated alginate capsules for

		concentration of chelating agents or degradative enzymes (74,75). – Gelation can be initiated internally by introduction of acid to insoluble calcium salts (76).	influenced by temperature (74). – Long-term stability is compromised by leaching of divalent ions into the surrounding aqueous medium (72,74).	cultivation of *S. cerevisiae* (78). – Encapsulation and enhancement of biocatalytic aminoacylase-producing *Pseudomonas* (63). – Long-term encapsulation and cultivation of mammalian cells within alginate-chitosan composite (79).
Photo crosslinking	– Crosslinked by light presence of reactive photoinitiators (80,81). – Methacrylate-functionalised poly(ethylene glycol) PEG, poly(vinyl alcohol) (PVA), poly(methacrylate) (PMA), gelatine or hyaluronic acid. PEG norbornene (PEGNB) (80,82).	– High spatial and temporal control of polymerisation with selective control of light exposure (83). – Controlled and varied microbead shapes are achievable by through stop-flow lithography (84). – Possible to fabricate hydrogels with multiple layers (85). – Superior stability and mechanical strength of capsules (80).	– Prolonged exposure to UV light leads to a reduction in cell viability (85,86). – Crosslinking agents and photoinitiators can be toxic to cells (80,81). – Homogenous polymerisation can be difficult to achieve in thick shells (86,87). – Less options for cell liberation or decapsulation (66,86).	– *E. coli* autoinducer-sensing bioreporters encapsulated within alginate-methacrylate shell capsules (88). – Formation of porous PEG-DA core-shell capsules for biocompatible cell cultivation (87). – Encapsulation of A549s carcinoma cells within biocompatible PEGNB capsules for long-term cultivation (89).

Table 1.1: Comparison of hydrogels for cell encapsulation and cultivation.

1.3.1 Thermoresponsive encapsulation polymers

Thermal cross-linking polymers are miscible when heated in solution but gelate once cooled under the polymer upper critical solution temperature (UCST) (66). Examples of natural thermoresponsive polymers include agarose, carrageenan, collagen and gelatine, while synthetics include poly(ethylene glycol) diacrylate (PEG-DA) and poly(N-isopropyl acrylamide) homo-polymer (PNIPAAm) (66,67). Agarose, derived from red algae, is a commonly used cell cultivation medium and encapsulant due to high biocompatibility, optical transparency, and ease of preparation. Standard agarose solution-gelation temperatures are approximately 40˚C. However, for cell encapsulation, hydroxyethylated agaroses are recommended as they exhibit lower gelling temperatures (20-30˚C), thus maintaining greater cell viability (69). Although biodegradable by enzymes of α-agarase, β-agarase and β-porphyranase, these seldom occur in non-marine bacteria and therefore offer a controllable and biocompatible mechanism for cell decapsulation (90).

1.3.2 Ionic-gelating encapsulation polymers

Ionic-gelating polymers comprise of polyelectrolytes and oppositely charged crosslinking ions. As gelation is rapid and initiated upon exposure to ions, greater control in crosslinking is achieved compared to thermal crosslinking (66). Alginate, k-carrageenan and chitosan are particularly suitable for cell encapsulation (66). Crosslinking can be initiated internally or externally. For example alginate, a linear copolymer of (1,4)-linked β-d-mannuronic (M block) and α-L-guluronate (G-block) derived from brown algae, can be externally gelated when extruded into a $CaCl_2$ solution. Here, Ca^{2+} ions substitute Na+ ions at carboxyl groups of the alginate G-block residues crosslinking in an egg-box type structure (74). Alternatively, internal, or delayed gelation is achievable using alginate solutions containing insoluble calcium salts such as $CaCO_3$, where lowering the pH liberates calcium ions initiating gelation (76). Other divalent cations such as Ba^{2+} and Sr^{2+} can be used, yielding gels with different strengths and properties (72). Gel dissolution is possible with addition of chelating buffers such as ethylenediaminetetraacetic acid (EDTA), or enzymes such as alginate lyase (74,75).

1.3.3 Photo-crosslinking encapsulation polymers

Photo-crosslinking involves exposure of a monomer and photo-initiator to light, usually in ultraviolet wavelength, whereby free radicals released by the exited photo-initiator covalently bond monomer chains, crosslinking the polymer (91). Natural polymers of alginate, collagen, hyaluronan or dextran can be photo-crosslinked after functionalisation with methacrylic anhydride (82). PEG, poly(vinyl alcohol) (PVA), or poly(methacrylate) (PMA) hydrogels are additional synthetic choices offering good biocompatibility with controllable mechanical properties by tuning polymer molecular weight and concentration (80). For example, PEG-DA has seen applications in encapsulation for biosensors, tissue culture and bioremediation (85,87,92,93). While capsules are structurally robust with higher Young's modulus than thermal or ionic-crosslinkable polymers, the biocompatibility of the encapsulation process is generally lower due to cell exposure to damaging UV radiation and free radicals (94,95).

1.3.4 Capsule surface coatings

An ongoing challenge in applications of hydrogel cell encapsulation is capsule instability, leading to potential cell leakage and posing issues for applications requiring robust cell containment. This instability can result in complications such as the rejection of transplanted cells by the host immune system, decreased bioreactor efficiency, and cross-contamination in high-throughput cell cultivation. (46,63–65,96).

Hydrogels used in cell encapsulation are amenable to chemical modifications for improved stability and cell containment. For example, the surface charge of alginate hydrogels is electronegative due to presence of carboxyl groups and therefore can be coated with oppositely charged polyelectrolytes such as chitosan, poly-l-lysine (PLL), poly-ornithine (PLO), polyallylamine (PAA) and polydiallyldimethylammonium chloride (PDADMAC) (73). Further oppositely charged layers may be added sequentially in a process termed layer-by-layer approach (LbL) (Figure 1.3A) (97,98). If chelating agents are applied after coating, hollow core-shell capsules are formed (99). Polyelectrolyte coatings may serve as catalysts for the condensation of silica precursors such as sodium silicate, tetramethoxysilane (TMOS) and 3-aminopropyl-trimethoxysilane, yielding silica-coated hydrogel capsules with superior mechanical stability (100–102). If two-component film coatings are used in separate oil/water immiscible phases, film deposition can be localised to the capsule surface at the oil/water interphase via an interfacial polymerisation (Figure 1.3B) (103).

Additional polymers can be coated directly on hydrogel capsule surfaces. Inspired by mussel adhesion complexes, polydopamine-coated alginate spheres have been used to encapsulate *Saccharomyces cerevisiae* preventing capsule cell leakage and with increased mechanical resistance (Figure 1.3C) (104). Agarose beads encapsulating environmental bacteria have previously been coated with porous polysulfone for contained *in situ* cultivation of novel species (53). Similarly, alginate beads subsequently coated with a rigid but diffusible alginate/acrylamide composite shell have recently been demonstrated for full *E. coli* containment for at least 48 hours (105). Despite these advances in cell capsule confinement, a common limitation is the low biocompatibility of capsule coating processes (57,97,100,101,104,105). Moreover, such coatings are typically permanent and thus require manual mechanical cutting or physical disruption to retrieve encapsulated cells after cultivation, limiting throughput (53,105).

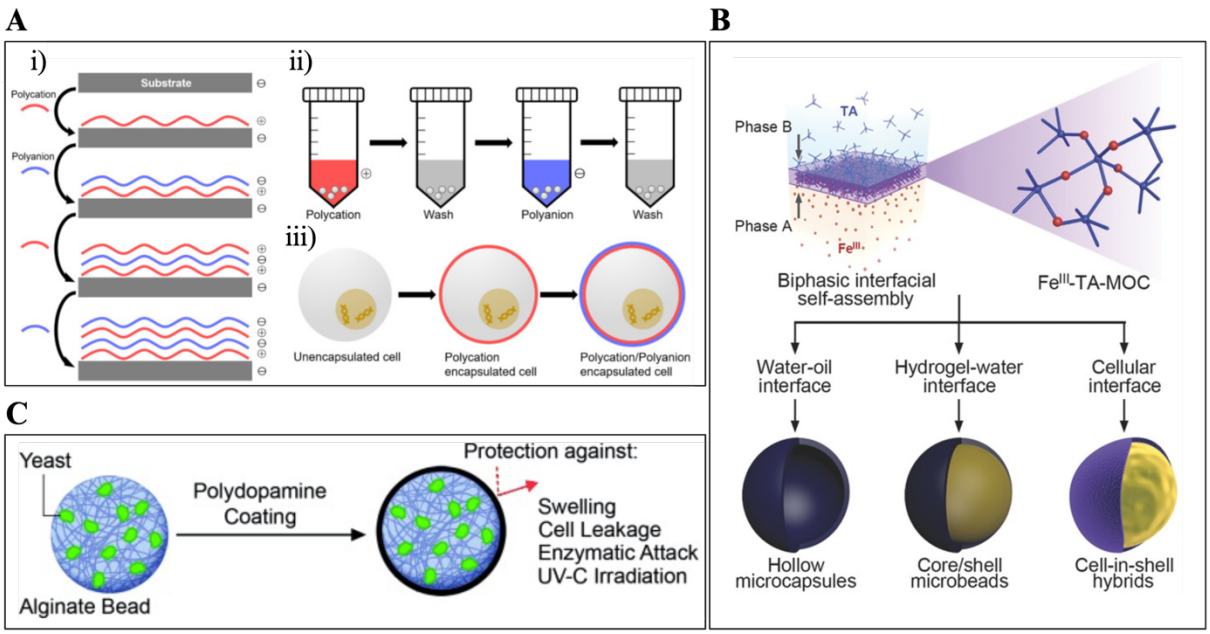

Figure 1.3: Microcapsule coating examples
(**A**) LbL approach for cell encapsulation. i) Negatively charged substrates, such as an alginate hydrogel, is incubated with polycation and polyanion alternatively to create polyelectrolyte coatings films by electrostatic force. ii) Coating can be performed by simple alternation between polyelectrolyte and wash containers. iii) Cell surfaces can additionally be coated directly by LbL self-assembly. Reprinted from (98) with permission from MDPI under CC BY 4.0 license, copyright (2022). (**B**) Schematic of interfacial self-assembly and polymerisation of Fe^{III} and tannic acid at various interfaces. Fe^{III} ions and tannic acid are dissolved separately in two immiscible phases whereby supramolecular self-assembly is localised at the surface interface generating a metal-organic complex (MOC). Reproduced from (103) with permission from John Wiley and Sons, Advanced Materials, copyright (2017). (**C**) Encapsulation of *S. cerevisiae* cells (green) within polydopamine-coated alginate beads to improve mechanical durability and prevent cell leakage Reproduced from (78) with permission from John Wiley and Sons, Angewandte Chemie International Edition, copyright (2014).

1.3.5 Enclosed channel microencapsulation devices

Microfluidics is a versatile methodology for micromanipulation of fluids and generation of emulsions gaining recent popularity for cell encapsulation and cultivation (106). Several enclosed microchannel geometries are possible for generating microdroplets depending on droplet size, throughput, or liquids utilised. The most common utilise passive T-junction (cross-flow), flow-focusing or co-flow geometries (66). Here, immiscible fluids intersect at a local flow field, which deforms the interface causing scission of a droplet. Commonly, cells are carried within an aqueous dispersed phase emulsified by a hydrophobic continuous phase, such as mineral or fluorinated oil, generating water-in-oil (w/o) emulsions (66,107). However, in circumstances when cells or proteins are sensitive to organic solutions, aqueous water/water emulsions (w/w) such as Poly(ethylene glycol) (PEG) and dextran can be used instead albeit with lower interfacial tensions, also known as aqueous two-phase systems (ATPS) (77,108). Furthermore, multi-layered emulsions can be created of water/oil/water (w/o/w) or oil/water/oil (o/w/o), for generating core-shell microcapsules (57,99).

Enclosed channel devices are commonly cast from PDMS, a highly biocompatible, transparent, inexpensive, and functionalisable material microfabricated through a combinational process of photo- and soft lithography (106). Here, a master template for the PDMS is first created using photolithography. A silicon wafer is spin-coated with a photoresist, such as SU-8, which is then covered with a stencil mask of the device channels. The exposed photoresist is then polymerised with UV light, and unpolymerised photoresist is washed away leaving a positive replica mould. In the next soft-lithography steps, PDMS is then combined with a crosslinking agent and poured over the template and cured at ~65 ˚C. The cross-linked PDMS now containing microchannels can be bonded to a glass slide via oxygen plasma treatment (81).

PDMS-microfluidic cell encapsulation offers high throughput (10 - >5000 Hz), high reproducibility (~2.5% coefficient of variation) and lower required resources compared to microwell cultivation methods (66). However, cells cultivated in static w/o emulsions are limited in adequate nutrient and oxygen exchange, as well as cell-cell communication (37,109). Therefore, cell cultivation in microfluidic preparations can be combined with hydrogel or core-shell encapsulation, whereby after crosslinking and removal of emulsions porous capsules may be subsequently incubated in aqueous media facilitating diffusion of signalling molecules, nutrients, and wastes (66).

Although lithographic approaches remain popular for microfluidic devices, they require specialist equipment and clean rooms that might not be accessible to non-disciplinary researchers. Moreover, such devices are limited to droplet sizes within nano- to micrometre range. Advances have therefore been demonstrated in non-lithographic devices fabricated from readily available glass capillaries and or 3D-printable materials. For example, co-axial flow microfluidic devices have been fabricated using concentrically aligned capillaries for generation of multi-layered emulsions and core-shell capsules (57,77,110,111). Recently, fully 3D-printable T-junction microfluidic devices have been demonstrated and utilised for cell encapsulation and cultivation (96,112,113). Although easier to manufacture, non-lithographic microfluidic devices have limited resolution and reproducibility compared to PDMS microfluidic chips.

1.3.6 Gravity-assisted microencapsulation devices

Gravity-assisted microencapsulation devices rely on extrusion of the cell-encapsulant medium through an orifice into air whereby gravity assists droplet formation (114). Gelation initiates once the polymer droplet contacts the crosslinking agent, cooling fluid or a combination of both. A simple example involves extrusion of an alginate-cell mixture through a needle bore held above a $CaCl_2$ crosslinking solution. The capsule size and shape are influenced by the diameter of the extrusion orifice, liquid viscosity, flow rate, and drop height or distance from crosslinking solutions (114). Numerous extrusion techniques have been developed to improve encapsulation efficiency, throughput, or incorporation of multi-phase liquids. These include droplet formation by electrospray, flow jet cutting, vibration dislodgement and coaxial/co-extrusion droplet formation (114).

Electrospray involves liquid dispersal into small droplets (~0.1–15 μm) using an electrostatic field. Here, a high voltage is applied across a needle or extruder and crosslinking solution. As a droplet is extruded, a Taylor cone is formed on the end of the extruder orifice due to a balance between electrical repulsions and surface tension. Once repulsion forces overcome surface tension and viscoelastic forces, one or several jets may erupt from the cone which fragment into ultra-small droplets which are then collected within the crosslinking solution (115).

In flow jet cutting, liquid extruding from the nozzle is segmented by a rotating cutting tool such as a perforated rotating disk or wire. The diagonal directionality of cutting minimises spraying and ensures uniform spherical droplets with higher throughput (116). Laminar flow

can be similarly disrupted by vibrational techniques. For example, pneumatically-drive micro-vibrators have previously been used for alginate encapsulation of chondrocytes (117). Flow jet cutting is particularly useful for flow scission of highly viscous fluid (114).

Multi-phase or core-shell capsules can be generated using coaxial or co-extrusion devices. Here, two phases such as an inner cell phase and outer polymer phase can be combined co-axially using concentrically aligned capillaries. The capsule size and shell thickness can thus be adjusted by controlling flow rates between phases. Such devices have been demonstrated with mammalian cell encapsulations using alginate core-shell spheres (118). Co-extrusion devices can be combined with electrospray or flow jet cutting systems for high-throughput core-shell encapsulation (116,118).

Gravity-assisted extrusion devices are often simpler, lower cost and milder in operational conditions, yielding higher cell viabilities. However, despite recent advances, droplet generation remains lower throughput and is limited to larger droplet sizes compared to enclosed channel microfluidic devices (114).

1.4 3D Printing Techniques and Applications in Cell Encapsulation and Cultivation

3D printing, otherwise known as additive manufacturing, has become increasingly prevalent in biotechnological laboratories allowing researchers to rapidly design, manufacture and share functional devices and equipment. Custom 3D models can be generated using computer-aided design (CAD) software such as AutoCAD or Solidworks. Models are then converted to standard tessellation language (STL) or 3D manufacturing format (3MF) files that can be read by open-source slicing software such as PruserSlicer or Ultimaker Cura to generate geometry code (g-code) containing printer commands. There are seven predominant additive manufacturing technologies, all based on sequential layer-by-layer deposition of print material into 3D objects. These are material extrusion, binder jetting, directed energy deposition, material jetting, powder bed fusion, sheet lamination and vat photopolymerization (119). Desktop material extrusion and vat photopolymerization printers are most frequently used in biomedical laboratories and therefore here will be of focus (Figure 1.4) (Table 1.2) (119).

1.4.1 Material extrusion 3D printers

Material extrusion 3D printers operate by extruding thermoplastic through a heated nozzle onto a build plate. First developed as fusion deposition modelling (FDM) by Stratasys in 1989, material extrusion 3D printers are better known by the parallel community-led technology fused filament fabrication (FFF), developed by open-source companies such as Prusa. Reduction of costs, printer sizes, high simplicity of operation as well as material flexibility in open-source environments has resulted in FFF printers being frequently utilised in research laboratories (119).

There are four main configurations of FFF printers categorised by the mechanism of moving parts or kinematics (Figure 1.4). The first and most common is the Cartesian-style that allows nozzle movement along the X and Y axis on a rail with either the printer bed or nozzle raised on the Z axis. This configuration is the simplest and provides high dimensional accuracy of ~50 µm. Alternatively, the extruder can be suspended above the build plate by a system on three pullies in an inverted Delta (Δ) shape configuration. Delta FFF 3D printers have the advantages of increased print speed and build hights at the expense of greater complexity and lower dimensional accuracy. Less commonly, polar FFF printers are utilised that in contrast to cartesian and delta printers operate on a polar coordinate system with a cylindrical build volume. Polar FFF printers are relatively obsolete but have high noise reduction due to fewer

moving parts. Lastly, Selective Compliance Articulated Robot Arm (SCARA) printers utilise precise robotic arms to move the extruder nozzle akin to laser-engraving instruments. SCARA printers are also uncommon but allow high precision, speed and compactness compared to cartesian printers (Figure 1.4) (120).

FFF printers have several advantages compared to other printer technologies. Printers are typically cheaper and simpler to operate, have a wider range of materials available and relatively large build volume. Furthermore, the ability to manipulate objects during printing as well as multi-material capabilities extends applications outside of single-polymer object usages. For example, if printing is paused midway through the print, non-printer materials such as metal nuts or porous membranes can be permanently integrated once inserted into a partially printed object before continuation of printing (121). Moreover, printers with multi-material capabilities or modifications can interchange different materials at different layers generating multi-material objects (120).

The limitations of FFF printers are warping or shrinkage of thermoplastic during the printing process. This results in print deformations or the loss of object adhesion to the build plate. While parameters can be optimised in slicing software to minimise warping, such as elephant foot compensation, printing with a brim or skirt, as well as the inclusion of draft shields, a heated build plate is usually essential, and may additionally require print speeds to be significantly reduced. Moreover, compared to vat polymerisation technologies, resolution is lower and therefore less suited to smaller detailed objects (120,122).

1.4.2 Material extrusion polymers

Material extrusion 3D printers have a large diversity of materials available, albeit limited to thermoplastics with compatible melting temperatures <300˚C. Most utilised are acrylonitrile butadiene styrene (ABS), polylactic acid (PLA), Polyethylene terephthalate (PET), polypropylene (PP), nylon/polyamide (PA), thermoplastic polyurethanes (TPU), and polycarbonates (PC) (Table 1.2) (120). Composites of these and others are additionally available for tailoring functional properties. For example, blends containing carbon nanotubes, metal powders or natural fibres can improve tensile strength, while poly(vinyl alcohol) (PVA) nanoparticle composites can create porous membranes (119,123).

PLA, a natural polymer derived from renewable sources such as sugar beets and corn, has high reported biocompatibility leading to applications in food packaging and biomedical devices (124,125). It is furthermore a convenient material to print owing to low warping, high

layer-layer adhesion and minimal nozzle stringing yielding fast, high quality prints (126,127). PLA does however experience poor temperature tolerance (glass transition temperate ~60˚C) and low chemical resistance and is thus infrequently used in mechanical applications (122,128).

PET, or more commonly in the form of polyethylene terephthalate glycol (PETG), offers higher chemical resistance, temperature tolerance and mechanical strength compared to PLA (129–132). It furthermore has reported biocompatibility with mammalian cells and is considered non-toxic, seeing usage in drink bottles and food packaging (122,125). Although relatively convenient to print with low warpages, PETG suffers from nozzle stringing leading to low quality in fine object details (129).

PC and PP offer superior chemical resistance, heat tolerance, biocompatibility, and mechanical strength compared to PLA and PETG. However, due to their sensitivity to temperature fluctuations and warping during printing, they are less commonly utilised. Achieving optimal results with PC and PP requires slower and more challenging printing processes, including the use of enclosures and specialised build plates (133,134). Notably, however, they are well-suited for autoclave sterilisation (135–137)

1.4.3 Vat photopolymerisation 3D printers

Vat photopolymerisation (VPP) utilises photo-sensitive photopolymers or resins that are exposed to directed light to obtain polymerised material layers. Here, liquid resins are a mixture of pre-polymer monomers/oligomers mixed with photoinitiators. Excitation of photoinitiators with the correct light wavelength (usually UV) generates free radicals or cationic species that react and crosslink pre-polymers. Depending on the mechanism of curing, VPP printers can be classified into stereolithography (SLA), digital light processing (DLP), and two-photon polymerization (2PP) (Figure 1.4) (83).

Developed as the first 3D printing technology in 1984, SLA printing utilises galvanometer scanners to trace a laser path, usually in UV wavelength, along each object layer upon a build platform. After each layer, the build platform is raised out of the resin vat and the next layer is polymerised. Printing speed is therefore correlated to curing depth and light penetration properties of the material being used and is typically slower compared to other VPP technologies. However, precise laser guidance in SLA printing offers superior details in complex geometries and fine features with layer resolutions around 10-100 µm (83).

DLP technology in contrast uses a digital micromirror device (DMD) or a digital light projector to generate light patterns for each object layer. The DMD consists of an array of

microscopic mirrors that can individually tilt to reflect or block light thus polymerising specific patterns onto the resin surface. The build plate is then raised to allow polymerisation of the next layer. Printing resolution and build space are therefore related to the size of the array, number of micromirrors, and the lenses used by the DMD. DLP projectors exist as arc lamps or more commonly LED arrays that offer greater control over intensity and wavelengths. Although having comparatively smaller printing areas than SLA printers (<3000 and <10,000 mm^2, respectively) DLP printers are optimal for smaller feature sizes of ~1 µm and greater print speeds (30mm3 s − 1) (83,138).

In 2PP printers, crosslinking is initiated by the simultaneous absorption of two low-energy near-infrared photons instead of a single high-energy photon. This greater confines the polymerisation volume (voxel) to the laser focal point allowing nanometre resolution (138). However, as printing is maintained in narrower dimensions, fabrication time for solid objects is significantly slower (i.e. printing a solid cubic structure of 50 µm × 50 µm × 10 µm can take ~ 3.5 h) (139). Furthermore, object sizes are limited to ~1mm^2. 2PP is therefore useful for objects in microfabrication, micro-optics, and microfluidics (138–140).

Overall, VPP printers offer greater resolution than material extrusion and are therefore better suited for smaller, detailed objects. Object surfaces are furthermore smoother and less prone to warping or shrinkage defects (83). Although DLP layer print speed may exceed that of material extrusion printers, the overall process speed is slower compared to FFF due to the necessary post-processing steps of curing and washing of unpolymerised material (83). In addition, print volumes are more limited and materials more costly (83).

1.4.4 Vat photopolymerisation polymers

Polymers used in VPP can be broadly categorised by their mechanism of polymerisation: free-radical or cationic photopolymerisation (141) (Table 1.2).

Free-radical polymerisation is the most commonly utilised mechanism involving Norrish type I or type II photoinitiators that split into free-radical intermediates upon UV photolysis, subsequently reacting with and covalently bonding polymer monomers (141). The photoinitiator employed determines the light wavelength necessary for crosslinking. For example, phosphine-oxide containing photoinitiators, such as diphenyl(2,4,6-trimethylbenzoyl)phosphine oxide (Irgacure-819) and lithium phenyl(2,4,6-trimethylbenzoyl)phosphinate (TPO) are compatible with relatively low activation sources (380–400 nm) utilised in DLP printers (141). Polymers are predominantly comprised of

acrylates/methacrylates with reactive double bonds (C=C) and can be selected for desired properties of mechanical strength, elasticity and transparency (141).

Hydrogel precursors can be photopolymerised when functionalised with acrylate and methacrylate groups, allowing their usage in VPP 3D printing. In contrast to other materials, hydrogels retain a porous and diffusible scaffold advantageous for biological applications. Examples include Gelatin methacryloyl (GelMA), PEG-DA, Chitosan Methacrylate, and HA-MA (Hyaluronic Acid Methacrylate) (141–146). Printing with functionalised hydrogels provides greater biocompatibility and hydrophilic objects for tissue scaffolding and remodelling. However, in comparison to non-hydrogel materials, specialist equipment and protocols are required, in addition to lower resolution, stability, and print speed (142,147).

In contrast to free-radical polymerisation mechanisms, cationic polymerisation utilises photoinitiators that generate reactive cations instead of free-radicals upon photolysis. Onium salt photoinitiators, such as triarylsulfonium or diaryliodonium salts, are typically used for crosslinking epoxide resins such as bisphenol A diglyceryl ether (141). In contrast to acrylate free-radical based polymerisations, cationic polymerisation is less sensitive to inhibition by oxygen, a prominent limitation in VPP (141). Furthermore, epoxides exhibit greater layer-layer adhesion and lower shrinkages (141). However, propagation of heavier acid or proton molecules within the resin is slower than a smaller, unstable radical, thus crosslinking is typically slower than free-radical systems (148).

The biocompatibility of materials printed with VPP is dependent on the selected resin, photoinitiator concentration, and post-processing washing steps (149,150). Polymerised resins from PEGDA, bisphenol A ethoxylate diacrylate (BEDA), and 1,6-hexanediol diacrylate (HDDA) have been demonstrated biocompatible for mammalian cells (149,150). Furthermore, several commercially available resins are formulated for medical use and therefore meet ISO 10993 standards for non-toxicity (151). Regardless, resins must be thoroughly washed of residual photoinitiator and uncured resin before use (149,152).

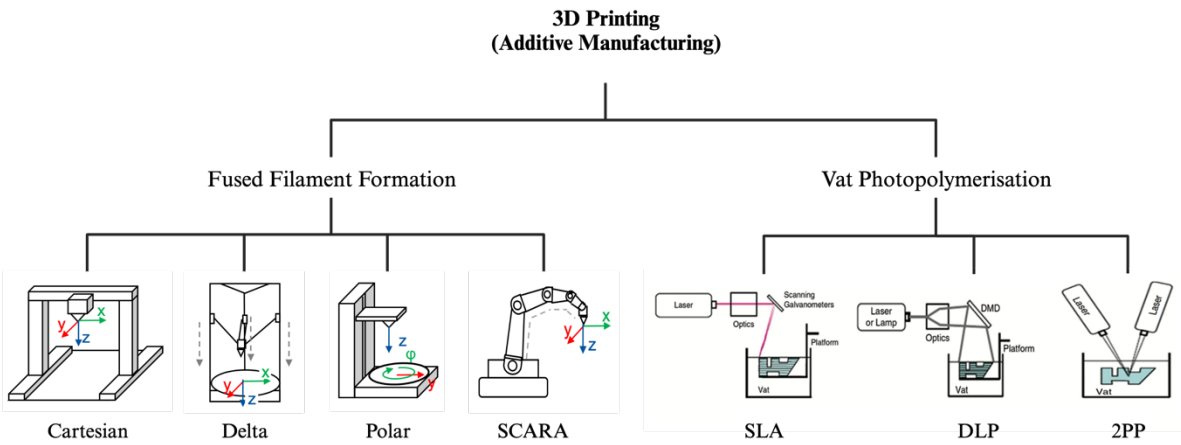

Figure 1.4: Comparison of FFF and VPP 3D printer technologies.
Diagrams of desktop 3D printer technologies. The FFF printers utilise a heated nozzle to extrude material in either the most common Cartesian configuration, or alternatively in delta, polar or SCARA types. In contrast, VPP utilise resin vats that are crosslinked by exposure to light excitation. In SLA printers, scanning galvanometers focus UV light to object layers paths, while DLP printers project light from DMD in single object layer patterns. The less commonly used 2PP employs two different wavelength laser sources for ultra-high resolution object layer paths. Reprinted from (260) and (261) with permission under CC BY 4.0 license.

Printer technology	Material examples	Advantages	Disadvantages	Examples in cell cultivation/encapsulation
Fused filament formation	Polylactic acid (PLA)	– Reported biocompatibility (124,125,153). – Good tensile strength (30-60 MPa) (127,132). – Low shrinkage and ease of printing (120,137). – Strong layer-layer adhesion (126). – Smooth surface finishing with low stringing. – Rigidity comparable to ABS (127).	– Low chemical resistance to solvents/acids (122). – Low temperature resistance (glass transition temperature 60 ˚C) (128). – Brittle (127). – Warped by autoclave heat (137).	– Isolation chips for bacterial *in situ* cultivation (154) . – Pathogen MIC determination. Bacterial culture transfer & replication (137). – Microfluidic devices in droplet generation and alginate cell encapsulation (113). – Stem cell culture perfusion bioreactor (155).
	Polyethylene terephthalate glycol (PETG)	– Reported biocompatibility (155). – Good impact resistance and tensile strength (40-60 MPa) (132). – Good thermal stability (glass transition temperature ~85 ˚C) (156). – Good chemical resistance to weak acids and alcohols (131). – Good translucency (155).	– Poor chemical resistance to strong acid/bases and aromatic/halogenated hydrocarbons (130). – Higher susceptibility to print warping (129). – Prone to print stringing and rougher surface finish (129). – Warped by autoclave heat (130).	– Centrifuge-driven microfluidic chip for urinary pathogen identification (157). – Mammalian stem culture within perfusion bioreactors (155). – Microfluidic devices in microdroplet generation (158).

	Acrylonitrile butadiene styrene (ABS)	– Reported biocompatibility (153) – Good tensile strength (30-40 MPa) (159,160). – High temperature resistance (glass transition temperature 105 ˚C) (161). – Good chemical resistance to weak bases and alcohols (160).	– Poor chemical resistance to strong acid/bases and aromatic hydrocarbons (160,162). – Higher susceptibility to warping (162).	– Isolation chips for bacterial *in situ* cultivation (154). – Porous support structure for mammalian perfusion cell culture bioreactor (163).
	Thermoplastic polyurethanes (TPU)	– Reported biocompatibility (164,165). – Flexible and shock-resistant (164). – Good transparency (165). – Good chemical resistance to alcohols and toluene (165).	– Easily deformed at elevated temperatures (164). – Prone to stringing and rougher surfaces (165). – Intolerable to autoclave heat (166).	– Fabrication of microfluidic channels and compatibility for mammalian cell culture (165).
	Polycarbonate (PC)	– Greater tolerance to autoclave heat (glass transition temperature 150 ˚C) (135). – High tensile strength (~60 MPa) (132). – Good chemical resistant to mild acids, bases, alcohols, and aliphatic hydrocarbons (167).	– Poor resistance to aromatic hydrocarbons (167). – Requires printer enclosure, slow printing, and specialised print beds (135,168). – High susceptibility to warping (135).	– Microfluidic devices for mammalian cell cytotoxicity assays (168).

	Filament composites	– Advanced and custom functionality (119). – Enhanced mechanical strength in natural fibre composites (169). – Electroconductivity in carbon and graphene composites (170). – Diffusible membranes in PVA nanoparticle/PLA composites (123).	– May require specialised printer nozzles (141,171). – More expensive and limited in source (141,171).	– Membranes and electrodes for microbial fuel cells (170). – Mammalian cell culture on porous membrane PVA/PLA composite (172). – Porous membrane integration in microfluidic devices (171).
Vat photo-polymerisation	(Methyl) acrylates	– Optical clarity and ease of visualisation (173). – Smooth surface finish and high dimensional accuracy (173). – Fast curing (141,148). – High mechanical strength (141). – Commercially available resins tolerant to autoclave heat (174).	– Low biocompatibility of unpolymerised components (174,175) – Polymerisation inhibited by oxygen (141). – Susceptible to shrinkage during polymerisation (148).	– Vessels for culturing umbilical vein endothelial cells (176). – Microfluidic devices for encapsulation of bacteria for *in situ* cultivation (49,50).
	Epoxides	– Less susceptible to shrinkage during polymerisation (141). – Tolerant to autoclave heat (177). – Polymerisation less susceptible to oxygen inhibition (148).	– Low biocompatibility of unpolymerised components (178). – Slower polymerisation with cationic photoinitiators (141). – Comparatively brittle (179).	– 3D printed iChips for *in* situ cultivation of bacteria (154). – Microfluidic actuator fabrication with PDMS bonding (180).

	Functionalised hydrogels	– Greater reported biocompatibility (80). – Forms diffusible hydrogels (80,82). – Greater biological relevancy with promotion of cell adhesion (80).	– Unpolymerised components cause toxicity (85). – Lower thermal and chemical resistance (147). – Higher cost and complexity of materials (80,147).	– Integrated diffusible PEG-DA membranes for cell-based microfluidic devices (181) – Mammalian cell-laden GelMA constructs within microfluidic devices (146).

Table 1.2: 3D printing materials for applications in cell encapsulation and cultivation.

1.4.5 Applications of 3D printing in cell encapsulation and microfluidics

The integration of 3D printing with cell encapsulation and culture has expanded new avenues for devices with non-traditional geometries, embedded sensors, and rapid optimisations. Advancements in material biocompatibility, print resolution, and the reduction in printer costs have increased applications for cell cultivation, encapsulation, and microfluidic devices.

Successful examples have demonstrated the capability of 3D-printed microfluidic devices to encapsulate and cultivate cells. Here, devices can be printed directly or indirectly. In indirect microfluidic device 3D printing, channels are printed in sacrificial materials which can be physically removed or dissolved by solvents after casting with PDMS (182) (Figure 1.5A). Alternatively, cell encapsulation microfluidic devices can be fabricated directly using either FFF or VPP technologies (Figure 1.5B). For example, Morgan et al. generated FFF-printed T-junction and flow-focusing microfluidic devices with 600 µm channels capable of encapsulating stem cells within alginate microbeads (113) (Figure 1.5C). Devices were comprised of PLA and found to withstand ~2000kPa, comparable to conventional PDMS devices (113). Although simple and rapid to fabricate, FFF microfluidic devices lack the resolution and channel smoothness of VPP-printed devices. Consequently, VPP printers are better suited for generating device microchannels of ~50 µm, albeit requiring optimisations of resin formulations and protocols for generating small voids (183,184). Alkayyali et al. utilised SLA printing to generate clear methacrylate cross-flow devices for agarose encapsulation of marine microorganisms. Encapsulated cells were furthermore cultured *in situ* within a saltwater aquarium using 3D-printed diffusion chambers (49,66).

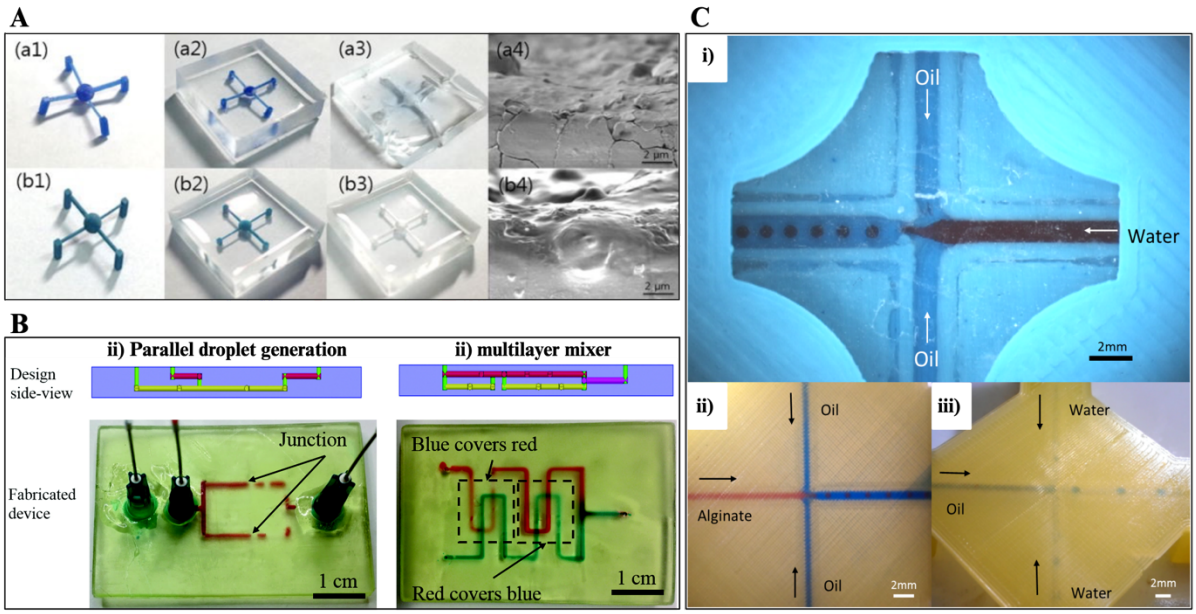

Figure 1.5. 3D printed microfluidics.
(**A**) PDMS channels formed using dissolvable VPP 3D-printed Moulds. (a1)–(a4) Mould made of Visijet M3 hi-cast is dissolved by n-hexane but causes damage to the PDMS structure. (b1)–(b4) Mould made of 3Z-model is successfully dissolved by acetone leaving microfluidic channels within the PDMS. Reprinted from (182) with permission from AIP, copyright (2018). (**B**) SLA-printed multilayer microfluidic devices for parallel droplet generation and fluid mixing. i) Parallel droplet generator with aqueous phase (red) supplied from the upper layer and the oil phase in the bottom layer with droplet generation occurring at a T-junction. ii) Multilayer mixer combining two aqueous fluids. Adapted from (184) with permission from Mary Ann Liebert, copyright (2017). (**C**) i) FFF PLA flow focusing junction for generation of water in oil droplets with glass observation window. ii) Alginate droplets in sunflower oil generated using a semi-transparent PLA. iii) Mineral oil droplets in water. Reprinted from (113) under CC BY 4.0 license.

1.4.6 Applications of 3D printing in cell culture

The ability to rapidly prototype custom devices with a diverse selection of materials has increased the prevalence of 3D printed devices in cell culture applications. Cultivation equipment comprised of PLA, including custom agar plates and replication pins, has been demonstrated for improving speeds of pathogen identification and minimum inhibitory concentration (MIC) testing (137). Recently, 3D-printable versions of the iChip have been developed using both FFF and VPP technologies for *in situ* cultivation of soil bacteria (154). During the investigation of plastic tolerance to environmental conditions, it was found after submersion in neutral or acidic (pH3) water for 28 days neither the ABS, PLA or epoxy plastics had significant loss of hardness or deterioration (154). However, water absorption was noted in the plastics of around 2% mass/volume coinciding with increases in layer thicknesses (154). Similar *in situ* diffusible devices have been demonstrated using FFF-printed PA for investigating pathogen phenotypes changes with exposure to soil (185).

Cell culture devices can be functionalisable with membranes expanding their applications for perfusion or multicellular cultivation (121). Dogan et al. printed stackable 96-well tissue culture inserts with integrated polytetrafluoroethylene (PTFE) and gelatine membranes for co-culture tissue models (186). Using SLA with biocompatible dental resin, PTFE membranes were integrated into the bottom of inserts by applying uncured resin to the object-membrane interface before UV bond-curing, creating a permanent water-tight seal (186). Similarly, Yuen integrated cellulose acetate membranes into PLA cell perfusion bioreactors in a print-pause-print technique (187). Such direct membrane integration streamlines post-processing and removes the requirement for adhesives with dubious biocompatibility (121,154,185).

Cell culture of environmental microorganisms or mammalian cells requires sterile technique and equipment. However, methods for sterilising 3D-printed objects have received relatively little attention. Notably, the high temperatures involved in FFF/FDM printing process provide intrinsic sterility to printed objects (188). This however requires the printer to be operated within a laminar flow hood with UV light illumination, of which air fluctuations increases object warping (188). Although the intrinsic sterility of VPP-printed objects has not been investigated, the combination of intense UV exposure along with post-processing washing steps in isopropanol would likely yield sterile objects. However, proprietary resins used on dental and surgical applications are available tolerant to autoclave sterilisation (152,189). Furthermore, thermoplastics with high temperature tolerance including PC, PP, PA as well as most VPP resins are autoclavable without significant deformations (185,190). PLA, PTEG and ABS in contrast are deformed by autoclave heat, although such deformations are minimised if an object is secured in metal supports (137). Sterilisation with 70% ethanol, 1,500 parts per million (ppm) sodium hypochlorite or hydrogen peroxide plasma vapour is instead recommended (154,185,191).

1.5 Conclusion

Standard cultivation techniques remain inadequate for the cultivation of most microorganisms. Cultivation of uncultivated bacteria remains a technical and philosophical challenge, with significant ramifications particularly for natural product discovery in the wake of an antimicrobial resistance crisis (13). Despite progress in cultivation methods, challenges persist, such as limited throughput, isolate diversity, and reliance on native environments for microorganism cultivation. The advancements of techniques, particularly in microfluidics and

cell culture, coupled with rapid prototyping and advanced fabrication technologies, will enable the exploration of innovative cultivation approaches.

1.6 Thesis Aims

This thesis aimed to devise methods that enhance microbial cultivation efficiency, thereby expanding the biodiversity accessible for research and biotechnological applications. By improving cultivation efficiency, it becomes possible to unlock a broader biosynthetic landscape, facilitating the exploration of novel natural products including antibiotics. Despite advances in cell cultivation and microfluidic techniques, methodological limitations remain. For example, cultivation methods for environmental cells encounter rapid transition of cells from native to laboratory media that may reduce viability of sensitive taxa (192,193). Moreover, utilisation of native media provided through extracts or diffusion chamber devices are limited by a lack of standardisation or requirement to return to source environments (7,14,194,195). This thesis therefore proposes an alternative approach of gradually acclimatising cells to cultivation media, thus facilitating adaptation to alternative media sources or tolerance to noxious media components. The effects of this approach were to be compared with the cultivation efficiencies using a standard instantaneous transition.

Additional limitations are found in the throughput of *in situ* cultivation methods, of which employ custom cultivation chambers that are not in a standardised format or readily scalable (11,154,195). While microfluidic approaches for *in situ* cultivation may significantly enhance throughput, such methods are hindered by poor containment efficiencies of cells within capsules or biocompatibility of encapsulation processes (22,38,49,50,53). This thesis therefore explores a biocompatible microfluidic approach for high-throughput *in situ* cultivation of bacteria contained within hydrogel beads.

Specific thesis aims were:

- Develop and experimentally assess a high-throughput cultivation platform capable of gradually acclimatising bacteria from native to laboratory cultivation media.
- Develop and experimentally assess a high-throughput method for contained *in situ* cultivation of microencapsulated bacteria.
- Screen any potentially superior cultivated biodiversity for antimicrobial activity against multi-drug resistant pathogens.

Chapter 2. Enhanced Cultivation of Bacteria by Acclimatisation to Cultivation Media

2.1 Introduction

2.1.1 Limitations of standard cultivation methods for environmental bacteria

Cultivation of bacteria remains an essential prerequisite for most microbiological research and biotechnology. Despite their ubiquity, only a minority of environmental bacteria are cultivable using standard cultivation techniques. Thus, there remains a vast microbial 'dark matter' yet to be accessed for valuable therapeutics or research potential (47,61). Several innovations have previously shown improvements in cultivation diversity and yield from environmental samples. These include optimisation of nutrient composition and concentration, temperature, aeration or provision of suitable electron acceptors (28,196,197). However, even with technological advances, elucidating optimal growth conditions for specific species remains laborious and at times necessitates environmental growth factors present in the native environment (39,40,198–201). Such growth factors may be provided directly by infusion of native extracts into cultivation media, or indirectly via diffusion chamber methodologies (14,15,46,48). A pioneering example is demonstrated with the iChip, used for high-throughput cultivation of bacteria *in situ* of native environments (11,13,46).

However, dependencies on native media for microbial cultivation bring disadvantages including the requirement to return to or replicate source environments that may vary seasonally (15). Moreover, encountered in standard cultivation methods are immediate transitions of microbes from a native, nutrient-scarce source to a substrate-rich cultivation medium that may reduce the viability of oligotrophic populations (35,192,202). Such laboratory cultivation media may contain components inhibitory to sensitive taxa such as inorganic phosphate (203). However, tolerance to initially suboptimal growth conditions may be established if given sufficient time for acclimatisation with incremental exposure (34,193,204). Previous work has demonstrated cultivation of greater previously uncultivated bacteria when acclimatised to nutrient-rich media, in conjunction with filtration-removal of larger fast-growing species (193). However, it remains unclear what effects media acclimatisation has on cultivation efficiency and diversity of microbial communities. Additionally, there remains a lack of readily available and reproducible tools for exploring alternative cultivation strategies.

2.1.2 Chapter aims and objectives

This chapter aimed to investigate if the acclimatisation of environmental bacteria to cultivation media (R2A) enhances cultivation efficiency compared to a standard instantaneous exposure or transition. Cultivation of previously uncultivated taxa was sought for increasing the likelihood of discovering new natural products (47). The efficiency of the method was to be compared by analysing changes in bacterial community structure, probability of microcolony formation and diversity of cultivated isolates. The specific objectives were:

- Develop and rapidly prototype cultivation devices for the gradual transition of bacteria from native to standardised cultivation media (R2A).
- Assess the effects of acclimatisation on community structure by 16S rRNA sequencing using an NGS Illumina platform.
- Assess the effects of acclimatisation on the probability of microcolony formation in agarose immobilised cells.
- Assess the effects of acclimatisation on the diversity of bacterial isolates by 16S rRNA Sanger sequencing.
- Screen enhanced microbial diversity for potential antimicrobial activity against multi-drug resistant pathogens.

2.2 Methods and Materials

2.2.1 Cells and media

Unless specified, all reagents were purchased from Sigma-Aldrich, UK. Reasoner's 2A (R2A) media (per litre; 0.5 g yeast extract, 0.5 g Proteose Peptone, 0.5 g Casamino Acids, 0.5 g glucose, 0.5 g soluble starch, 0.3 g dipotassium phosphate, 0.05 g magnesium sulfate heptahydrate, 0.3 g of sodium pyruvate and 15g bacteriological agar) was used to cultivate all strains and environmental cells (21). *Bacillus subtilis* 168 was kindly donated by Josef Altenbuchner, University of Stuttgart, Germany. *Escherichia coli* K-12 was purchased from ATCC (ATCC 10798). Clinical isolates of methicillin-resistant *Staphylococcus aureus* (MRSA) or *E. coli* extended spectrum beta-lactamase (ESBL) were kindly donated by Shiranee Sriskandan, Colebrook Laboratory, NIHR Imperial Biomedical Research Centre. Pond water with sediment was obtained 10 cm below water surfaces from King's Mere, Putney Heath, UK (51° 26' 42.7194" N, 0° 13' 48.1908" W) in high-density polyethylene buckets. Sterile-filtered pond water (SFPW) media was prepared by centrifugation of raw pond water at 4,000 g for 10 mins followed by vacuum filtration using a 0.1 µm polyether sulfone filter (ThermoFisher).

2.2.2 Cell extraction and quantification

Environmental cells were extracted by diluting 1 ml of pond sediment samples in 9 ml of SFPW before vortexing with 3 g of 1 mm sterile borosilicate glass beads for 15 minutes. Homogenised samples were filtered through a 20 µm filter (pluriSelect) and stained with 5 µM carboxyfluorescein diacetate, succinimidyl ester (CFDA SE, ThermoFisher) in R2A medium for 30 minutes at 23ºC before quantifying fluorescent cell abundances with a haemocytometer.

2.2.3 Fabrication of Enhanced Domestication platform (EDEN)

EDEN models were designed using AutoCAD 2022 (Autodesk) software and exported as STL files for digital slicing with Ultimaker-Cura (205). Gcode was uploaded to a Prusa i3 MK3S+ FFF 3-D printer equipped with natural PLA thermoplastic (Polymaker) and a smooth polyetherimide (PEI) build plate heated to 65 ºC. Extrusion was maintained at 220 ºC at 100 µm layer height with 100% infill density, 105% flow rate, and 60 mm/s speed. After printing the lower reservoir of an EDEN, the print was paused and a 0.05 µm polycarbonate track-etched membrane (Sterlitech) was affixed over the top of the reservoir and secured to the printer bed with PVA glue. The first layer printed directly on the membrane was completed at 6 mm/s

speed. The EDEN tubing connectors had support materials removed and were polished with P100 sandpaper.

2.2.4 Biocompatibility assessment

The biocompatibility of the PLA plastic was assessed by comparative microcolony growth rates of *B. subtilis* or pond microorganisms with commercially available clear 384-well plates (Greiner Bio-One) and 3D-printed PLA 384 plates. For *B. subtilis*, a single colony was grown overnight in 10 ml R2A medium, 30 ˚C. Cells were then washed once with R2A and diluted in 1% ultra-low melting point agarose (LMPA) R2A maintained at 37 ˚C to achieve approximately single cell per well concentrations (2.44 x 10^{-6} dilution from OD 600 of 0.1). The same procedure was performed for CFDA SE-quantified extracted pond microbial cells. 20 µl of agarose-cell suspension was inoculated into each well of the standard or PLA microwell plates. Plates were sealed with clear polyester self-adhesive film (Starlab) and incubated at 23 ˚C for two weeks. Microcolonies >100 µm were quantified by light microscopy.

2.2.5 Automated pump system and validation

The automated EDEN media delivery comprised a series of NEMA 17 stepper motor peristaltic pumps (Yanmis) driven by DRV8825 drivers (Youmile) controlled by an Arduino Uno microcontroller. Ratios of 1mm-filtered native raw pond water and R2A were combined in 4-hour intervals in separate mixing vessels (custom 500 ml Duran bottles fitted with 0.2 µm air filter) before being immediately delivered to EDENs in 10 ml volumes (1x EDEN reservoir volume). Waste from reservoirs was drip-collected in waste containers. Native pond water was mixed with R2A starting at 99.9/0.1% concentration and exponentially alternated to 0/100% concentration, respectively, over 28 days.

Pump system validation was performed using 10 µM fluorescein sodium salt in 10 mM Tris-pH8 mixed with unstained buffer in the same protocol. Wells and reservoir contents from EDENs were quantified for dye concentrating with fluorescence measurement on a CLARIOstar plate reader (BMG labtech) at timed intervals with comparison to expected measurements.

2.2.6 EDEN acclimatisation and cultivation experiments

The effects of media acclimatisation were examined using three different EDEN methods. These were community cultivations in liquid 96-well EDENs, microcolony cultivations in agarose 384-well EDENs, and isolate cultivation in liquid 384-well EDENs. This allowed investigation with broad high-throughput Illumina sequencing, PCR-bias free colony quantification and single isolate Sanger sequencing, respectively. 5 independent replicates were collected from community experiments, while 3 replicates were collected from microcolony and isolate cultivation experiments.

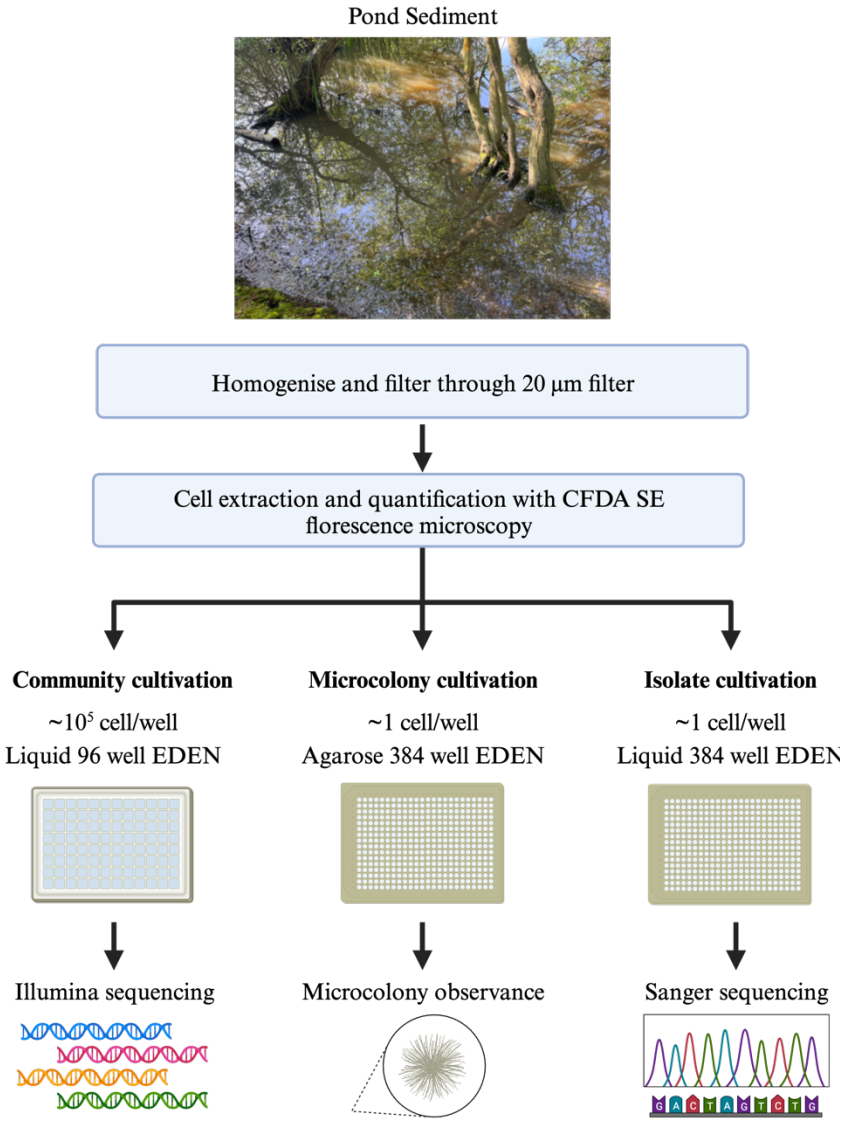

Figure 2.1: Overview of cultivation experiments.
Microorganisms were sourced from a freshwater pond sediment and homogenised before filtering through a 20 µm filter. Samples were then quantified for viable cell abundances by CFDA SE fluorescence microscopy using a haemocytometer. For community cultivation, ~10^5 cells were inoculated into individual wells of 96-well EDENs. After cultivation and acclimatisation, well contents had DNA extracted with sequencing on an Illumina MiSeq platform. For microcolony cultivation, microbes were diluted in molten agarose and dispensed into individual 384-EDEN wells to achieve approximately single cell/well concentrations. Cultivated microcolonies were counted by light microscopy. For isolate cultivation, microbes were inoculated into liquid 384-EDENs to achieve approximately single cell/well concentrations. Cultivated isolates were sequenced by colony PCR and Sanger sequencing.

EDENs were washed with distilled water before submerging overnight in 70% ethanol for sterilisation. Sterilised EDENs were then washed with sterile distilled water before air drying in a biosafety cabinet. Reservoirs were flushed with sterile distilled water prior to use.

Environmental cell extraction and quantification was performed as previously (Methods 2.2.2) Cells were diluted in SFPW for acclimatisation experiments or R2A for standard cultivation comparisons. EDEN bacteria acclimatised to R2A were initially suspended in SFPW with 0.1% R2A and exponentially transitioned to 100% R2A over 28 days. Alternatively, EDEN bacteria were inoculated in SFPW or R2A and pumped with pond water or R2A alone, respectively. Cultivations were left on benchtops at room temperature (23 ˚C).

For Illumina sequencing community experiments, 96-well EDENs were inoculated with 10^5 cells in 50 µl and sealed with clear polyester self-adhesive film (Starlab). Parallel cultivation comparisons were made with cells streaked on 1.5% agar R2A petri dishes. After cultivation or acclimatisation, EDEN wells were harvested and resuspended with 50 µl R2A media by repeated pipetting, while colonies from R2A agar plates were scraped using 1 ml R2A and collected in Eppendorf's. Samples were freeze-thawed at -20˚C before DNA extraction with a commercially available environmental DNA extraction kit (MP Biomedicals).

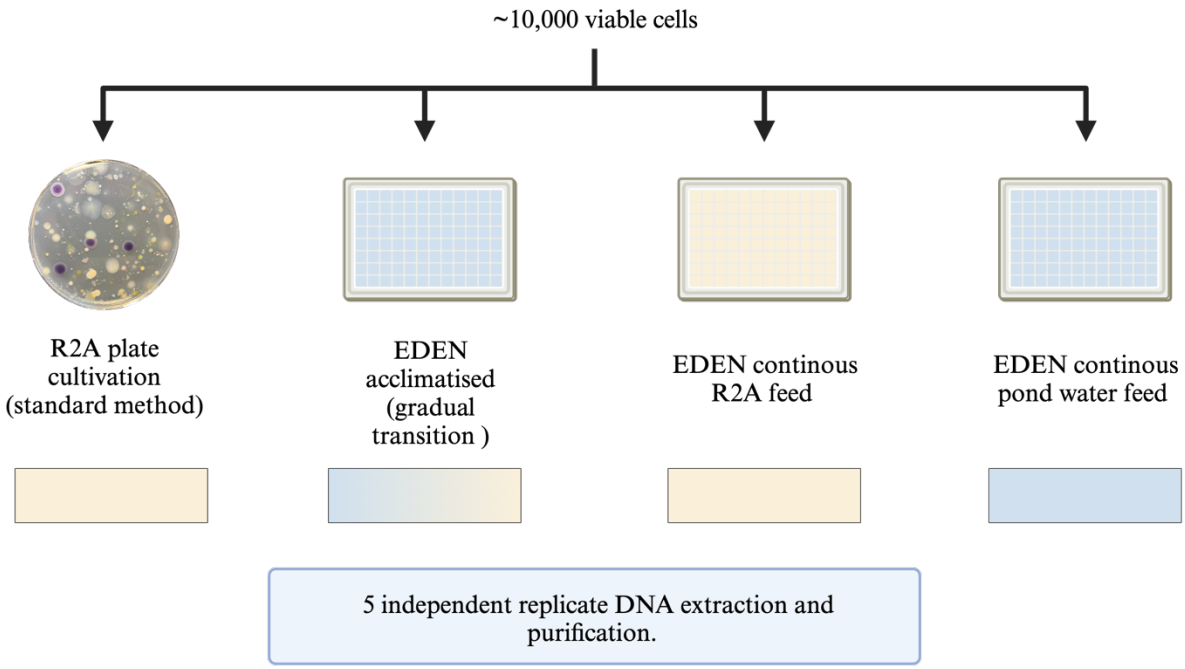

Figure 2.2: Community cultivation experiment for NGS Illumina sequencing.
Bacteria were sourced and extracted from a freshwater pond sediment. A portion (500 µl) was retained for analysis of the undiluted community. 10,000 CFDA SE+ viable cells were inoculated onto R2A agar for standard method comparison, or individual wells of a 96-well EDEN for acclimatisation to R2A. As additional controls for effects of EDEN format, parallel EDENs were set up with R2A or pond water alone. After 28 days incubation, a single random well was selected from 5 independent EDENs of each cultivation condition in addition to plate scrapings from 5 R2A plates for DNA extraction and Illumina 16S rRNA sequencing.

For cultivated isolates for Sanger sequencing, 384-well EDENs were inoculated with ~1 cell/well in 20 µl liquid medium and centrifuged at 500 rpm for 2 seconds. EDEN bacteria were acclimatised with control EDENs as previously. Parallel cultivation comparisons were made with cells cultivated in 20 µl R2A in commercially available clear 384 microwell plates (Greiner Bio-One).

For visual microcolony counts, the same media solutions were boiled with 1% LMPA, sterile-filtered at 0.2 µm and inoculated with bacteria after cooling to 37 ˚C. After cultivation, EDEN reservoirs were physically separated from growth chambers and grown microcolonies >100 µm were counted by light microscopy.

2.2.7 Illumina community sequencing and analysis

Sequencing analysis was carried out in collaboration with Dr Raphaella Jackson, Imperial College London, Faculty of Medicine, Department of Infectious Disease. Library preparation and sequencing were performed using an Illumina MiSeq platform with a 2 x 300 bp paired-end read module by Eurofins Genomics (Germany). Libraries were generated by a two-step

PCR with first amplification of the bacterial 16S rRNA gene V3-V4 region (forward: 5-' TACGGGAGGCAGCAG -3' and reverse: 5-' CCAGGGTATCTAATCC -3') followed by appending of amplicons with sample barcodes (206,207). Raw sequences were processed using the Ampliseq pipeline available from nf-core (revision 2.4.0) (208). First, quality assessment was reviewed using FastQC (v 0.11.9) (209). Adapter sequences were removed using cutadapt basic (v 3.4) (210). Denoising, filtering of low-quality reads. inference of amplicon sequence variants (ASVs), merging of paired-end reads and removal of chimaeras was performed using DADA2 (v 1.22.0) (211). ASVs were assigned taxonomic labels based on the Silva SSU database (release 138) (212). ASVs annotated as mitochondria or chloroplasts were removed, as well as ASVs not detected in the original pond source material. The ASV table with taxonomic assignments were further analysed in R with vegan package (v 2.4.3) (213).

The non-metric multidimensional scaling (NMDS) plot was generated by first transforming raw counts ASVs into proportions, with low-level variation filtered by setting proportions below 0.005 to zero. Subsequently, a Bray-Curtis dissimilarity matrix was computed on the transformed data. The metaMDS function was called with iterative optimisation for a stable solution. Permutational multivariate analysis of variance (PERMANOVA) was conducted to assess the significance of sample type in shaping community composition.

For filtering of ASVs unique to cultivation conditions, only distinct ASVs observed more than once across replicates and only in one cultivation condition were quantified. For quantification of likely uncultured ASVs, ASVs observed in more than one replicate and greater than 100 in abundance across conditions were filtered by either having no genus-level classification, <97% 16S rRNA sequence identity or specifically labelled 'uncultured' in Silva taxonomic classification.

2.2.8 Isolate sequencing and analysis

Isolates for Sanger sequencing were obtained directly from 384-EDEN wells with cell lysis and direct 16S rDNA PCR. 10 µl of EDEN well contents were mixed with 40 µl lysis buffer (10 mM Tris-pH8, 1 mM EDTA, 1% Triton X-100, final concentration) and boiled for 12 minutes with pipetting agitation. Lysates were placed on ice before 16S rDNA amplification with 27F (5-' AGA GTT TGA TYM TGG CTC AG -3') and 907R (5-' CCG TCA ATT CMT TTG AGT TT -3') primers (214). 5% v/v lysate volume was added to each PCR reaction with a programme of pre-denaturation at 98 °C for 2 min, 35 cycles of denaturation at 98 °C for 30

s, annealing at 54 °C for 40 s, elongation at 72 °C for 40 s, and final elongation at 72 °C for 5 min. Sanger sequencing of amplicons was performed by Eurofins Genomics using 907R primer. High quality reads Q30 and >300 bp length were filtered using Geneious Prime (Biomatters) and exported as FASTA files. Sequences were classified using SILVA Incremental Aligner (SINA) (v1.2.12) and classification with a minimum query sequence identity threshold of 0.95 (215).

2.2.9 Antimicrobial detection assay

For detection of antimicrobial activity, colonies from acclimatised EDENs were transferred to the centre of a new R2A agar dish and cultivated for 14 days at 23˚C. Reporter cells of *B. subtilis* 168, MRSA, or *E. coli* ESBL were cultivated in 10 ml Muller Hinton broth overnight at 30˚C before diluting 1/500 in Muller Hinton 1% agar maintained at 40˚C. The agar-cell suspension was then mixed and dispensed on top of the EDEN colonies and allowed to solidify before overnight incubation at 30˚C. Antimicrobial activity was detected by clearance zones on reporter cell lawns surrounding the EDEN isolates.

2.3 Results

2.3.1 Cultivability of pond water microorganisms

Prior to the investigation of media acclimatisation on the cultivability of pond water microorganisms, the effects of media composition were first compared on the cultivability of isolates. R2A was selected as a growth medium and was compared with native sterile-filtered pond water (SFPW) or mixture ratios. Microorganisms were extracted from pond water sediment and quantified using CFDA SE-staining fluorescent microscopy. Viable cells were then diluted in agarose with media mixtures to yield approximately one cell per well in sealed 384-microwell plates. After incubation of multiple time points, the number of cultivated microcolonies was quantified by light microscopy. Greater cultivation efficiency was found when R2A was diluted in native SFPW compared to pure water. The highest microcolony counts were observed in mixtures comprising 50% native SFPW and 50% R2A media, a significant increase in comparison to the standard 100% R2A media formulation by day 28 ($P=0.002$, $F(4, 21) = 26.73$) and all additional timepoints (Figure 2.3A-D). Furthermore, cultivation yield was dose-dependent with R2A addition, indicating nutrient concentration is rate-limiting for most isolates before plateauing at 50% R2A (Figure 2.3A-D). Slow-growing microorganisms represented a relatively minor proportion of culturable cells, with only ~4% increase in microcolony growth observed between 14 days and 4 months across all conditions (Figure 2.3A-D). Cells cultivated with native nutrients alone were comparable but not superior to counts with 100% R2A media. Interestingly, notable (~1% yield) microcolonies were observed under extreme oligotrophy with 1000-fold less added R2A medium (Figure 2.3A-D). No microcolonies or CFDA SE+ viable cells were observed in SPFW or agarose solutions without bacteria introduced.

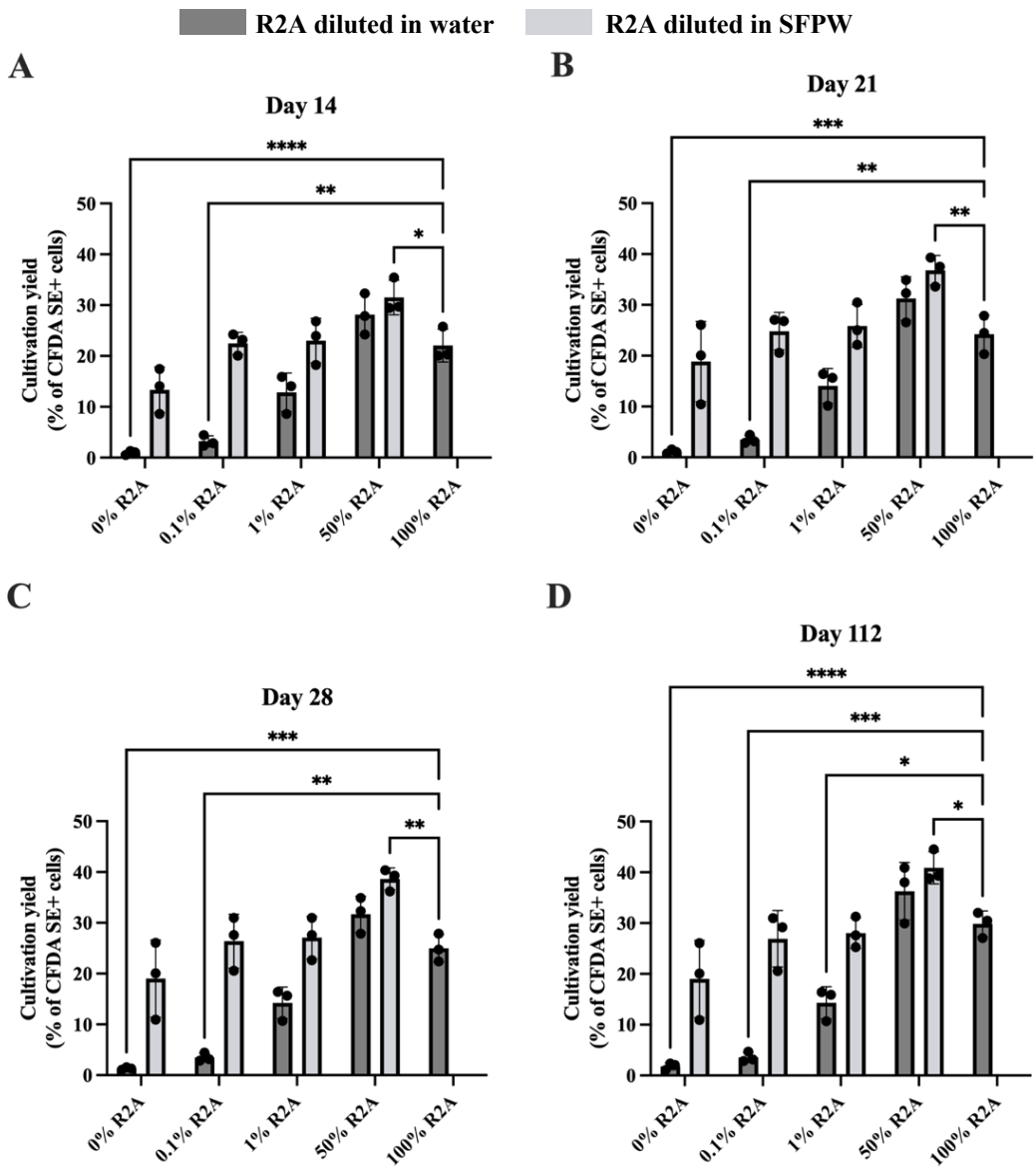

Figure 2.3: Cultivability of pond water microorganisms with dilution mixtures of R2A and SFPW.
Pond water microorganisms were inoculated into agarose containing R2A diluted in water (dark grey) or SFPW (light grey) at approximately single viable cell/well concentrations. Cultivated microcolonies were quantified after (**A**) 14 days, (**B**) 21 days, (**C**) 28 days and (**D**) 112 days. Data shown as proportion of CFDA SE viable cells yielding microcolonies, with two-way ANOVA and Tukey's multiple comparison test. * = $p < 0.05$, ** = $p < 0.01$, *** = $p < 0.001$, **** = $p < 0.0001$.

2.3.2 EDEN design and optimisation

To test if the acclimatisation of bacteria to cultivation media enhances cultivation efficiency and diversity, a novel device was conceptualised termed Enhanced Domestication Platform (EDEN) capable of transitioning bacteria from native to cultivation media over an extended period (Figure 2.4).

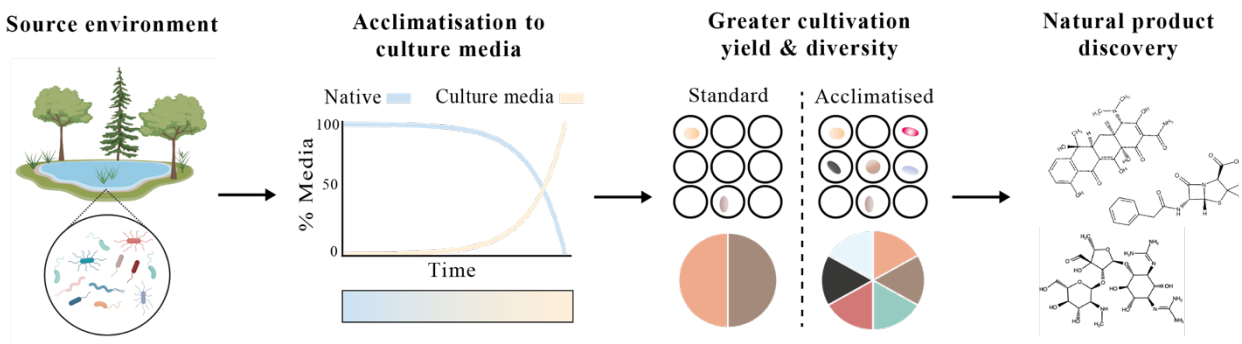

Figure 2.4: Acclimatisation to culture media for enhancing microbial cultivation. Environmental microorganisms extracted from a source environment such as pond water are gradually acclimatised to cultivation media by exponential replacement of native media. Acclimatisation may enhance microbial cultivation (shown as coloured microcolonies in wells) yielding novel taxa that may produce new natural products of interest.

The EDEN device comprised a changeable reservoir separated from a growth chamber via a diffusible 0.05 µm-pore PC membrane that enabled diffusion of nutrients but prevented migration of cells. A freshwater pond located in Putney, UK was sourced for the native environment. This was optimal as the EDEN reservoir requires liquid media. Native media (collected raw pond water) was mixed with R2A at initially at 0.1% R2A concentration and increased to 100% over 28 days, with exponential increments (to the power of 1.00017134 per minute). The required mixture ratio was prepared and immediately delivered to the EDEN reservoirs in 4-hour intervals, where contents within the reservoir diffuse to bacteria within the growth chambers. A prototype device was first developed comprising a Delrin ring plastic reservoir sealed with a PC membrane by a PLA 3D-printed frame in the dimensions of a 90 mm petri dish (Figure 2.5A). Agar was then cast on top of the membrane which diffused with the contents of the reservoir. Microorganisms were extracted from pond sediment and plate-streaked on EDENs at approximately 100 viable cells per plate concentrations. However, during preliminary testing it was found that the agar absorbed too much moisture resulting in biofilm plaque formation with cross-contamination of growing colonies into a mixture lawn of cells (Figure 2.6).

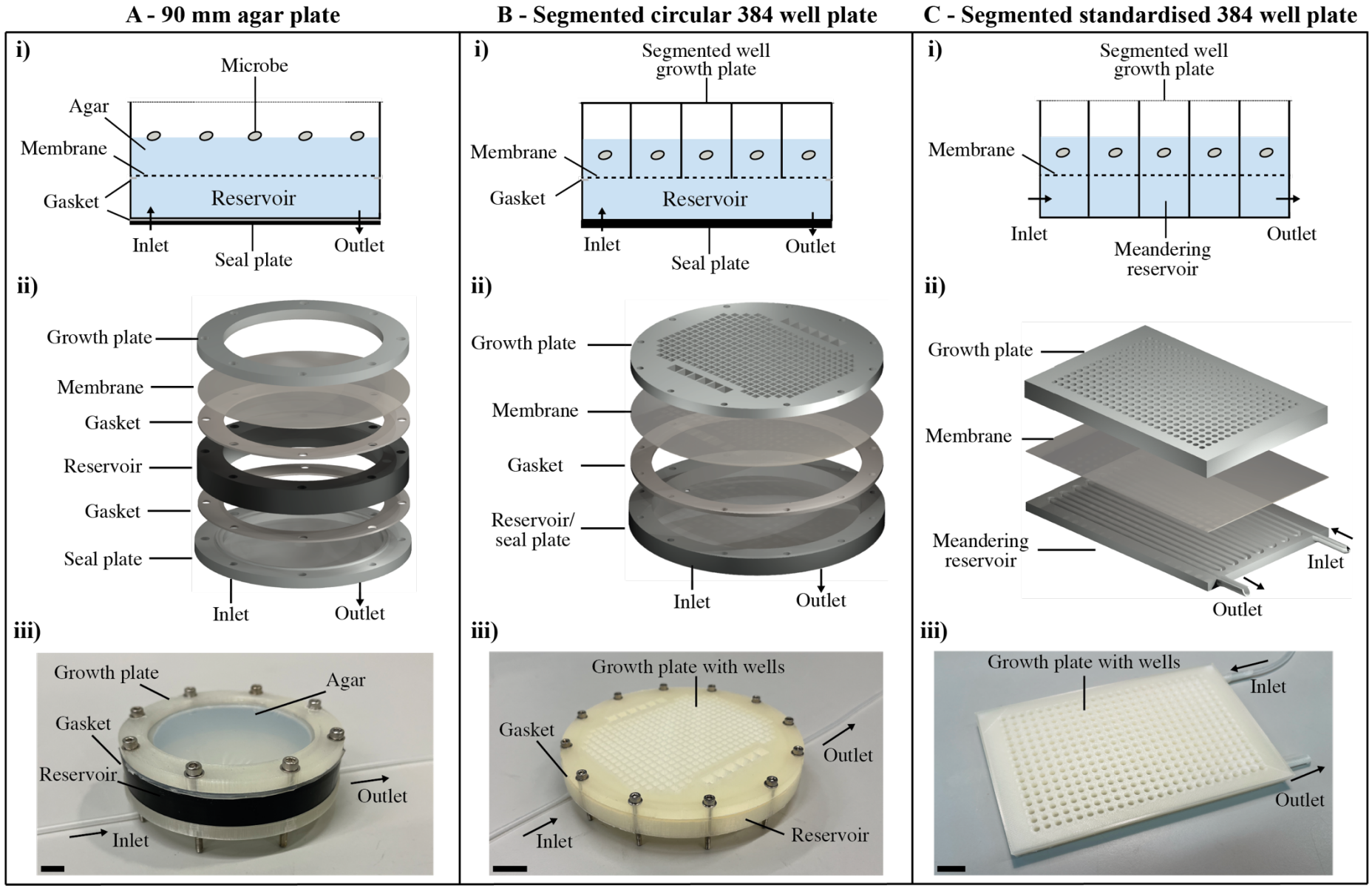
A - 90 mm agar plate
B - Segmented circular 384 well plate
C - Segmented standardised 384 well plate
i)
Microbe
Agar
Membrane
Gasket
Reservoir
Inlet
Seal plate
Outlet
Segmented well growth plate
Meandering reservoir
ii)
Growth plate
Membrane
Gasket
Reservoir
Gasket
Seal plate
Inlet
Outlet
Reservoir/ seal plate
Meandering reservoir
iii)
Growth plate
Agar
Gasket
Reservoir
Outlet
Inlet
Growth plate with wells
Gasket
Outlet
Inlet
Reservoir
Growth plate with wells
Inlet
Outlet

Figure 2.5: EDEN development.
(**A**) i) Cross-section of prototype 90 mm agar plate EDEN featuring a continuous reservoir that diffuses with agar cast within the growth plate on top of a porous PC membrane. Microorganisms are then streaked and cultivated on top of the agar. ii) 3D render of Delrin reservoir (black) with PC membrane and seal plates sealed with silicone gaskets. iii) Assembled single-plate EDEN displaying agar cast on top of the membrane and reservoir. (**B**) i) The growth plate was segmented into 384-wells for greater through-put and prevention of cross-contamination of colonies. Microorganisms were mixed with molten LMPA or liquid before dispensing into wells. ii) 3D render displaying continuous reservoir that is screw-assembled to the membrane and growth plates with a silicone gasket. iii) Image of assembled circular 384-EDEN. The circular format was required to accommodate the circular membrane available at the time. Larger square wells were provided as control wells. (**C**) i) Cross-section of EDEN in standardised 384 microwell format with linear meandering reservoir that reduced dead volumes and compatibility with automated media exchange pumps. ii) 3D render displaying meandering reservoir and membrane heat-bonded together with growth chambers iii) Image of final EDEN version fabricated as a single printed object without screws or adhesives.

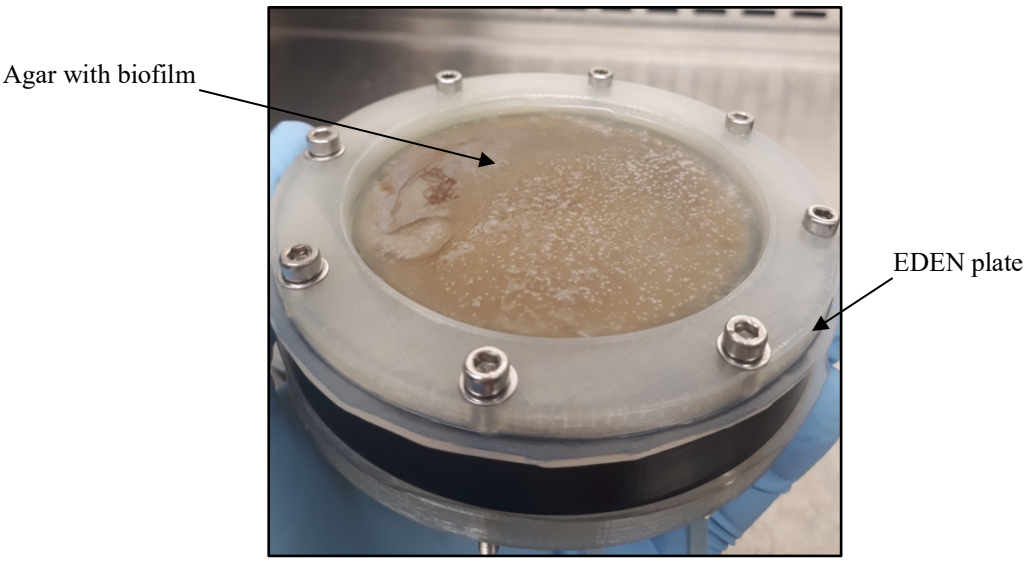

Figure 2.6: Single plate EDEN with biofilm.
A single agar plate EDEN was streaked with pond water microorganisms and incubated with exponential increases of R2A in reservoirs over 28 days. However, by 10 days a biofilm had formed on the agar with lack of isolatable colonies.

To mitigate cross-contamination of colonies and enhance throughput, the single agar growth plate was redesigned to a 384-microwell plate format, which allowed for physical separation between growing colonies (Figure 2.5B). For increased speed of manufacturing and prototyping, EDEN growth well plates and reservoirs were 3D-printed with PLA and screw-assembled using silicone gaskets (Figure 2.5B). The circular EDEN format was required to accommodate the 142 mm circular polycarbonate membrane utilised.

Physical compression of the growth chamber walls against the PC membrane was not sufficient to maintain a water-tight seal between the bottom of the growth chambers. It was therefore necessary to glue the membrane to the bottom of the growth chamber plates. Despite

being previously applied in the literature, the biocompatibility and effectiveness of acetoxy silicone or polyurethane-based adhesives has not been described effectively (15,216). To investigate, ~10 µl of either acetoxy silicone or polyurethane adhesive was dropped into the bottom of a 96-well plate and allowed to cure before the introduction of a *B. subtilis* or *E. coli* culture. Both adhesives were found to be significantly inhibitory to *B. subtilis* growth regardless of curing time ($F(8, 18) = 6149$, $P<0.0001$) (Figure 2.7A), while *E. coli* was only capable in tolerating silicone adhesive ≥ 6hr cure time ($F(8, 18) = 118.0$, $P<0.0001$) (Figure 2.7B). Furthermore, it was noted the adhesive strength of acetoxy silicone to the PC membrane was weak and prone to removal. It was therefore determined the use of adhesives was unsatisfactory.

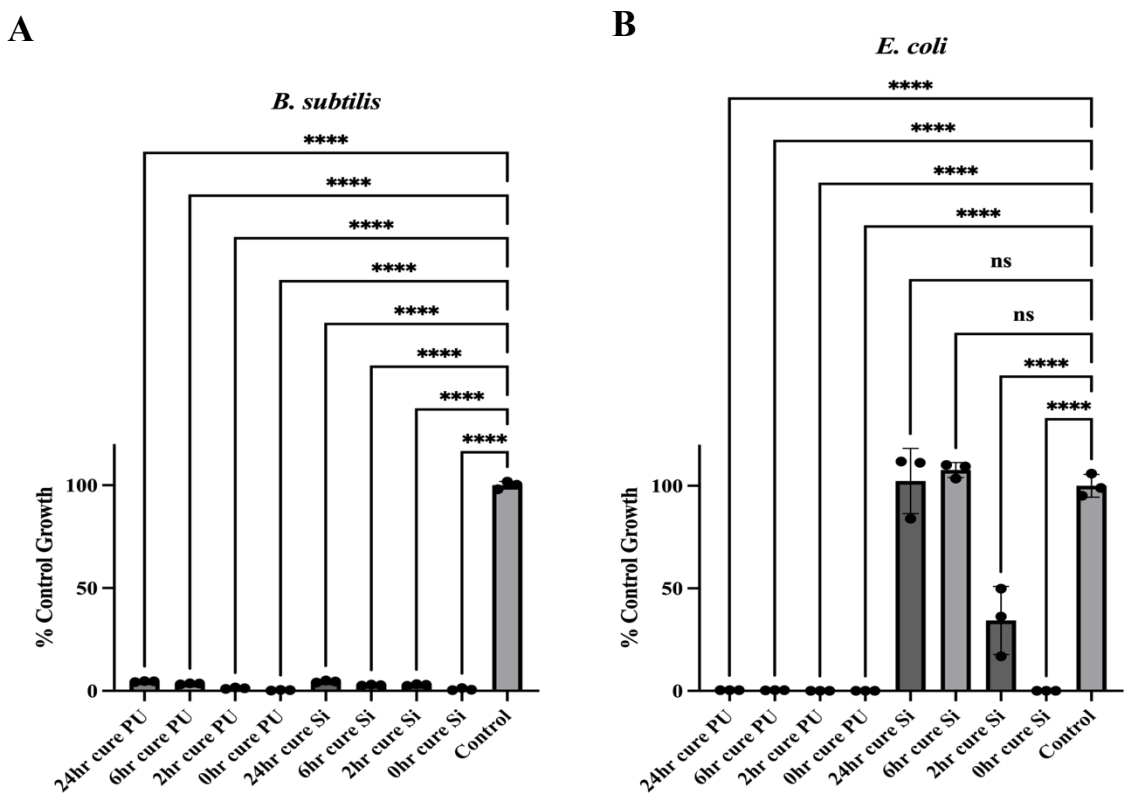

Figure 2.7: Biocompatibility of adhesives with *B. subtilis* and *E. coli*.
Approximately 10 µl of either silicone (Si) or polyurethane (PU) based adhesives were placed within microplate wells and allowed to cure for 24 hrs, 6 hrs, 2 hrs or 0hr before addition of (**A**) *B. subtilis* or (**B**) *E. coli* R2A liquid cultures for overnight incubation. Relative growth to control of R2A with one-way ANOVA and Tukey's multiple comparison test. ns= non-significant, * = $p < 0.05$, ** = $p < 0.01$, *** = $p < 0.001$, **** = $p < 0.0001$.

2.3.3 EDEN optimisation and fabrication using direct membrane 3D printing

To address the limitations of using adhesives in fabrication of EDENs, and with consideration of the high temperature tolerance of PC (glass temperature 260 ˚C), it was hypothesised the growth chambers could be heat-bonded to the PC membrane if the growth chamber model was extruded directly on top during printing. Optimisations in first-layer printing settings allowed successful printing and bonding of PLA or PETG growth chambers to PC membranes (Figure 2.8A-B). Compared to chambers printed in PETG, PLA exhibited superior print quality, lower liquid adhesion to well walls, and fewer instances of stringing or blockages in wells, therefore, PLA was selected for EDEN fabrication. Additionally, printing circular wells instead of square was found to result in more reliable watertightness between wells, due to thicker walls. Using the CuraSlicer software instead of PrusaSlicer also resulted in significantly fewer well obstructions due to optimised nozzle travel with fewer migrations over well chambers that lead to stringing (205,217). Further optimisations were made, such as procurement of rectangular PC membrane so EDENs could be printed in standardised microwell dimensions. The continuous reservoir required manual draining and replacement with correct ratio mixtures of native and culture media each day. Thus, the continuous reservoir was replaced with a linear meandering reservoir channel that allowed spent fluid to be more efficiently ejected with media flow and thus compatibility for an automated pump system (Figure 2.5C).

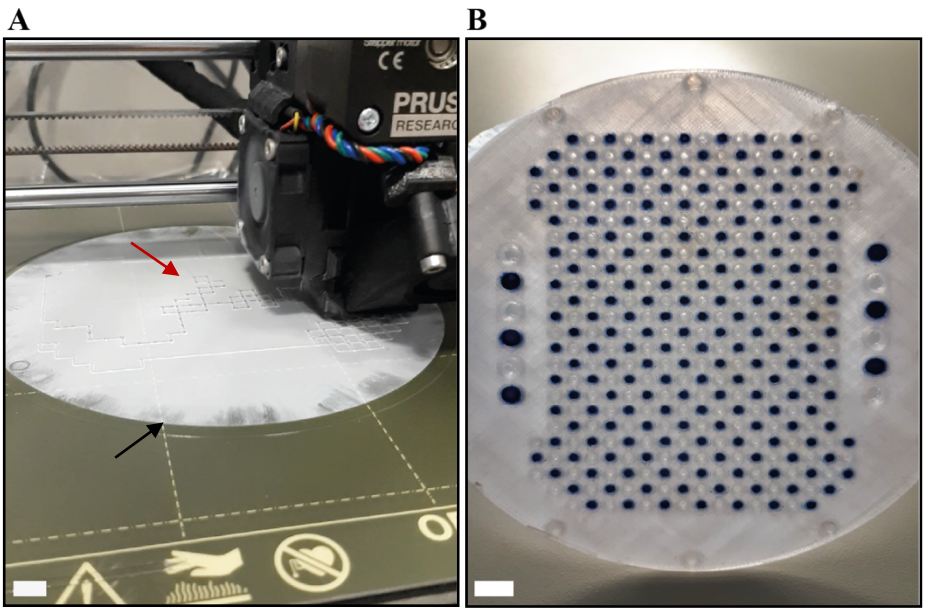

Figure 2.8: Demonstration of EDEN fabrication by direct membrane printing.
Example of heat-bonding of growth chambers to PC membrane by direct 3D printing. (**A**) Circular EDEN fabrication with first layer of growth wells (red arrow) being directly 3D printed onto PC membrane (black arrow). (**B**) Finished circular well 384-EDEN growth plate with heat-bonded PC membrane. Checkerboard pattern alternating with blue dye and clear water demonstrate watertightness between wells and membrane. Scale bar = 1 cm.

Despite the removal of toxic adhesives, fabrication of EDENs still required manual assembly of EDEN growth chambers to reservoir parts using gaskets and screws. To improve EDEN fabrication throughput, it was hypothesised the PC membrane could be incorporated directly into EDENs by print-pause-print technique thus allowing the fabrication of EDENs as a single ready-made object (121). After 3D-printing the lower reservoir portion, the PC membrane could be affixed on top, with the printing of the growth chambers continuing directly on top of the PC membrane (Figure 2.9A-C). Direct 3D print integration of PC membrane was successfully achieved for 384- and 96-well EDENs (Figure 2.9D). To test if direct-membrane printing compromises the membrane integrity, EDEN wells were filled with sterile media while reservoirs were pumped with confluent cultures of *E. coli* and allowed to incubate for 28 days. Only 2/288 96-EDEN wells and 1/1152 384-EDEN wells tested were found to be contaminated with *E. coli* from reservoirs, indicating direct integration of PC membranes did not significantly compromise membrane integrity. Additionally, it was observed in optimising printing temperature to 220˚C, that the bacterial growth plate bonded stronger to the membrane than the reservoir portion allowing the latter to be cleanly removed using a prying tool. This allows compatibility of EDEN growth plates with high-throughput liquid handing robots and microscopic visualisation.

Despite recent demonstrations of PLA used in cultivation of bacteria, the biocompatibility of PLA with environmental bacteria remains unclear (137). To assess biocompatibility, cells of *B. subtilis* or extracted pond microorganism communities were diluted to approximately single-cell concentrations and dispensed into commercially available 384 or PLA 3D-printed wells. Microcolonies were then quantified by light microscopy after 28 days incubation. No significant differences in microcolonies were observed between the commercially available 384 plates or PLA 3D-printed wells for either *B. subtilis* or pond communities ($t=0.5315$, $df=4$, $p= 0.6232$ and $t=0.8176$, $df=4$, $p= 0.4595$, respectively) (Figure 2.10A-B).

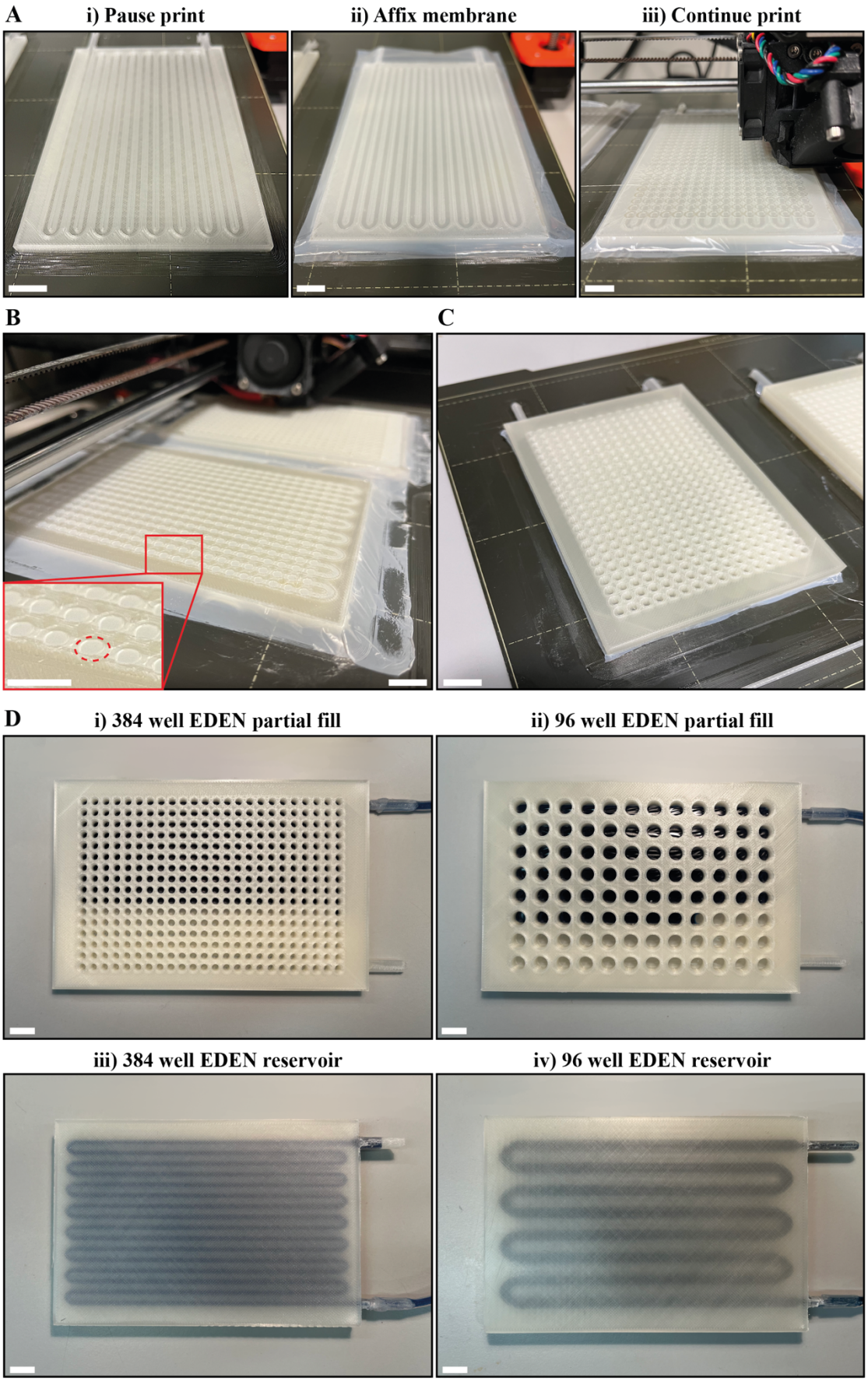
A
i) Pause print
ii) Affix membrane
iii) Continue print
B
C
D
i) 384 well EDEN partial fill
ii) 96 well EDEN partial fill
iii) 384 well EDEN reservoir
iv) 96 well EDEN reservoir

Figure 2.9: EDEN fabrication by print-pause-print technique with direct membrane integration.
Demonstration of screwless and adhesive-free fabrication of EDENs by incorporation of PC membrane by print-pause-print technique. (**A**) i) The EDEN reservoir is first 3D printed and automatically paused before the first layer of the growth chambers. ii) PC membrane is placed over the printed object and secured to the printer bed with PVA glue. iii) The first layer of the growth chambers is printed and heat-bonded to the PC membrane. (**B**) Partial print of growth chambers showing zoom and well outline (dotted red line). The bottom of the well is unobstructed and diffusible with the reservoir channels beneath. (**C**) Completed EDEN on printer bed. Two EDENs are printable simultaneously on a Prusa MK3S+ 3D printer bed. (**D**) Views of i) top of 384-well EDEN and ii) 96-well EDEN with partially filled reservoir with blue dye. Underside of iii) 384-EDEN and iv) 96-EDEN displaying reservoirs when filled with dye. Scale bar = 1 cm.

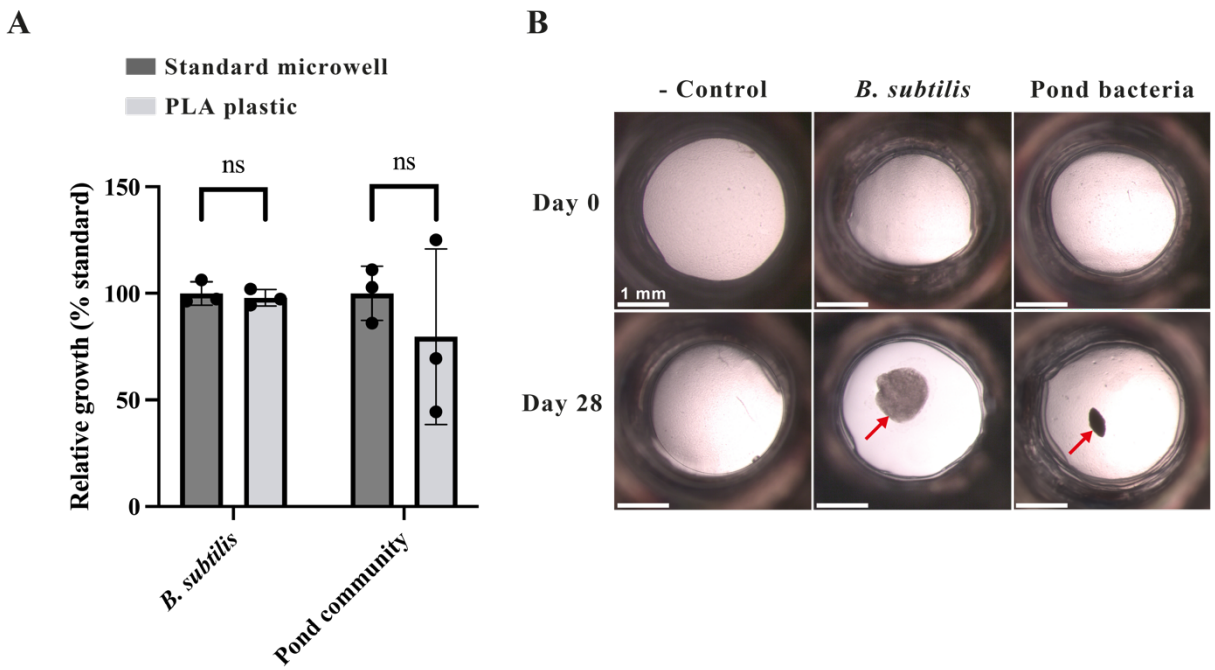

Figure 2.10: Biocompatibility of PLA plastic with *B. subtilis* and pond water microorganisms.
(**A**) Relative growth of *B. subtilis* or pond water microorganism communities in 3D printed PLA wells plates compared to standard commercially available microwell plates. Results of unpaired t-test. (**B**) Example microcolonies (red arrows) in 3D printed PLA wells after 28 days incubation.

2.3.4 Construction of an automated EDEN liquid media delivery system

To acclimatise EDEN bacteria through the gradual introduction of culture (R2A) medium, an automated media delivery system was developed. Here, native pond water was mixed and exponentially replaced with R2A media over 28 days using a series of peristaltic pumps controlled by a programmable Arduino microcontroller. To control for potential excess EDEN nutrient availability and format differences, parallel EDENs were set up and fed R2A or native pond water alone (Figure 2.11A). To prevent spoilage of media and stocks, required ratios of

pond water and R2A were mixed in a separate mixing vessel at 4-hour intervals before being immediately delivered to EDEN reservoirs (Figure 2.11A-C). During preliminary testing, it was found that tubing for directing waste from EDENs into waste collectors caused siphoning and drainage of EDEN well contents. Conversely, when the waste tubing was positioned above or in line with the EDEN, the wells would flood. Consequently, the waste outlet of EDENs was left without connected tubing and allowed to passively drip into waste containers (Figure 2.11C).

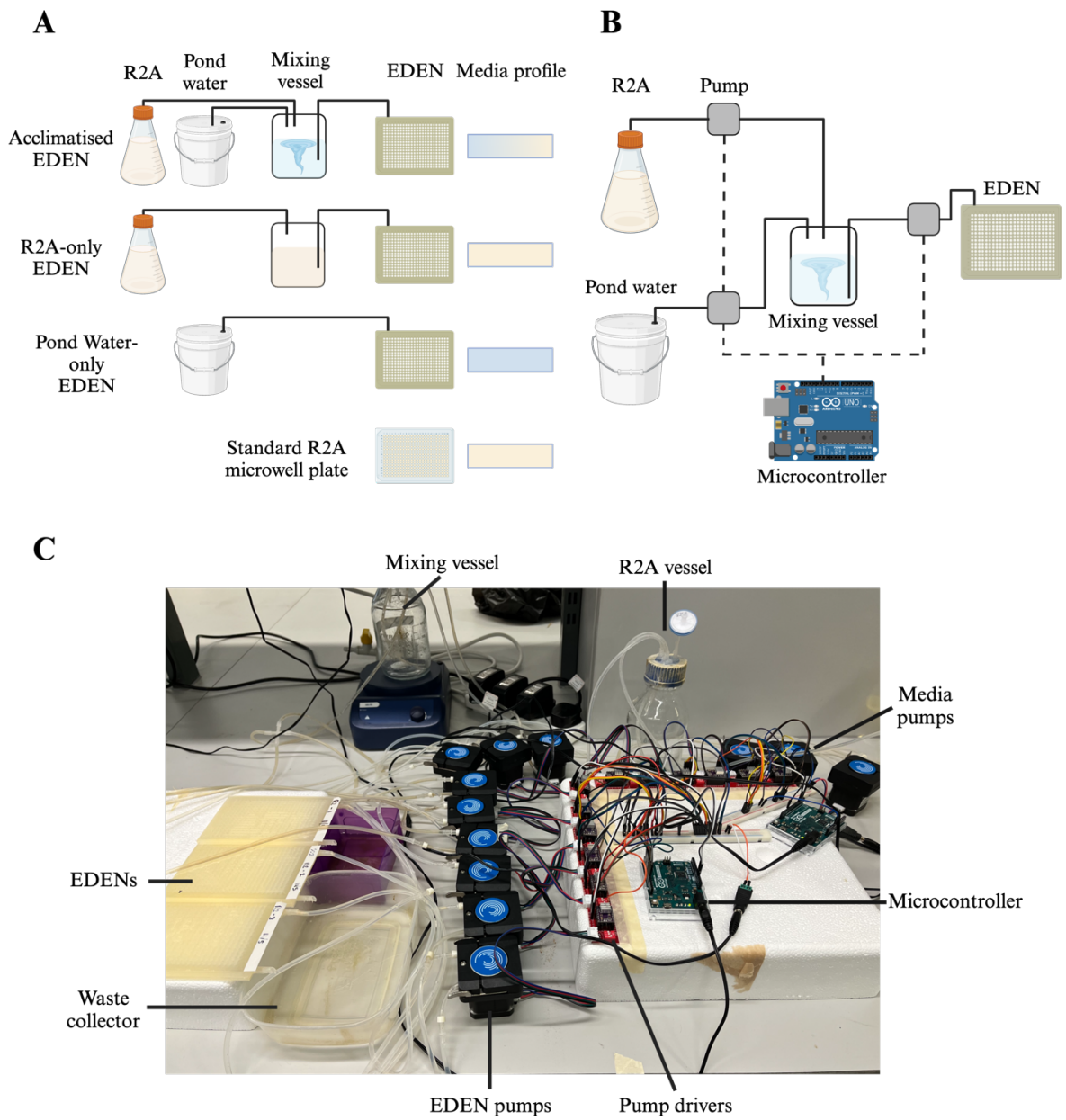

Figure 2.11: Automated EDEN media delivery system and variables.
(**A**) Liquid delivery variable comparison for experimental setup. For acclimatisation, R2A (light brown) and raw pond water (blue) were combined at 4-hour intervals into a mixing vessel before immediate delivery to EDENs. R2A-only EDENs were provided media from stocks indirectly via intermediate vessels to prevent stock spoilage, while pond water-only EDENs were directly pumped with raw pond water. R2A agar plates or microwell plates were used as standard cultivation comparison. (**B**) Diagram of acclimatised EDEN pump system whereby peristaltic pumps deliver media to mixing vessels before immediate delivery to EDENs through an EDEN pump. Pumps were automated by connection (dotted line) to an Arduino microcontroller. (**C**) Picture of automated EDEN liquid delivery system. Media pumps deliver mixture ratios of native and culture media to mixing vessels on magnetic stir plates. Media is then immediately delivered to each EDEN by the EDEN pumps with waste drip-collected in waste containers.

To validate the pump system and ensure nutrients could efficiently diffuse into wells, the pump system was set up using the fluorescent dye fluorescein instead of the nutrient medium, allowing quantification of diffusion within the EDEN reservoir and wells. The measured concentration of fluorescein was consistent with that expected at each timepoint in both the EDEN reservoir and diffused well contents, albeit greater variance was observed in wells, likely due to well volume fluctuation (Figure 2.12A-B). These data validate the automated pump system as well as the diffusibility of EDEN for at least low molecular weight hydrophilic compounds.

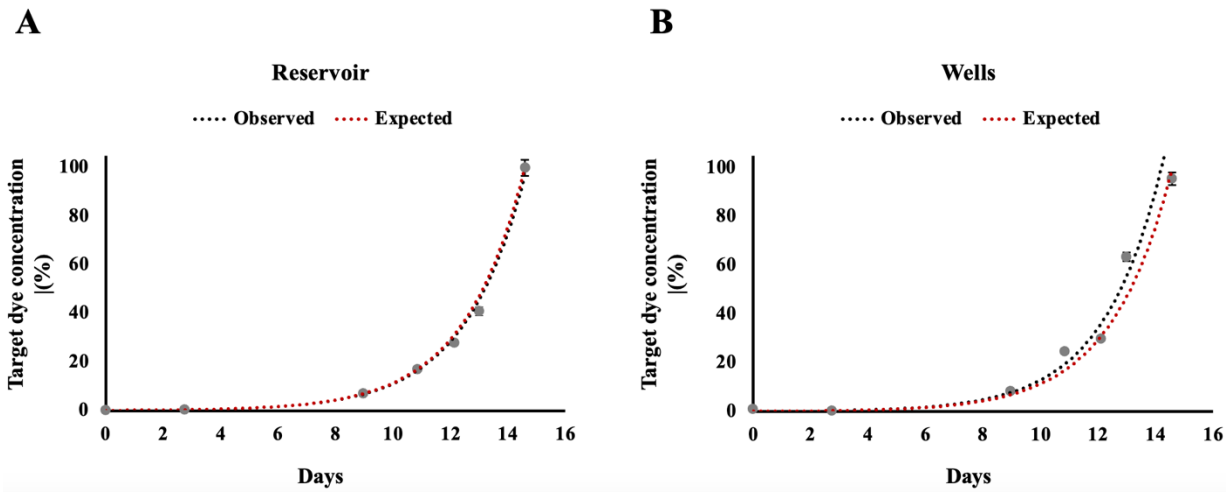

Figure 2.12: Validation of automated media delivery system and diffusibility of EDEN.
The automated media delivery system and diffusibility of EDEN wells were validated with the use of the dye fluorescein in replacement of media. Using a 14-day exponential increase protocol, increases in dye concentration measured were consistent with expected concentrations in both (**A**) EDEN reservoir contents and (**B**) EDEN well contents.

2.3.5 EDEN acclimatisation enhances community cultivation diversity and novelty

To assess the effectiveness of EDEN acclimatisation in enhancing bacterial cultivation, a comparative analysis was conducted on the diversity of acclimatised bacterial communities in contrast to those cultivated using standard R2A agar plate techniques. Here, ~10^5 viable cells of extracted pond water bacteria were inoculated into individual 96-EDEN wells or plate-streaked onto R2A agar petri dishes. Bacteria in EDENs were acclimatised to exponentially increasing amounts of R2A over 28 days. Parallel EDENs were set up and fed R2A or native pond water alone. After incubation, bacteria from EDEN wells or petri dishes were collected for DNA extraction with sequencing of 16S rDNA amplicons on an Illumina MiSeq platform. Five replicate sequencing libraries were obtained for each cultivation method along with the source 20 µm-filtered pond water samples. Significant cell densities were observed from the

wells of R2A-acclimatised and R2A-only EDENs, averaging 1.18×10^8 and 4.41×10^8 CFDA SE+ cells/ml, respectively (Figure 2.13A). No appreciable growth was observed in EDEN communities with only pond water as a nutrient source, with only an average cell density of 8.30×10^5 cells/ml (Figure 2.13A). Consequently, 3 out of 5 pond EDEN samples had failed library preparation due to insufficient cell and DNA concentration and were therefore excluded. Additionally, 1 out of 5 pond source samples had failed library preparation and were excluded.

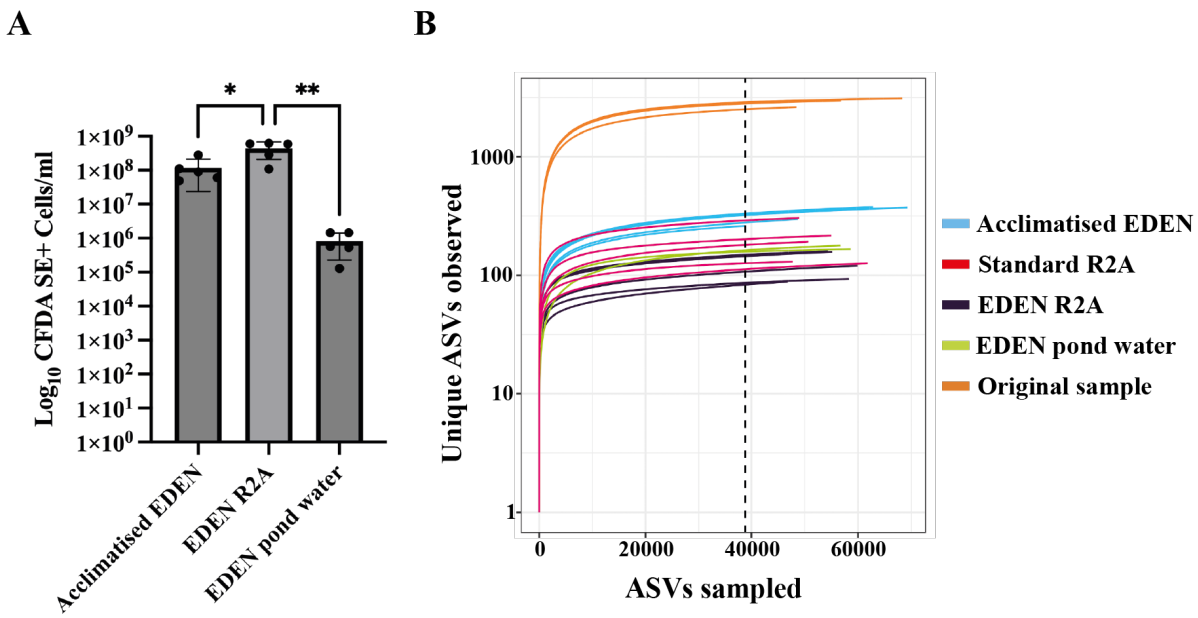

Figure 2.13: Cell densities of EDEN wells and rarefaction curve of samples.
(**A**)After acclimatisation or cultivation, wells from EDENs were harvested with cell densities quantified by CFDA SE fluorescence microscopy. Results of one-way ANOVA and Tukey's multiple comparison test, * = $p < 0.05$, ** = $p < 0.01$. (**B**) Rarefaction curve illustrating the cumulative number of ASVs as a function of sequencing depth with subsampling threshold (dotted line).

The following sequencing analysis was aided in collaboration with Dr Raphaella Jackson, Imperial College London, Faculty of Medicine, Department of Infectious Disease. Sequencing libraries were processed using the nf-core/ampliseq pipeline with high-quality reads inferred into amplicon sequence variants (ASV) (208). ASVs were then assigned to provisional taxa using Silva SINA classification. Samples were rarefied at an equal sequencing depth to prevent bias caused by variable library size (25) (Figure 2.13B). To explore differences in community structures for the different cultivation approaches, an unconstrained ordination was performed using Bray–Curtis distance. Significantly distinct microbial communities were observed (Permanova: $F_{4,16} = 2.30$, $P = 0.001$, Beta-dispersion: $F_{4,16} = 0.33$, $P = 0.85$) (Figure 2.14).

Under pairwise comparison, all conditions were significantly distinct from each other (FDR-adjusted P<0.05), except for the pond water-only EDEN communities, likely attributable to insufficient sample size. These data indicate that each cultivation condition had a significant and reproducible effect on cultivated community composition (Figure 2.14).

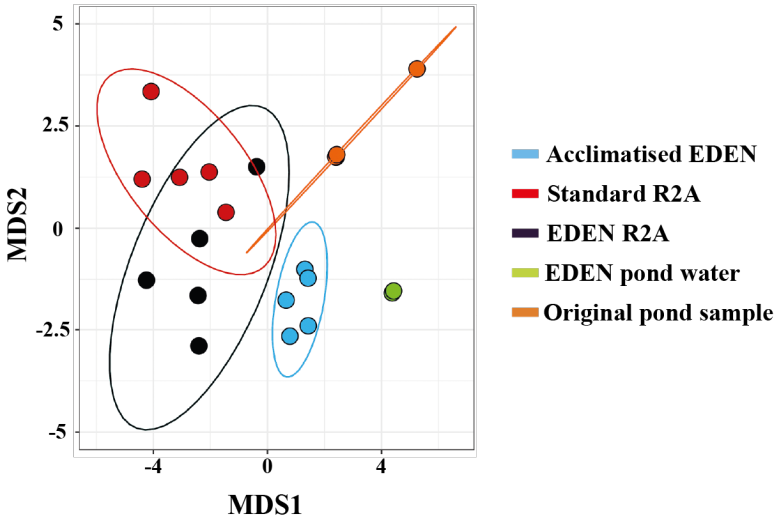

Figure 2.14: MetaNMDS plot of communities cultivated by different cultivation methods. Multi-dimensional analysis demonstrating dissimilarities of cultivated communities and original pond sample source. The stress for the meta-NMDS plot is 0.09. Dots represent different samples, while colours represent different cultivation conditions. Data ellipses represent the clustering of points under a multivariate t-distribution at a 90% confidence interval.

Next, the taxonomic diversity of cultivated communities was compared. ASV diversity within the original pond sediment was dominated by Proteobacteria, Bacteroidota and Acidobacteriota phyla (Figure 2.15A). This proportionality was skewed towards Proteobacteria in cultivated communities, except in acclimatised EDENs that retained greater Acidobacteriota and Desulfobacterota compared to other methods (Figure 2.15A).

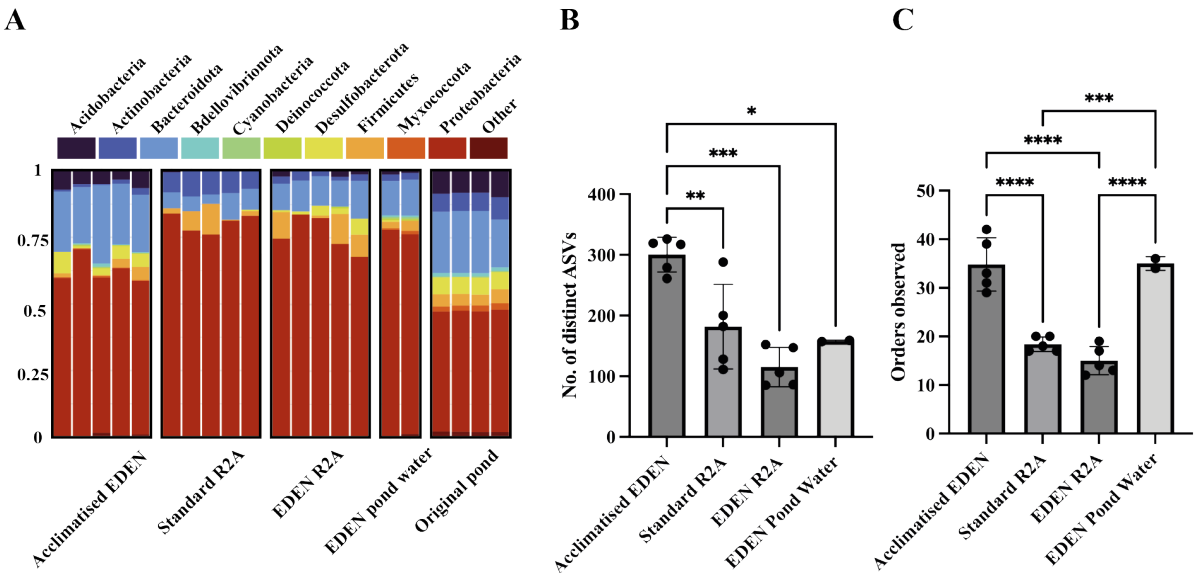

Figure 2.15: EDEN acclimatisation cultivates significantly greater community diversity. (**A**) Relative abundance of ASV phyla in each sample. Each grouped column represents a different cultivation condition nested with individual samples nested within. Different colours represent different proportional ASV phyla observed. Original pond represents undiluted original source material. (**B**) Number of distinct (non-redundant) ASVs and (**C**), number of distinct bacterial orders detected in cultivated communities. Results of one-way ANOVA and Tukey's multiple comparison test. * = $p < 0.05$, ** = $p < 0.01$, *** = $p < 0.001$, **** = $p < 0.0001$.

Acclimatised EDENs provided significantly greater species richness (distinct ASVs) compared to all other cultivation conditions ($P<0.0002$, $F(3, 13) = 14.59$) (Figure 2.15B). Moreover, significantly greater bacterial orders were observed in EDEN acclimatised and pond water-only communities compared to the standard R2A plate streaking and R2A-only EDEN methods ($P<0.0001$, $F(4, 16) = 181.1$) (Figure 2.15C). Investigation of distinct ASVs at the order taxonomic level revealed stark presence/absence differences between acclimatised and standard R2A cultivated communities (Figure 2.16). In addition to broader cultivated diversity, acclimatised EDENs enriched difficult to cultivate taxa within Holophagales and Acidobacteriales (Figure 2.16A) (6). In contrast, standard R2A cultivation displayed greater enrichment of Xanthomondales and Reyranellales (Figure 2.16). All order taxa cultivated with standard R2A cultivation were also found in acclimatised EDENs at least once (Figure 2.16). Comparable results to the standard R2A cultivation were found with R2A-only EDENs (Figure 2.16).

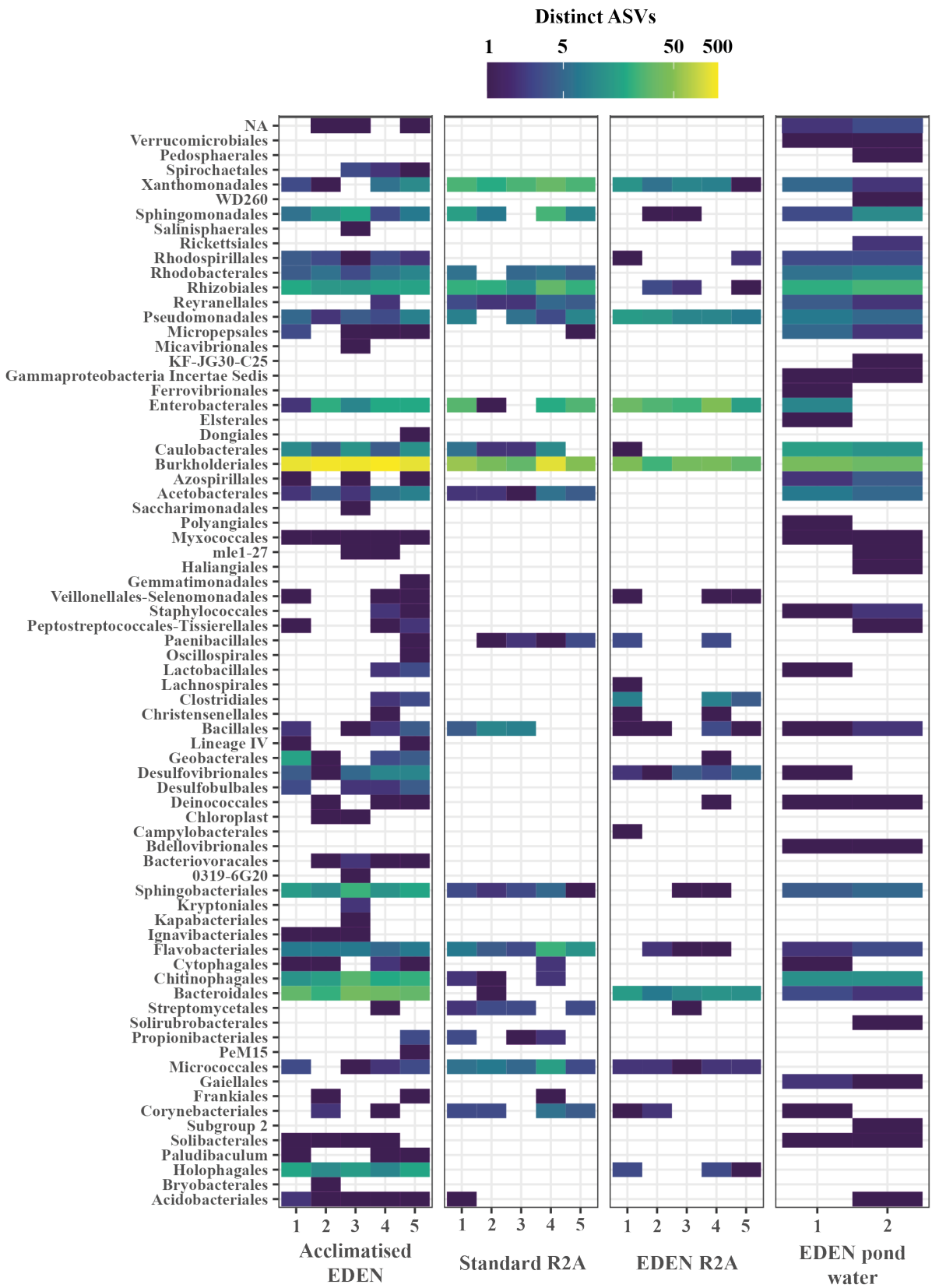

Figure 2.16: Heatmap of order-level bacterial taxonomy of cultivated communities. Distinct ASVs detected in each cultivation condition by bacterial order. Conditions are separated by segmented columns and numbers relate to samples of independent replicates.

2.3.6 EDEN acclimatisation cultivates unique and likely uncultivated taxa

Next, the abundance of ASVs that were uniquely cultivated by each cultivation method was compared. Analysis within an order-level heatmap indicated that EDEN acclimatisation produced the greatest and most diverse abundance of uniquely cultivated ASVs (Figure 2.17A). Most taxa uniquely cultivated in acclimatised EDENs were within the order Burkholderiales (~30% of unique ASVs). An additional high abundance within Holophagales is notable (~9% of unique ASVs). In contrast, fewer taxa were unique to other cultivation conditions (Figure 2.17B). Most unique ASVs within standard R2A cultivated communities were of Xanthomondales (~22% of unique ASVs), while ASVs unique to R2A-only EDENs were mostly within Enterobacterales (~31% of unique ASVs) (Figure 2.17A). These data indicate acclimatisation to R2A facilitates cultivation of greater and more diverse unique taxa.

Having observed greater unique taxa in acclimatised EDENs, the abundance of likely previously uncultivated ASVs was next compared. To improve the validity of such events, distinct ASVs were filtered by appearance in more than one replicate per condition and abundance greater than 100. Likely uncultivated ASVs were then defined as those without genus-level classification, <97% 16S rRNA LCA sequence identity or specifically labelled 'uncultured' in Silva SINA taxonomic classification. Acclimatised EDENs cultivated significantly greater likely uncultivated ASVs compared to the standard R2A cultivation and all other methods ($P<0.0001$, $F(3, 13) = 31.32$) (Figure 2.17C). Overall, these data indicate acclimatisation to R2A cultivates unique communities that are otherwise uncultivable with standard R2A cultivation with immediate media exposure, with greater access to previously uncultivated species.

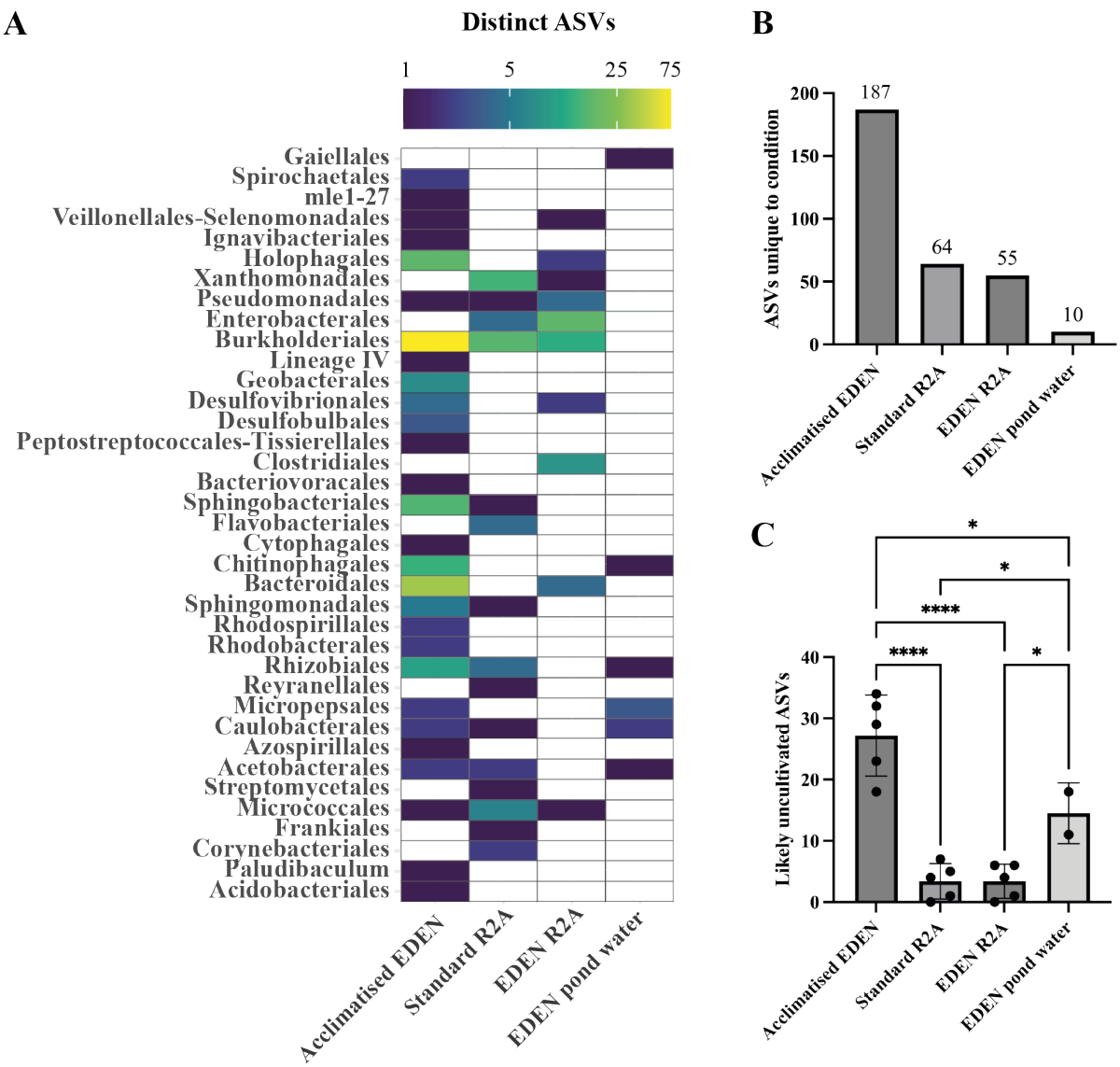

Figure 2.17: EDEN acclimatisation cultivates greater unique and likely uncultivated ASVs. (**A**) Heatmap of bacterial orders and (**B**) bar chart of distinct ASVs that were unique to each cultivation method. (**C**) Number of likely uncultivated ASVs. Results of one-way ANOVA and Tukey's multiple comparison test. * = $p < 0.05$, ** = $p < 0.01$, *** = $p < 0.001$, **** = $p < 0.0001$.

2.3.7 EDEN acclimatisation significantly increases cultivation yield

The relativistic effects on cultivation yield were next compared for each cultivation method at approximately single cell per well concentrations. Here cultivation yield was quantified by presence of microcolonies cultivated in wells with agarose, or PCR products obtained from lysed liquid wells cultures. Using 384-EDENs or standard commercially available plates, bacteria were acclimatised and cultivated as previously. Bacteria acclimatised to R2A in agarose EDENs displayed significantly greater microcolony cultivation yield than the standard R2A agarose cultivation condition (= 0.0248, F (3, 8) = 13.62) (Figure 2.18A). No

improvement in microcolony yield was observed in EDENs with R2A or pond water only (p= 0.0098 and 0.0012, respectively) (Figure 2.18A). Additionally, microcolony growth was not improved by the initial mixture ratio of 0.1% R2A in SFPW (p= <0.0001), indicating the enhancement of cultivation was specific to the EDEN acclimatisation process (Figure 2.18A).

In contrast to agarose cultivation, isolates cultivated in liquid format observed approximately twice the cultivation rate by detection of PCR amplicons from well lysates (Figure 2.18B). However, differences between cultivation conditions were not significant (P=0.5311, F (3, 8) = 0.7932), likely influenced by large variance in replicates (Figure 2.18B). The limit of detection of the PCR protocol was found to be ~100 CFU cells/µl, respectively for *B. subtilis* and *P. putida*. No PCR products were obtained from uninoculated wells, R2A medium or SFPW alone.

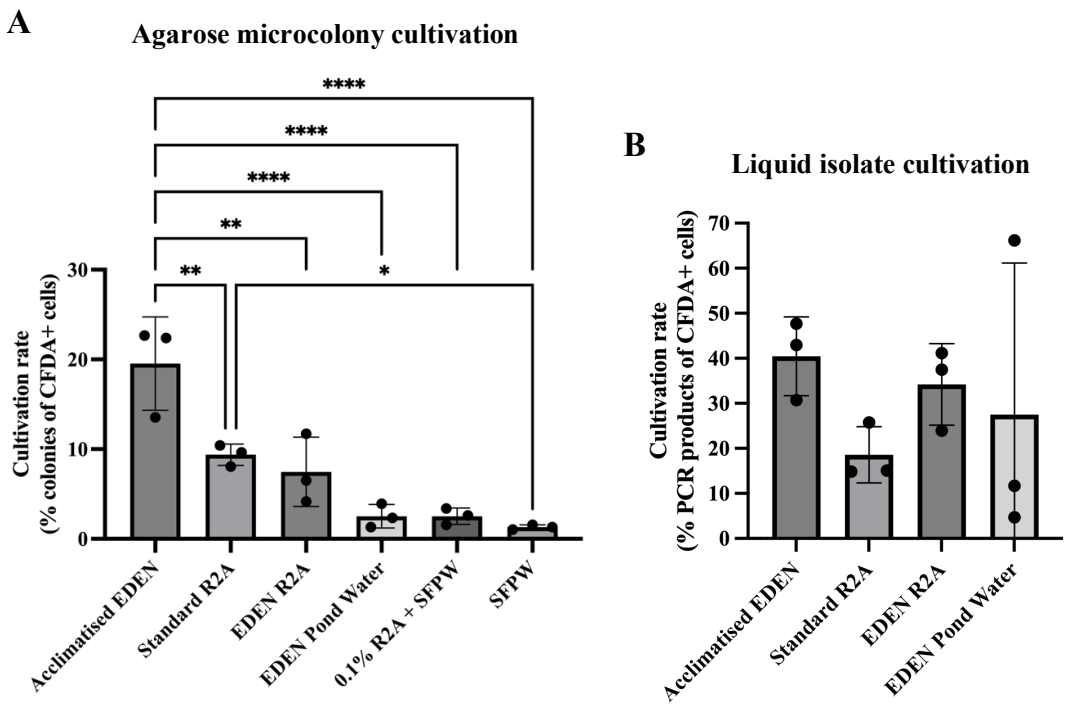

Figure 2.18: Acclimatisation to R2A with EDEN enhances microcolony cultivation probability. (**A**) Extracted pond water microorganisms were quantified using CFDA SE fluorescence microscopy before diluting into LMPA agarose to achieve approximately single cell per well concentration. Cultivated microcolonies were quantified by light microscopy after 28 days acclimatisation and cultivation. (**B**) Cultivation with same concentration of cells but within liquid wells. Bacterial isolate growth was detected with presence of PCR amplicons from lysed wells. Results of one-way ANOVA and Tukey's multiple comparison test with only significant differences shown, * = p < 0.05, ** = p < 0.01, *** = p < 0.001, **** = p < 0.0001.

2.3.8 EDEN acclimatisation enhances isolate cultivation diversity and novelty

Having observed significantly greater community cultivation diversity and colony yield with EDEN acclimatisation, the effects of each cultivation method were next compared with examination of the liquid-cultivated isolates by cell lysis and direct 16S rDNA PCR. 50% of detected PCR products for each condition were attempted for Sanger sequencing and assignment of provisional taxa using Silva SINA classification.

Isolates cultivated by EDEN acclimatisation yielded greater order taxonomic diversity as well as greater unclassified and novel taxa compared to all other cultivation methods (Figure 2.19A-E). Furthermore, notoriously difficult to cultivate taxa from Verrucomicrobiales, Opitutales, Kryptoniales and Gemmatimonadales were uniquely detected from acclimatised EDENs (Figure 2.19A). Additionally noteworthy is the enrichment of Sphingomonadales, previously reported to be susceptible to nutrient shock by R2A (192) (Figure 2.19A). Although exhibiting the lowest cultivation rate, the pond water EDENs exhibited the lowest average 16S rDNA % identity to reference LCAs (Figure 2.19B).

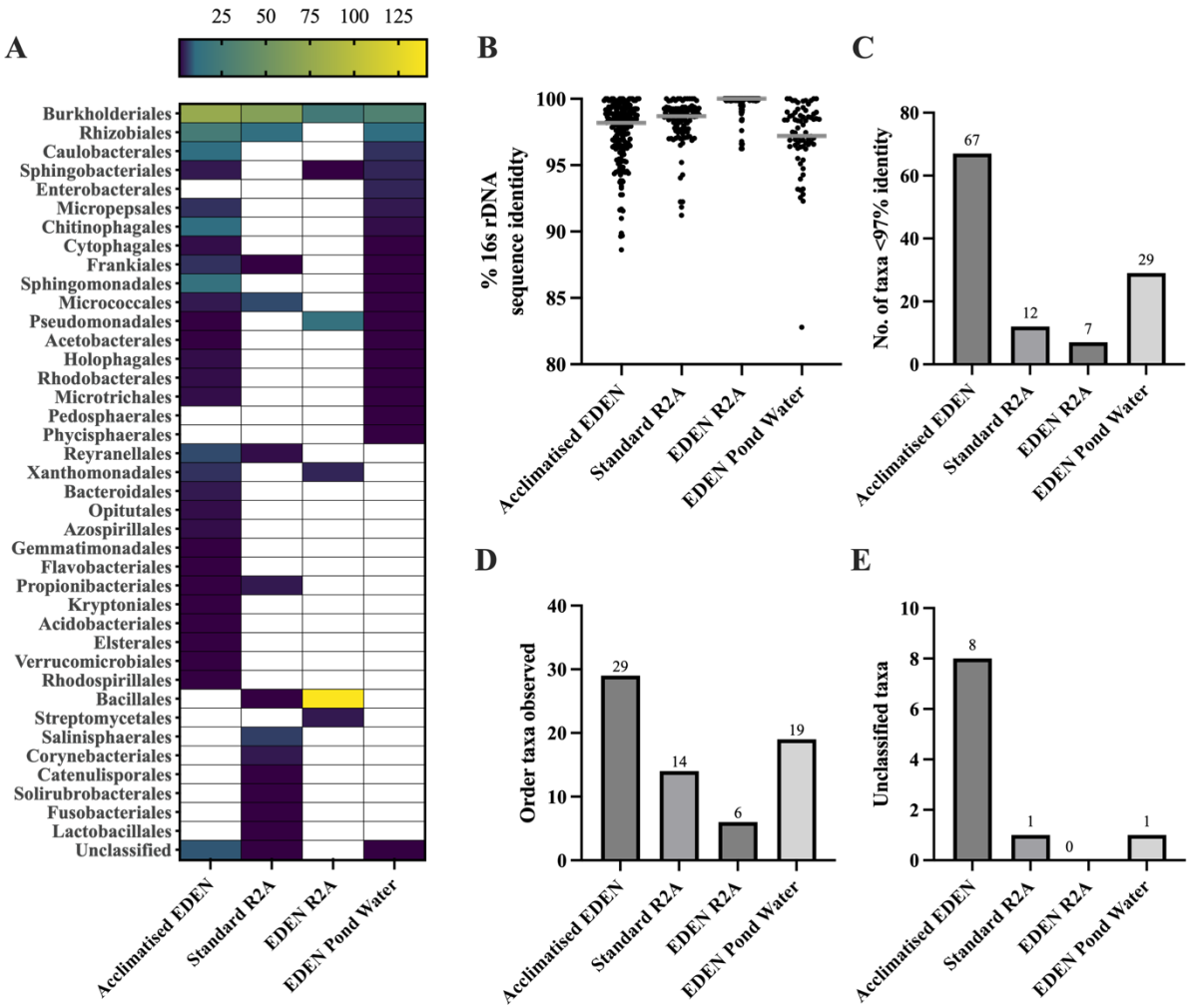

Figure 2.19: EDEN acclimatisation enhances greater diversity and likely uncultivated isolates. (**A**) Heatmap of cultivated isolates at the bacterial order taxonomic level. (**B**) Scatter plot of isolate percentage identity to Silva reference LCA. Mean is shown in grey bar. (**C**) Number of isolate taxa that are likely uncultivated (<97% 16S rRNA sequence identity to Silva reference LCA). (**D**) Total distinct orders observed in cultivated isolates. (**E**) Number of isolates without known identity in Silva database. Results of 50% of cultivated isolates in 1152 wells per cultivation condition.

2.3.9 Antimicrobial activity of acclimatised bacteria

Taking advantage of the greater diversity available from EDEN acclimatisation, colonies obtained from acclimatised EDENs were replicated in the centre of individual R2A plates for detection of antimicrobial compounds through reporter overlay assays (Figure 2.20). Isolate screening assays were aided by the help of Caitlin McShane. Of 400 isolates, 12 exhibited antimicrobial activity against *B. subtilis* (Table 2.1) (Figure 2.20). Of these, 7 displayed additional activities against MRSA. No activity was detected against *E. coli* (Figure 2.20). Colony 16S rDNA PCR and Silva SINA classification identified the MRSA-inhibiting isolates to be closely related novel taxa within the genus *Rhodobacter*, alongside a likely non-novel

isolate of *Variovorax* (Table 2.1). Additionally, an isolate of *Pseudomonas* exhibited inhibition of *B. subtilis* as well as the fungus *A. niger* (Table 2.1).

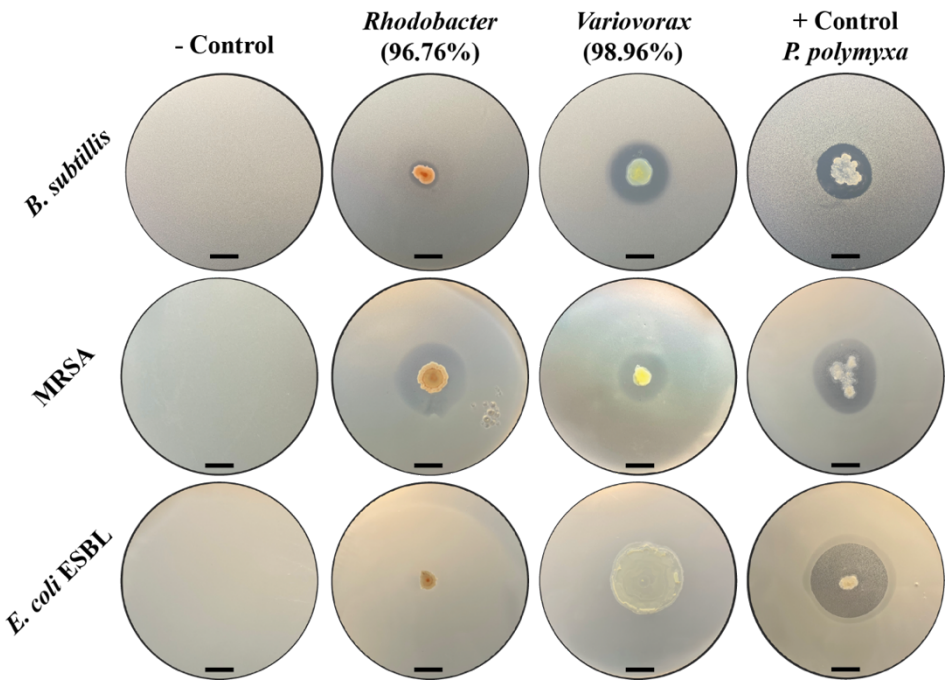

Figure 2.20: Microbial inhibition assay for detection of antimicrobial compounds from EDEN isolates.
Example of acclimatised EDEN hit isolates displaying antimicrobial activity. Isolates are spotted in the centre of agar petri dishes and allowed to cultivate before overlay with reporter cells of *B. subtilis* or drug-resistant pathogens MRSA and *E. coli* ESBL. A likely novel isolate *Rhodobacter* (isolate B2_95), alongside an isolate of *Variovorax* (B1_120) displayed inhibition against *B. subtilis* and drug-resistant pathogen MRSA. No comparable inhibition was observed against *E. coli* ESBL. Positive controls were performed with the known polymyxin producer *P. polymyxa*. Percentage 16S rRNA identity to Silva SINA LCA is shown in brackets. Scale bar 1 cm.

EDEN Hit Isolate	Silva LCA Genus	16S rRNA ID to LCA	*B. subtilis*	MRSA	*E. coli* ESBL	*A. niger*
B1_107	*Variovorax*	98.82 %	12 mm	X	X	X
B1_61	*Variovorax*	99.50 %	1 mm	X	X	X
B2_6	*Pseudomonas*	99.30 %	3 mm	X	X	10 mm
B2_91	*Rhodobacter*	96.07 %	1 mm	1 mm	X	X
B2_96	*Rhodobacter*	96.37 %	7 mm	6 mm	X	X
B2_95	*Rhodobacter*	96.76 %	2 mm	6 mm	X	X
B2_70	*Rhodobacter*	95.95 %	1 mm	6 mm	X	X
B2_71	*Rhodobacter*	95.99 %	1 mm	X	X	X
B2_30	*Burkholderia-Caballeronia-Paraburkholderia*	99.61 %	10 mm	X	X	X
B1_120	*Variovorax*	98.96 %	6 mm	3 mm	X	X
B2_68	*Rhodobacter*	96.37 %	1 mm	1 mm	X	X
B2_74	*Rhodobacter*	95.68 %	4 mm	X	X	X
B2_92	*Rhodobacter*	96.00 %	2 mm	1 mm	X	X

Table 2.1: Silva classification and antimicrobial activity of EDEN acclimatised isolates. Isolates obtained from acclimatised EDENs were cultivated on individual agar petri dishes for detection of antimicrobial activity via an agar inhibition overlay assay with *B. subtilis* and pathogens MRSA, *E. coli* ESBL or fungus *A. niger*. The size of the zone of inhibition is shown in mm for each tested reporter cell type. The percentage identity (ID) of 16S rRNA sequences to Silva classification LCA genus is shown. Results of 400 isolates.

2.4 Discussion

2.4.1 Cultivability of pond water bacteria

Cultivation of environmental bacteria remains a fundamental yet bottlenecked microbiological procedure. Here, it was hypothesised the efficiency of bacterial cultivation could be enhanced by gradual transition to culture medium such as R2A. The effects of media composition and acclimatisation were compared on the cultivation of pond water bacteria.

Initial investigations into the cultivability of pond water bacteria, using the conventional R2A cultivation media, revealed ~25% of CFDA SE-viable cells yielded microcolonies after 28 days incubation (Figure 2.3). This cultivability of bacteria with R2A contradicts the narrative of "less than one percent of bacteria are cultivable" commonly recited in review or research article sources (14,15,50,203,218). The cited source is that of Staley &

Konopka, 1985, indeed that quote – "*Only approximately 0. 1-1 .0% of the total bacteria can be enumerated by the plating procedure. Indeed, as a general rule we have found that the maximum recovery of heterotrophic bacteria is 1% of the total direct count using plating procedures or other viable enumeration methods from a variety of oligotrophic to mesotrophic aquatic habitats*" utilising a medium similar in composition to R2A (5). However, as directly follows in the source – "*whereas, higher recoveries (approaching 80-90%) can be achieved from eutrophic habitats*" (5). Thus, as described in the aforementioned and reaffirmed by others, cultivation yield or recovery of bacteria varies considerably on the source environment, cultivation conditions and quantification methods employed, and such a statement has been recommended to be retired (5,8,9,219,220). Nonetheless, it is clear standard cultivation methods remain inadequate for cultivating most environmental cells, and that the high variability of environments indicates there is unlikely a universal method for cultivating all species (19).

It is noteworthy to highlight increases of cultivation alongside mixing R2A with pond water filtrates (SFPW), compared to using either alone (Figure 2.3). Such results may reflect the nutritional deficiency of native pond media, while absence of potential essential native growth factors within the R2A cultivation medium. However, any approach utilising native media is impractical due to a lack of control in formulation and seasonal variability. Thus, microorganisms should be adapted or acclimatised to a standardised culture media if possible.

The observed cultivation of microcolonies under extreme oligotrophy (≤0.1% R2A concentration) is additionally noteworthy (Figure 2.3). Similar nutrient concentrations have previously been shown to cultivate oligotrophs such as the previously uncultivated Pelagibacterales (SAR11 clade) (7). Additionally, dilution of R2A to 10% and 1% concentration has been shown to favour different taxa cultivation in a similar quantitation, with examples of obligatory oligotrophic growth for taxa such as *Actinoplanes* (221). However, microcolonies cultivated (average 3/384 wells) at concentrations <1000x diluted medium, without light sources for photosynthesis, is unexpected (Figure 2.3). In this condition, trace amounts of R2A would be introduced alongside bacteria inoculation into the pure H_2O-agarose solution at ~0.01% media final concentration. However, such isolates could additionally be metabolising the agarose hydrogel as a nutrient source, or capable of alternative autotrophic metabolism (90).

Although ultramicrobacteria <0.1 μm^3 are known to occupy freshwater environments, we did not detect microbial growth in 10 ml preparations of 0.1 µm-filtered SFPW media on solid agar, inside solid agarose, or in liquid culture (193,222). There was furthermore no

detection of viable cells under CFDA fluorescence microscopy or PCR products from uninoculated controls.

2.4.2 EDEN fabrication

By use of the 3D print-pause-print technique, EDENs can be fabricated as a single object thus avoiding laborious assembly steps or use of toxic adhesives (121,187) (Figure 2.9). Such adhesives, particularly silicone-based, were previously utilised for adhering diffusible membranes to similar cultivation devices (15,46,216). Although generally accepted as biocompatible once cured and available in applications for medical devices, solvents within partially cured adhesives may leach and negatively affect cell growth (Figure 2.10A). The Nature Protocols article for the assembly of the iChip recommends at least 30 minutes cure time or "until the smell of glue is no longer detectable" (216). Although curing time varies with manufacturer, it was found here using similar adhesives even after 24 hours cure time, it was unlikely to be biocompatible in direct exposure (Figure 2.10A). Moreover, the adhesive strength to PC was clearly inadequate. Thus, the method to fabricate EDENs proved highly advantageous alongside adhesive-free heat bonding of the polycarbonate membrane to the PLA plastic. It is further noteworthy that although the PLA utilised here had non-significant effects on bacterial cultivation, the large standard deviation of the pond community in PLA growth wells and EDEN wells compared to standard plates indicates that some species may be differently affected (Figure 2.10A & 2.16). Thus, although PLA provided the greatest print fidelity, alternative materials should be explored that have greater chemical resistance or biocompatibility. The use of proprietary 3D printing materials has disadvantages in that exact compositions are unknown.

Further improvements for 3D printing of EDEN devices could be made using VPP printer approaches instead of FFF used here, providing greater resolution and smoothness of wells, faster printing time, and more reliable water-tight bonding (138,183). Challenges, however, would be met in integrating PC membranes without degradation by UV light and optimisation of post-curing steps to remove toxic unpolymerised components (174,176). However, the fabrication of similar devices has recently been demonstrated with multi-material 3D printing of porous PEG-DA layers that could replace UV-sensitive and expensive PC membranes used here (181). Further optimisations could be made in simplifying the automated pump system, where an array of solenoid valves could be used to direct flow to individual EDENs instead of peristaltic pumps used here.

Additional challenges encountered in EDEN optimisation were stability in liquid levels within wells. Fluctuations or pressure differentials across the membrane would cause flooding or drainage of liquid, particularly if tubing were connected to the outlet and held below or above the EDEN. Such fluctuations were mitigated by pumping media discontinuously in 10 ml volumes, as well as leaving EDEN outlets without connected tubing. Additional work should explore non-3D printed microfluidic devices that would be miniaturised, have greater throughput, and ensure stability of well liquids.

2.4.3 Effectiveness of R2A acclimatisation on bacterial community cultivation

The effectiveness of R2A acclimatisation on bacterial cultivation was compared and analysed in three EDEN formats. These were community cultivations analysed by Illumina 16S rRNA sequencing, microcolony cultivations quantified by light microscopy and isolate cultivation analysed by 16S rRNA Sanger sequencing (Figure 2.1).

In community cultivations, acclimatisation of bacteria to R2A resulted in distinct cultivated bacterial communities. Analysis through NDMS highlighted significant differences between cultivation conditions that were further reflected in unique taxonomic profiles in the heat maps (Figure 2.14-16). Although proportional differences in taxonomy were explored, the use of 16S rRNA Illumina sequencing is unlikely to accurately reflect direct cell counts (Figure 2.15). This is due to significant distortion arising from primer bias, strain 16S rRNA copy number and intra-genomic heterogeneities (223,224). Diversity metrics that incorporate proportionality, such as Shannon and Simpson indices, would be similarly unreliable. Future analysis should include quantification standards or microbial spikes of a known concentration, that could be added to aid analysis in proportional differences in communities (225). Thus, the analysis here focused on presence/absence relationships as opposed to proportional relationships.

Acclimatised communities observed significantly greater distinct ASVs and bacterial orders compared to the standard R2A and EDEN R2A-only methods (Figure 2.15-17). Interestingly, all bacterial orders cultivated with standard R2A were also found in acclimatised EDENs, with few ASVs found unique to standard R2A cultivation (Figure 2.16). This indicates the acclimatisation process does not negatively impact the majority of cultivable taxa. ASVs that particularly benefited from the acclimatisation process were within the order Burkholderiales and Holophagales. The former is notable due to having significant applications in bioremediation, biopesticidal and antimicrobial drug discovery (226–228). Thus, the

cultivation of novel Burkholderiales species could be particularly advantageous for combating antimicrobial resistant pathogens (226,227). Enrichment of Holophagales is additionally noteworthy due to their underrepresentation in standard cultivation efforts (6). Thus, the EDEN acclimatisation process may enrich difficult-to-cultivate taxa with biotechnological importance that otherwise are recalcitrant to standard cultivation methods. Further evidence is demonstrated by the significant increases of taxa without similarity to cultivated representatives (LCA), indicating acclimatisation enhances the cultivation of previously uncultivated bacteria (Figure 2.17).

It is acknowledged that the low sample size limits the reliability of the analysis. Future work should incorporate a larger sample size to improve statistical rigour. Techniques such as shotgun metagenomics should be explored for analysing effects on all microbial communities including fungi and archaea. Additionally, potential primer bias in library PCR amplification may be mitigated with greater species-level resolution (229).

2.4.4 Effectiveness of R2A acclimatisation on bacterial microcolony cultivation

Acclimatisation significantly increased microcolony cultivation probability compared to the standard R2A microwell plate cultivation method (Figure 2.18A). Similar to results from community cultivations, EDENs continuously pumped with R2A or pond water alone did not show such improvement and thus effects are unlikely attributable solely to the EDEN device (Figure 2.18A). Native media were again found to be an inferior media choice for cultivation (Figure 2.18A). This contrasts with previous reports utilising similar diffusion chamber setups with native media (14,15,48,216). However, it is acknowledged that different native media may yield different results, including if cultivation is performed *in situ* instead from a collected bucket. For example, in comparable conditions, cultivation yield was lower during the colder March experiments compared to those conducted in September, which could reflect seasonal variabilities and temperature influences (15). This is illustrated in the ~2-fold difference in R2A cultivability between the preliminary and EDEN experiments (Figure 2.3 and 2.18, respectively).

Unlike 16S rRNA sequencing analysis, the observance of microcolony cultivation was not biased by primer selection or 16S rRNA copy number. However, attempts to sub-culture microcolonies onto larger agar petri dishes were hindered by difficulties in liberating them from agar plugs. Future work could investigate methods to liberate and re-streak microcolonies,

such as the use of the enzyme agarase. Future work should also investigate the sub-cultivability of the acclimatised colonies on R2A media and to validate independent growth adaptation.

2.4.5 Effectiveness of R2A acclimatisation on bacterial isolate cultivation

In addition to the community and microcolony cultivation experiments, the effects of media acclimatisation were examined on the diversity of cultivated isolates (Figure 2.19). This format has the advantage in that competition from neighbouring species is mitigated, akin to the dilution to extinction cultivation technique (7,22). The limit of detection for the PCR protocol from well lysates was ~ 100 cells/µl, or ~500 cells/µl in EDEN wells. Thus, positive PCR products would be indicative of significant cell proliferation, as the starting inoculum cell concentration was 1.0×10^4-fold below the limit of PCR detection. However, compared to the counts of microcolonies, liquid culture growth yields were generally higher (i.e. ~40% for liquid cultivation instead of ~25% for acclimatised EDENs) but non-significant likely due to greater variance among replicates (Figure 2.18B). Such variance could be explained by contamination in some EDENs; for example, in the R2A EDENs there were abnormally high reads of *Bacillus* compared to other EDEN conditions (Figure 2.19A). Nonetheless, there remained sufficient reproducibility of EDEN diversity among replicates. Due to the lack of sample size, a diversity comparison of the 3 independent cultivation runs was pooled for a single analysis. Greater sample sizes and replicates would provide sufficient data for a robust statistical analysis.

Proportional to growth in wells, the EDEN-acclimatised isolates yielded the greatest bacterial order coverage and number of likely novel and unclassifiable isolates (Figure 2.19C-E). Furthermore, isolates belonging to difficult to cultivate taxa were uniquely detected including Verrucomicrobiales, Opitutales, Kryptoniales and Gemmatimonadales (6,230) (Figure 2.19A). Although detected as singletons, their unique presence from acclimatised EDENs may indicate acclimatisation may enhance cultivation of these taxa. The NCBI taxonomy database lists only 6 non-candidatus species within the phylum Gemmatimonadota, 5 of which are within the class Gemmatimonadales, despite comprising ~1% of soil and aquatic bacteria worldwide (231). One of the validly published Gemmatimonadota species, *Longimicrobium terrae*, was isolated via an *in situ* cultivation diffusion chamber technique with reported oligotrophic nature (232). Additionally enriched in acclimatised EDENs were isolates of Sphingomonadales previously reported to be susceptible to nutrient shock by R2A (192) (Figure 2.19A). The EDEN acclimatisation method may therefore provide appropriate

conditions for these cultivation-recalcitrant taxa. However, future work should also investigate the sub-cultivability of isolates outside of EDENs to fully appreciate the effectiveness of media acclimatisation.

2.4.6 Potential mechanisms for enhanced cultivability with EDEN acclimatisation

Although few to date have investigated the effects of media acclimatisation on the cultivation of microorganisms, several non-exclusive mechanisms can be hypothesised to describe the enhanced cultivability of bacteria alongside media acclimatisation:

1) Increased mutational adaptation through incremental exposure and directed evolution (233).

This hypothesis features a greater literature background due to relevant phenomena within the facilitation of antibiotic resistance and selective laboratory evolution (233). For example, spatiotemporal gradients of trimethoprim or ciprofloxacin have been shown to facilitate resistance of *E. coli* up to 3000x MIC (204). Additionally in *E. coli*-rifampicin resistance models, gradual antibiotic introduction gives rise to greater mutational diversity, growth rate and survival compared to ancestorial strains once challenged with high antibiotic concentration (234). In this mechanism, gradual antibiotic exposure allows accumulation of greater but individually less effective mutations that concert a highly resistant phenotype that otherwise would be improbable to emerge during an instantaneous high exposure (235,236). Additional instances are observed outside of antibiotic resistance models. Abrupt changes of atmospheric CO_2 have been shown to significantly decrease plant mycorrhizal fungi species richness compared to those gradually adapted (237). Mutational adaptation of wild-type strains to laboratory media is furthermore well documented (238). Although plausible, these examples alone may be unlikely to explain the improvements in cultivation seen here with media acclimatisation. Firstly, the aforementioned share a methodological commonality in that populations are serially transferred to new vessels or continuously siphoned in a chemostat with acclimatisation (235–237). This is not comparable to the EDEN device that maintains a closed system. Additionally, selection of beneficial mutants from a high-density cell population would not explain the results of the single-cell EDEN experiments and cultivation yields shown here (Figure 2.18-19) (204,234,236).

2) Awakening from dormancy or VBNC state (239–241).

Dormancy and VBNC states are widely used by prokaryotes and eukaryotes to facilitate survival under unfavourable environmental conditions (241). While both dormant and VBNC

cells share a recalcitrance for cultivation on laboratory media, dormant cells are characterised by low or undetectable metabolic activity whereas VBNC cells retain metabolic activity (239). Mechanisms for recusation or awakening from such states remain unclear but may include signalling molecules, removal of stress variables, secreted enzymes, temperature, presence of nutrient or stochastic events (239,242–245). Therefore, it can be hypothesised the gradual introduction of nutrients may induce resuscitation from starvation or dormant states in EDEN acclimatised bacteria, potentially from signalling molecules produced from reservoir native bacteria that would not be present in the R2A or pond water-only conditions tested. Further research could elucidate the dependency on native bacteria for resuscitation by attempting acclimatisation with cell-free native pond water in reservoirs.

3) Facilitating transcriptional and metabolic adaptation to alternative media.

Microorganisms respond to changing environmental stimuli by regulating gene expression and metabolism (246). Such changes alter metabolic pathways, allowing alternative nutrient acquisition, execution of stress response pathways, and adaptive phenotypes. However, the time taken to alter gene expression and physiology in response to stimuli could range from minutes to hours. This is furthermore concerning well-studied fast-growing species such as *B. subtilis* or *E. coli* that may differ in kinetics from quiescent environmental species. For example, in osmotic shock of *B. subtilis* to NaCl (6% w/v, ~1 M), mRNA transcripts alternate within 30-60 minutes of exposure, whereas changes in effector proteins were significantly slower and likely take over 120 minutes (247). Thus, it can be hypothesised gradual transition to culture media may provide sufficient time for an effective gene regulatory response, thereby increasing the probability of survival. An overlapping but less well described phenomenon is nutrient shock, whereby nutrient-starved cells receive accelerated death once exposed to relatively high carbon nutrients such as 10 mM glycerol (248). Such accelerated death was furthermore prevented by the oxidative phosphorylation uncoupler 2,4-dinitrophenol and therefore could be indicative of 'metabolic overload', although the exact mechanism has yet to be described (248). Future work could investigate potential metabolic and transcriptomic responses of acclimatised cells to cultivation media and avoidance of nutrient shock (22,192,247,248).

2.4.7 Methodological utility in natural product discovery

Uncultivated bacteria offer a rich source of untapped biosynthetic potential including antimicrobials (13,47,61). The utility of the EDEN cultivation platform was demonstrated with

the cultivation of likely novel species exhibiting antimicrobial activity against MRSA and *B. subtilis* (Figure 2.20). Although not directly compared with antimicrobial screening using standard R2A cultivation, the significantly greater novel and diverse species cultivated through EDEN acclimatisation may increase the probability of discovering novel compounds of interest (13,61). Furthermore, the EDEN microwell format provides compatibility with high-throughput screening assays (37). Future work will investigate the producer isolates and compounds of interest, starting with full-genome sequencing to obtain a better taxonomic assignment and bioinformatic interrogation of the genome for putative BGCs using tools such as AntiSmash (249). Furthermore, subjecting the isolates to diverse culture conditions and/or elicitors should be performed to maximise the detection of antimicrobial activity through the stimulation of cryptic or quiescent BGCs of interest (227). Repurposing of EDEN for stimulation of antibiotic production (for example by delivery of an eliciting agent such as sub-MIC antibiotics) could be conveniently implemented after the acclimatisation and cultivation process in a single EDEN (226,227).

2.4.8 Conclusion

In conclusion, this chapter provided new insights into the effects of media composition and acclimatisation on the cultivability of pond water bacteria. By use of the novel EDEN cultivation device, acclimatisation to R2A media was found to enhance diversity in community cultivations, microcolony cultivation probability and yield a broader spectrum of isolates, including those from difficult-to-cultivate taxa. Moreover, the utility of the EDEN platform in enhancing antimicrobial discovery was demonstrated alongside the cultivation of likely novel taxa exhibiting antimicrobial activity against MRSA. Further work may optimise EDEN performance and elucidate possible mechanisms for enhanced cultivability of bacteria. The findings propose a novel cultivation strategy for unlocking the untapped biosynthetic potential of environmental bacteria.

Chapter 3. Encapsulation of Environmental Bacteria for Contained *In Situ* Cultivation

3.1 Introduction

3.1.1 Challenges of a microfluidic approach for *in situ* cultivation of environmental bacteria

In situ cultivation entails the isolation and incubation of bacteria within their native environment utilising diffusible membrane chambers (11,13,46). Placement of cells within such chambers permits the diffusion of native nutrients and growth factors while restricting cell migration. Several device formats have been implemented for *in situ* cultivation, including the iChip, hollow-fiber membrane chambers, as well as 3D-printed devices (48,49,154,185,216). *In situ* cultivation formats, however, remain imitated in throughput and compatibility for downstream cultivation or analytical techniques. Microfluidic cell encapsulation has proven to be a promising solution, potentially providing magnitudes greater throughput (10 - >5000 Hz) while simultaneously facilitating diffusion between neighbouring cells and external environments (49,66). Although attempts have been made to combine *in situ* cultivation with microfluidics, the full requirements of such a method have not yet been fulfilled, including (49,50,56):

1) Biocompatible encapsulation within a capsule capable of containing but not restricting cell proliferation.
2) Efficient diffusion of environmental nutrients or growth factors.
3) Efficient cell decapsulation and recovery of cultivated cells from capsules.

Concurrently with experiments of this chapter, others had attempted microencapsulation of bacteria for cultivation *in situ* of native environments within commercially available Slide-A-Lyzer cassettes or custom diffusion chambers termed microbial domestication pods (MD) (49,50). It was found that the agarose microbeads were unable to prevent cell outgrowth into the surrounding medium. The authors additionally limited the duration of *in situ* incubation to 7 days, less than the recommended 14-21 days thus potentially limiting the efficacy of the method for slow-growing bacteria (49,50,53). Therefore, the development of a cell encapsulation method capable of containing cell growth for a longer *in situ* cultivation time may increase the effectiveness of the method.

3.1.2 Chapter aims and objectives

This project aimed to develop a high-throughput method for encapsulation and *in situ* cultivation of previously uncultivated bacteria. Such a method could provide unprecedented access to new microbial species and thus increase likelihood of discovering novel natural products such as antibiotics. Significant challenges remain in developing a cell encapsulation and *in situ* cultivation method offering cell biocompatibility, containment, and efficient diffusion of natural growth factors while retaining throughput and recovery of cultivated cells. Specific objectives were to:

- Develop a cell encapsulation technique capable of containing bacterial growth for the period of *in situ* cultivation.
- Develop a diffusible chamber for *in situ* incubation and cultivation of encapsulated bacteria.
- Compare the efficiency of cultivation methods by colony recovery and 16S rRNA sequence identification.

3.2 Materials and methods

3.2.1 Cells and media

Unless specified, all reagents were purchased from Sigma-Aldrich, UK. R2A media was used to cultivate all strains and environmental cells prepared as previously described (21). *B. subtilis* 168 was kindly donated by Josef Altenbuchner, University of Stuttgart, Germany. *E. coli* K-12 was purchased from ATCC (ATCC 10798). *Streptomyces coelicolor* A3(2) was kindly donated from the John Innes centre, Norwich, UK. Environmental cells were sourced from pond water sediment samples 10 cm below water surfaces collected at Silwood Lake, Ascot, UK (51°24'49.6"N 0°38'53.9"W).

3.2.2 Modification of *B. subtilis* for constitutive sfGFP expression

To generate GFP-fluorescent *B. subtilis*, the sequence of an optimised constitutive superfolder GFP (sfGFP) construct, designed by Guiziou et al., was synthesised (Twist Biosciences) and inserted into the pBS3C backbone by isothermal assembly (250). For transformation and chromosomal integration, the "Paris method" was employed using Spizizen's minimal medium as previously described (251).

3.2.3 PDMS chip microfluidic encapsulation and cultivation of bacteria

An overnight culture of *B. subtilis* sfGFP grown in R2A at 30 ˚C. Cells were diluted to single cell concentrations in R2A with 1% ultra-low melting point agarose (LPMA) (ThermoFisher) maintained at 37 ˚C. Heating pads were wrapped around the PDMS flow-focusing microfluidic device (Wunderlichips GmbH) as well as the tubing (Masterflex Transfer Tubing, PTFE, 1/32). Steel tube connectors (SC20/15) and 0.7 mm syringe needles were used to connect tubes to the device and syringes, respectively. The aqueous cell suspension was pumped through a custom T-junction PDMS microfluidic device (Dolomite Microfluidics) using a syringe pump (World Precision Instruments) at 80 µl/hr flow rate. Fluorinated oil (Fluro Surf 2% in HFE-7500, Dolomite Microfluidics) was used at 2000 µl/hr to emulsify ~50 µm agarose microdroplets and collected in a 1.5 ml Eppendorf. The emulsion was then cooled at room temperature (RT) for crosslinking. To purify agarose beads, 10 µl of beads were mixed with 20 µl of R2A media and 30 µl of Fluro-Stop (Dolomite Microfludics). After a 15 second spin at 1000 rpm, the aqueous

top layer was removed and mixed with 60 µl R2A media. Encapsulated cells were grown in 1 ml R2A at 20˚C in a 15 ml Falcon without shaking.

3.2.4 Surface modifications of agarose droplets

Experiments involving surface-modified agarose beads were conducted using 50-300 µm beads. These beads were created by vortexing 100 µl of 3% LMPA inoculated with *B. subtilis* in 500 µl mineral oil containing 4.5% Span 80 and 0.5% Tween 20 in a microcentrifuge tube. The emulsions were then placed on ice for 30 minutes to solidify before undergoing two washes to remove residual oil, using 0.5 ml R2A at 2000 rpm for 10 seconds.

For double-layering the beads in agarose, 86 µl of washed agarose beads containing *B. subtilis* were mixed with 514 µl of 7% agarose. The mixture was vortexed in oil, and the crosslinking and washing steps were repeated.

Polydopamine film deposition was performed by mixing 500 µl of 10 mg/ml dopamine hydrochloride, dissolved in sterile distilled water, with 500 µl of beads suspended in 20 mM Tris-HCL (pH 8.5). Layering was maintained for one hour at 8 ˚C with 200 rpm orbital shaking. Afterwards, the coated beads were washed twice with 1 ml R2A at 2000 rpm for 10 seconds before cultivation.

Aqueous layering with Fe(III)-tannic acid involved mixing 250 µl of 0.2 mg/ml ferric chloride with 250 µl of beads suspended in 0.8 mg/ml tannic acid. Subsequently, 500 µl of 20 mM MOPS (pH 7.4) was immediately added, and layering was carried out for 30 seconds before washing the beads three times with R2A.

ZIF-8 coating involved mixing 500 µl of 20 mM zinc acetate with 500 µl of beads suspended in 160 mM 2-methylimidazole. Layering was conducted for 20 minutes before washing the beads three times with R2A.

For interphase layering with Fe(III)-tannic acid, 100 µl of bacteria in molten 37˚C LMPA agarose with 2.5 mg/ml tannic acid was mixed with 500 µl of hexadecane oil containing 5% Span 80 and 1 mM iron(III) acetylacetonate. The mixture was vortexed for 10 seconds, and the emulsion was incubated at 18 ˚C for bead solidification and interfacial layering with Fe(III)-tannic acid. The beads were then washed three times with 800 µl hexadecane, followed by three washes with R2A.

3.2.5 Fabrication of non-3D printed alginate encapsulation device

The components used for the concentric capillary device included 1.5 ml Eppendorf microcentrifuge tubes, 1.83 mm and 0.6 mm inner diameter (ID) blunt steel needles (Shintop, 1.8 mm), 0.3 mm glass capillary (CM Scientific CV3040-B-100), 1.8 mm glass capillary (Samco G119/02), 1mm ID silicone tubing and rapid two part-epoxy (Araldite ARA-400007). Glass capillaries were hydrophobically coated by incubation in a solution of 94% acidic methanol (0.15 M acetic acid), 4% ddH20 and 2% 1H,1H,2H,2H-Perfluorooctyltrimethoxysillane (252).

3.2.6 Fabrication of 3D printed capillary mount

The 3D models for the alginate encapsulation capillary mount were designed using AutoCAD 2022 (Autodesk) software and exported as STL files for digital slicing with Ultimaker-Cura. The Gcode was uploaded to a Prusa i3 MK3S+ FFF 3-D printer equipped with natural PLA thermoplastic (Polymaker) and a smooth PEI build plate heated to 65 ºC. Extrusion was maintained at 220 ºC at 100 µm layer height with 100% infill density, 105% flow rate, and 60 mm/s speed. After printing the devices, hydrophobically-coated glass capillaries of 1.8 mm and 0.3 mm ID were concentrically aligned and glued in place with epoxy glue. The 1.83 mm ID blunt steel needles were glued to the device inlets for the connection of 1 mm ID silicone tubing. The mount and tubing were sterilised in 70% ethanol overnight before washing with sterile distilled water.

3.2.7 Pneumatic oscillating pressure apparatus for centralised alginate bead encapsulation

For the pneumatic oscillating pressure apparatus, a 1 ml syringe (Terumo) was connected tangentially to the inner-phase (IP) tubing (silicone, 1.5 mm ID) via a 3 mm ID T-junction halfway between the syringe pump and encapsulation device (20 cm). 7.5 cm of tubing was connected between the pump syringe and the T-junction. The syringe was fixed within a custom PETG 3D-printed holder and adaptor linking the plunger to a reciprocating linear actuator (AZSSMUK) driven by a Nema 17 bipolar stepper motor (Rtelligent) and DRV8825 driver. Silicone grease (Beckman) was applied to the syringe plunger to maintain an airtight seal. Approximately 0.5 cm^3 of air was displaced on each actuation, causing pressure in the IP tubing to oscillate and deliver ~40 nl of IP in synchronisation with each outer-phase (OP) alginate drip. Synchronisation was automatically maintained by a programmable Arduino Uno microcontroller that received trigger events from each alginate drip and actuator engagement

via LM393 photointerrupter sensors (Hailege). Two M3 x10 mm screws with nuts were used to fix the photointerrupters to the BEAD device and actuator using pre-defined holes in the 3D models.

3.2.8 Environmental cell extraction and quantification

Environmental cells were extracted by diluting 1 ml of pond sediment samples in 9 ml of 0.1 µm SFPW, before vortexing with 3 g of 1 mm glass beads for 15 minutes. Homogenised samples were filtered through a 20 µm filter (pluriSelect) and stained with 5 µM carboxyfluorescein diacetate, succinimidyl ester (CFDA SE, ThermoFisher) in R2A medium for 30 minutes at 23ºC before quantifying fluorescent cell abundances with a haemocytometer.

3.2.9 Fabrication of cultivation cassettes

Chambers for cultivation cassettes were CNC-drilled from a 12 mm thick acetyl homopolymer sheet (Delrin) in the size of 10 x 8 cm at Imperial College Hackspace (Figure 3.1). Gaskets were manually cut from a 1.5 mm silicone rubber sheet and hole-punched for screw holes (Figure 3.1). Holes for screws were melted through a 0.05 µm-pore polycarbonate track-etched membrane (Sterlitech) using hot metal tweezers. Cassettes were assembled and sealed with

twelve M3x35 316L screws, washers, and hex nuts (RS Components) with 3D-printed PLA screw frames (Figure 3.1).

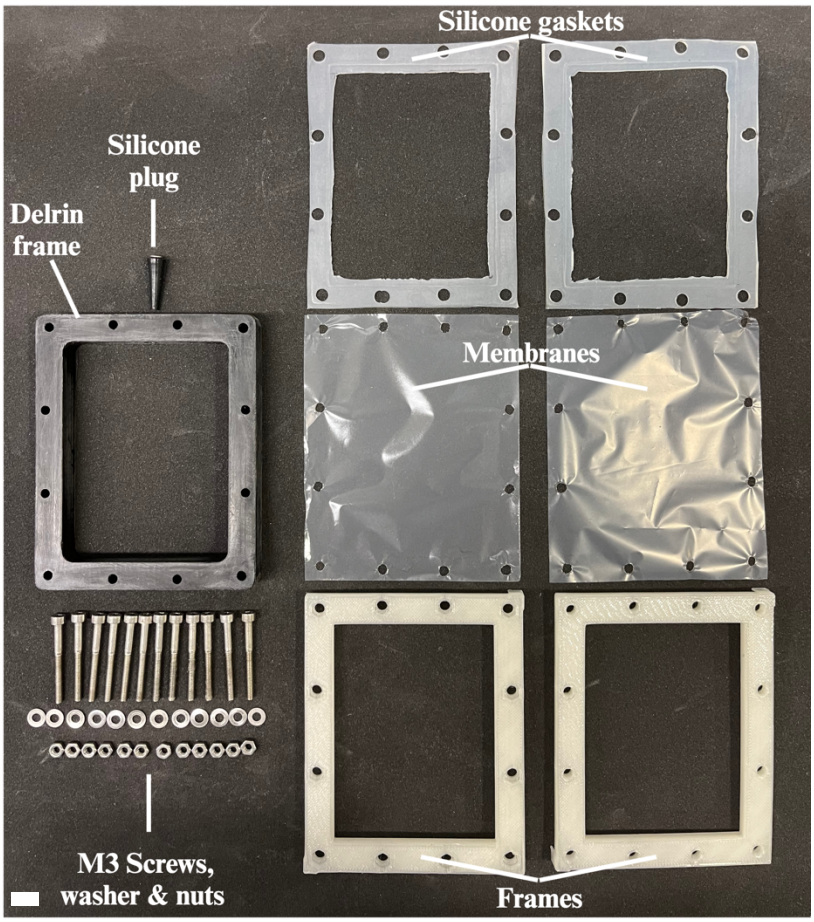

Figure 3.1: Cultivation cassette components.
Cultivation cassettes were assembled from a Delrin frame chamber that was sealed with porous PC membrane by silicone gaskets and PLA frames. Silicone plugs allowed filling and drainage of contents prior to incubation and extraction, respectively. Scale bar 1 cm.

3.2.10 Alginate cell encapsulation and *in situ* cultivation

To encapsulate cells using the concentric capillary mount device, extracted environmental cells from Imperial Silwood Park were prepared in an IP medium of SFPW with 10% (w/v) dextran sulfate (Mw 500,000 kDa) to achieve approximately single cell/bead concentrations. The OP medium comprised 5% alginic acid sodium salt and 4% PEG 35K dissolved in distilled water, with filtering through a 5 µm pore filter (Minisart) to remove impurities. Flow rates were 0.424 ml/min and 1.2 µl/min for the outer and inner phases, respectively, generating ~30 beads/min. cells within the IP were microinjected into cores of nascent OP drips by the automated pneumatic pump apparatus. The capillary mount was held by a clamp 10 cm above a vortexing

200 ml solution of 100 mM $CaCl_2$ and 0.01% Tween 20 in a 250 ml glass beaker. After 45 minutes of solidification, the alginate beads were washed four times with 200 ml of SFPW. Residual SFPW was removed, and beads were loaded into partially assembled autoclaved cultivation cassettes. The top half of the cassettes was then screw-sealed. ~60 ml of SFPW was then injected into the cassettes through an access port on the top of the Delrin frames before sealing the port with a 3.18 mm x 6.35 mm tapered silicone plug (Vital Parts). The sides of the cassettes were wrapped in waterproof tape (Gorilla) before being sealed in a nylon mesh bag. Cassettes were submerged in high-density polyethylene buckets containing 10 L Silwood Lake pond water with sediment for 2 weeks of *in situ* incubation. After incubation, cassettes were retrieved and washed with distilled water and wiped with 70% ethanol.

3.2.11 Recovery of cells from alginate beads

For recovery of cells in alginate beads, single beads were picked up by suctioning with a 10 ml stripette tip and placing on a 5 ml 60 mm R2A agar. 3 ml of 1U/ml alginate lyase was then added and left to digest at 26˚C at 90 rpm. Alternatively, beads were dispensed into wells of a 96-well deep block with 5-10 1 mm glass beads and 1 U/ml of alginate lyase in 0.25 ml volume. Plates were then shaken at 1000 rpm for ≥4 hours at RT.

3.2.12 16S rDNA amplification and analysis for isolate identification

Discrete colonies were picked and homogenised in a PCR tube of 50 µl of 10 mM Tris-HCL pH 8, 1 mM EDTA, 1% Triton X-100. Colonies were then boiled at 100 ˚C for 12 minutes, with pipette agitation halfway through boiling. Lysates were used as templates for 16S rDNA amplification as previously described (Methods 2.2.8).

3.3 Results

3.3.1 Microfluidic encapsulation of bacteria within agarose microdroplets

To investigate the feasibility of a microfluidic approach for *in situ* cultivation of bacteria, cells were encapsulated in agarose microbeads using a commercially available PDMS flow-focusing microfluidic device (Figure 3.1A). The ~50 µm size of the crosslinked agarose beads was selected for maximising throughput and compatibility with FACS. Containment efficiency was initially evaluated by encapsulating *B. subtilis* constitutively expressing sfGFP, serving as a model environmental bacterium. Growth of the encapsulated cells was monitored daily at 20 ˚C in 500 µl R2A medium. It was observed as early as day 1, however, that the dividing *B. subtilis* colonies could penetrate the agarose matrix and egress into the surrounding medium ((Figure 3.1B). Free cell contaminants were unable to be removed from the agarose beads using membrane filtration or washing.

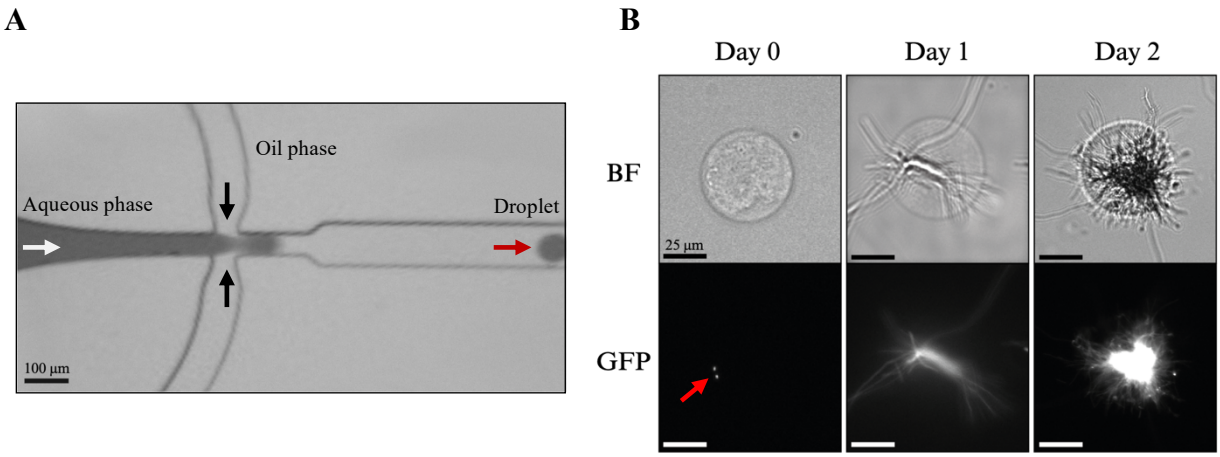

Figure 3.2: Microfluidic encapsulation and cultivation of *B. subtilis* within agarose microdroplets. (**A**) Microscope image of formation of 50 µm agarose microdroplets encapsulating *B. subtilis* via a PDMS microfluidic device. The aqueous phase (white arrow) containing molten LMPA and *B. subtilis* is intersected by an oil phase (black arrows) causing scission of flow and generation of microdroplets (red arrow). (**B**) After solidification of agarose, encapsulated *B. subtilis* expressing GFP (red arrow) were cultivated at RT within R2A media. Cells were observed to outgrow capsules into the surrounding medium. Comparison of cultivated microcolonies under brightfield (BF) or fluorescence (GFP).

3.3.2 Agarose encapsulation method modifications

After observing insufficient containment of microbial growth within the unmodified agarose microbeads, it was next hypothesised surface or functional modifications could be made to limit cellular outgrowth. In subsequent experiments, encapsulated cells were generated by

vortexing the agarose-cell mixture with oil within a microcentrifuge tube to generate ~150 µm particles as this substantially reduced experimental set-up time compared to the microfluidic

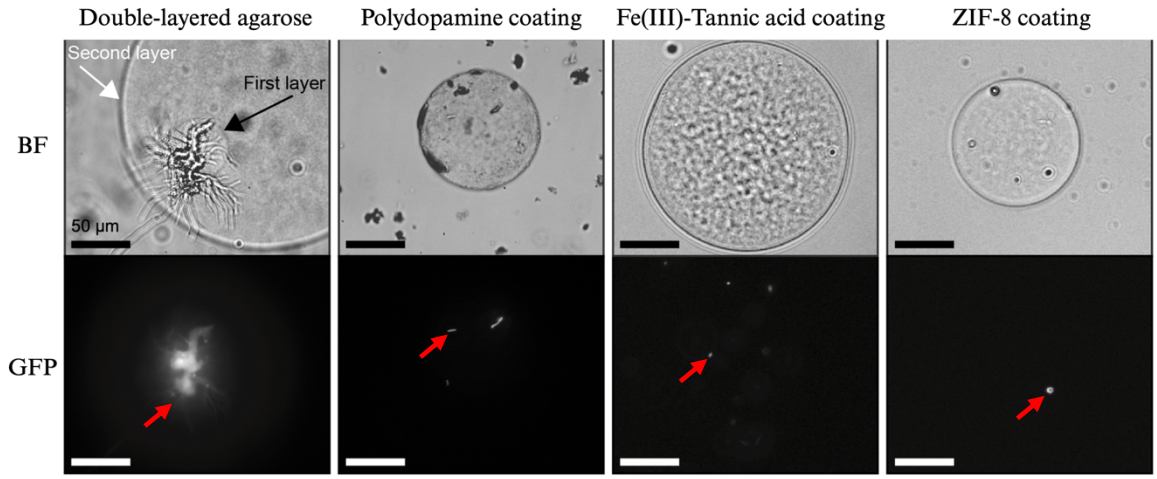

Figure 3.3: Evaluation of capsule coatings for cultivation and containment of *B. subtilis*. Microscope images of encapsulated *B. subtilis* expressing GFP (red arrows) after 2 days cultivation with capsule coatings with a double-layer of agarose or surface coatings of polydopamine, Fe(III)-tannic acid, or ZIF-8. The second, high percentage agarose layer was insufficient in containing *B. subtilis* growth, whereas the surface layer coatings appeared to restrict cell division.

device. Using higher concentrations of agarose (up to 6%), as well as double layering capsules in a second hydrogel layer proved ineffective in containing *B. subtilis* for the required *in situ* incubation time (1-4 weeks) (Figure 3.3). A selection of agarose surface modifications was evaluated for the containment efficiency of agarose-encapsulated *B. subtilis*. Such a film would require high porosity, biocompatibility, and the ability to readily self-assemble on agarose surfaces. Three self-assembling films were identified to fulfil these criteria and have been previously used to limit cell division or prevent cell outgrowth from hydrogel capsules. Films of polydopamine, Fe(III)-tannic acid, and zinc 2-methylimidazole (ZIF-8), rapidly form on the bead surfaces upon the introduction of soluble precursors and were applied to the *B. subtilis* microbead surface as previously described (78,103,253,254). Although fluorescence was retained, cell division was abrogated resulting in the absence of colony formation (Figure 3.3). It was hypothesised that the lack of colony formation was consequential to polymer precursors diffusing into the beads and inhibiting cell division by coating cells directly (253). To localise film deposition to the bead surface, a water-oil interphase layering approach was performed using the Fe(III)-tannic acid film (255). Here, ferric iron dissolved in the oil phase reacts with tannic acid at the aqueous interphase forming a localised metal-organic complex localised on the bead surface. Although colony growth was improved with evidence of improved

containment, it was shown Fe(III)-tannic acid film was not sufficient in containing colony growth over 2 days (Figure 3.4).

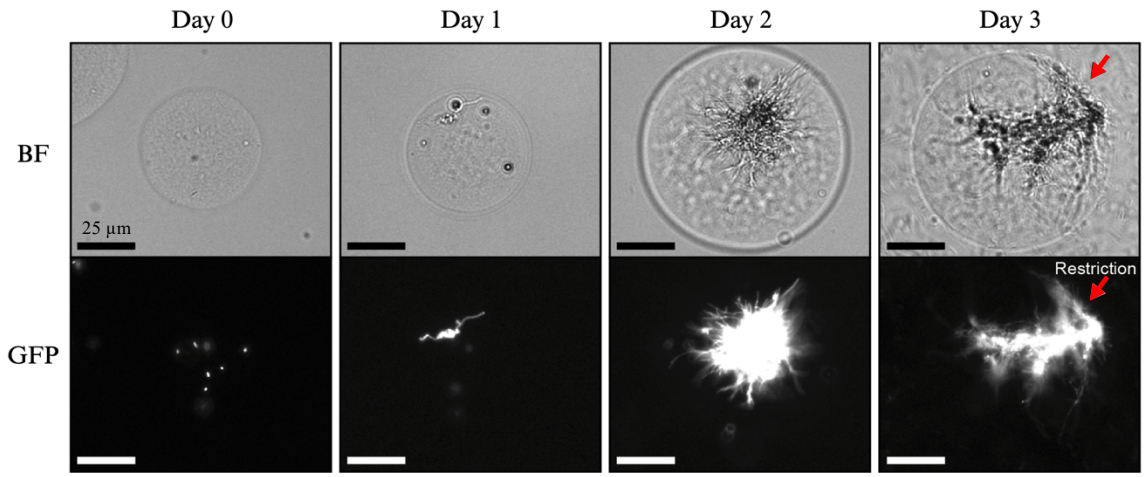

Figure 3.4: Interfacial polymerisation of Fe(III)-tannic acid restores but does not contain microcolony growth.
Microscope images of encapsulated *B. subtilis* expressing GFP after localised interfacial polymerisation of Fe(III)-tannic acid to the agarose bead surface. Colony cultivation was restored, with restriction of colony growth at the bead surface (red arrows). However, outgrowth of cells was still observed after 3 days incubation.

3.3.3 Spatial containment of cells within alginate capsules

Having observed insufficient containment within the agarose microbeads, it was hypothesised that bacteria centralised in larger beads may remain contained for long-term colony growth. Alginate was selected over agarose for superior control in gelation and avoiding complexities in maintaining a heated apparatus. First, the growth and colony size of *B. subtilis* encapsulated in alginate were monitored over time. *B. subtilis* cells mixed in 5% alginate were dripped through a 1.8 mm ID capillary into $CaCl_2$, generating ~5 mm diameter beads encapsulating ~10 cells per bead. After 14 days of incubation in R2A medium, the colony size within the beads increased to approximately 1.7 mm (SD± 0.22) (Figure 3.5). It was therefore hypothesised that colony growth might be contained within the alginate capsules after 14 days of in situ incubation if colonies were sufficiently centralised.

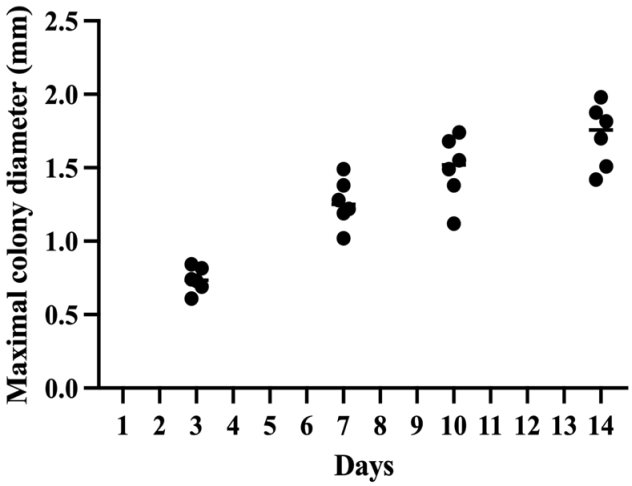

Figure 3.5: Colony growth of randomly dispersed *B. subtilis* within alginate beads.
Alginate was mixed with *B. subtilis* and extruded into a $CaCl_2$ solution yielding beads encapsulating ~10 cells per bead. Beads were then incubated in R2A with the maximal colony diameter averaged from cells in 6 beads.

3.3.4 Development of the BEAD method

To contain and cultivate bacteria within alginate capsules, a new method was developed, termed Bacterial Encapsulation and Containment (BEAD), capable of centralising and cultivating bacteria within alginate beads. The method utilised a 3D printed capillary mount containing two concentrically aligned capillaries. The outer capillary (1.8 mm ID) serves as an outlet for the outer alginate phase (OP), while the inner capillary (0.3 mm ID) microinjects the bacterial inner phase (IP). The alginate OP and bacterial IP were deliverable by two syringe pumps connected to the mount inlets with silicone tubing (Figure 3.6).

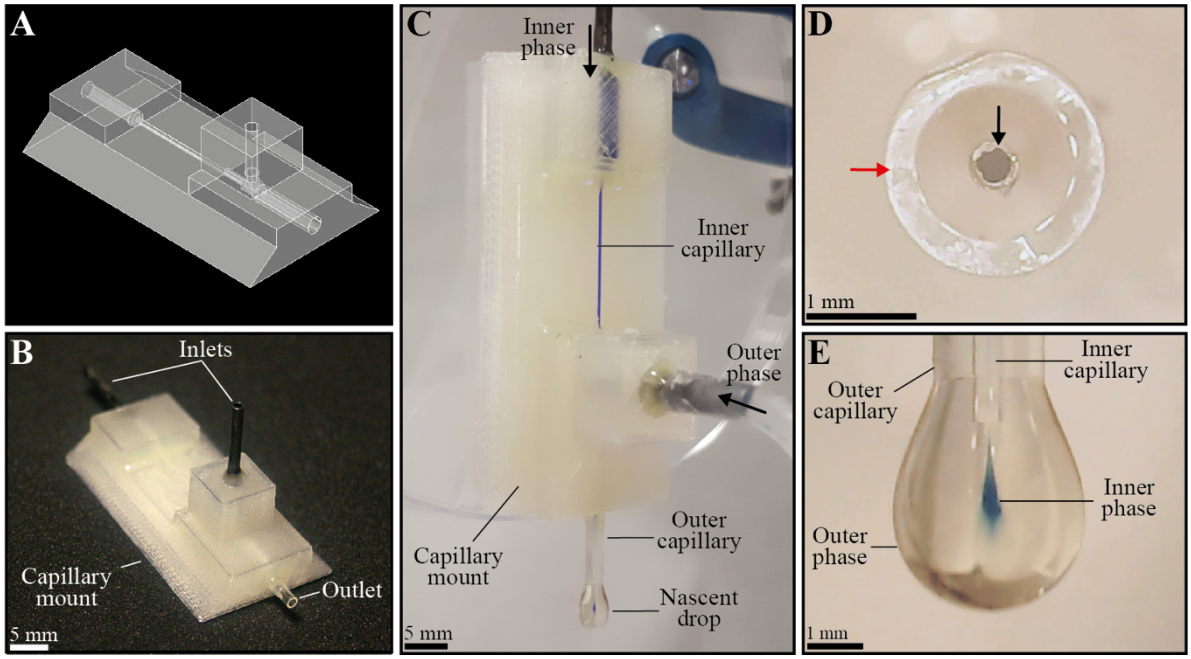

Figure 3.6: Capillary mount for microinjection of bacterial IP within alginate OP droplets. (**A**) X-ray 3D model of capillary mount. (**B**) Image of mount with inlets and outlets inserted. (**C**) Connected mount with blue-stained IP microinjected into the OP nascent droplet. (**D**) Cross-section of concentrically aligned inner (black arrow) and outer (red arrow) capillary. (**E**) Zoom of alginate OP receiving microinjection of blue-stained IP. Alginate drops encapsulating IP fall into a $CalCl_2$ solution for crosslinking.

3.3.5 Development of automated pneumatic pump and ATPS for microinjection of bacteria

First, a pneumatic pump system was developed to allow the synchronous injection of bacteria into the core of alginate beads before crosslinking. Here, a syringe air piston was connected in tandem with the IP tubing, thereby oscillating IP pressure by the reciprocal push and pulling of the syringe plunger. The pneumatic piston was actuated by a linear reciprocating actuator driven by a DC motor that could be manually controlled with a pulse width modulation speed controller. Thus, with the use of an IP tracer dye, synchronisation of IP injection inside OP drips could be maintained.

Without further chemical modification, the bacterial IP and alginate OP lacked sufficient phase separation and rapidly diffused, leading to bacteria in the periphery of the alginate beads. To improve phase separation and containment of bacteria, an aqueous two-phase system (ATPS) comprising PEG and dextran was employed (72,103). Here, a mixture of 5% v/w alginate with 8% PEG 35000 as the OP and 10% dextran as the IP displayed sufficient phase separation and spatial localisation of IP within the alginate bead core (Figure

3.7). The flow rate was set to ~30 beads/min, as this was found to maintain uniform OP drips and accurate IP injection. However, the syringe flange would buckle under pressure while attempting the necessary flow rate for the highly viscous fluid (~840 µl/min). The amount of PEG was therefore reduced to 4% v/w without significant losses of phase separation. Due to phase density differences, the denser dextran IP was observed to sink to the bottom of the OP bead during crosslinking. This was mitigated by vortexing the bead-crosslinking solution.

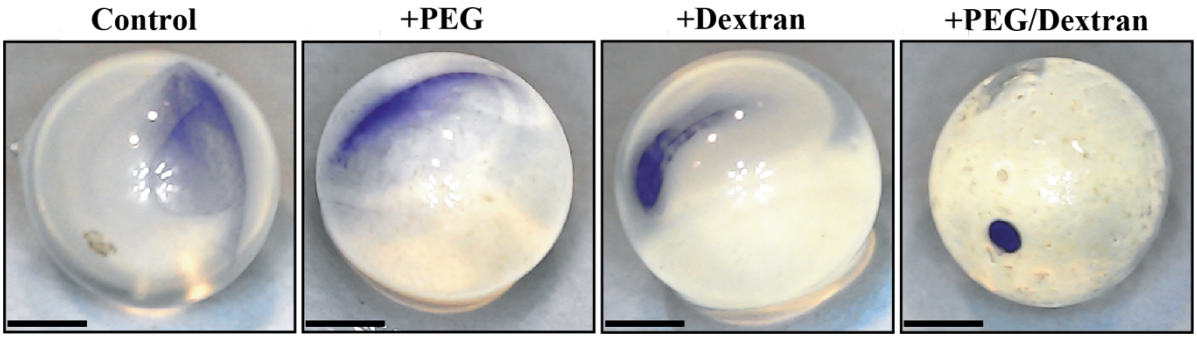

Figure 3.7: ATPS to maintain phase-separation and localisation of IP within beads.
Use of the ATPS comprising 4% PEG OP and 10% dextran IP for maintain phase-separation and preventing immediate diffusion of IP (stained blue). Compared to the control of no additives, or beads with only one of either PEG or dextran, PEG/dextran combined displayed greater phase-separation demonstrated by the spatial focusing of IP. Peripheral localisation is due to sinking of IP without a vortexing crosslinking solution. Scale bar 1 mm.

Several limitations were, however, noted in the aforementioned apparatus. Firstly, the synchronisation required frequent manual adjustment, as the DC motor driving the pneumatic IP injection did not maintain a consistent speed. Secondly, although biocompatible, the use of the indigo carmine tracer dye should be optimally removed to prevent potential interference with encapsulated cells. To address these limitations, a new automated pneumatic pump system was developed that would automatically maintain synchronisation of IP injection with each alginate drip, thus also eliminating the necessity for a visualisation dye (Figure 3.8).

First, the actuator DC motor was replaced with a significantly more precise bipolar stepper motor. Next, the capillary mount and syringe pump motor were each fitted with photointerrupter trigger sensors to monitor the timing of the alginate drip and pump actuation. The speed of the IP injection pump motor and thus synchronisation was automatically adjusted by an Arduino microcontroller with data received from the photointerrupters (Figure 3.9A-D).

To test the precision of automated IP injection into each alginate bead, the IP was stained with the fluorescent dye fluorescein, and dye-injected beads were collected in a microwell plate for fluorescence dye quantification. With measurements at 30, 60, and 90

minutes of operation, the average IP injection volume was calculated to be close to the expected 40 nl at 38.53 nl (SD± 4.63) with a coefficient of variation (CV) of 12%. The IP core was found to be consistently centralised within 1 mm from the bead surfaces (mean 1.6 mm n=26) (Figure 3.10).

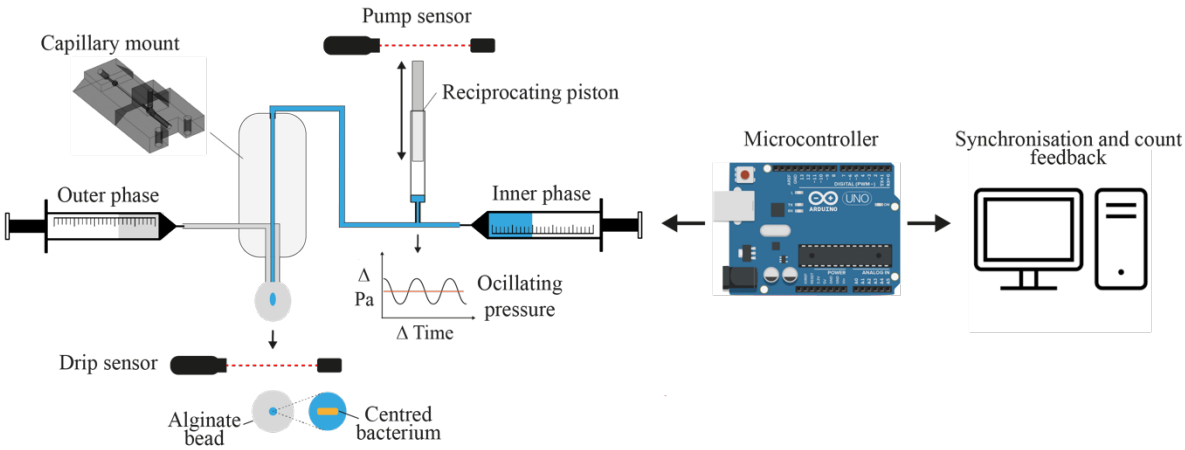

Figure 3.8: Automated phase synchronisation for microinjection of IP into OP droplets. Syringe pumps maintain a consistent flowrate of OP and IP to the capillary mount. The IP tubing connects to a reciprocating piston that oscillates pressure. Photointerrupter sensors on the piston pump and below the drip path of the capillary mount send timing data to an Arduino microcontroller that automatically synchronises the actuation of the piston with each alginate drip. Synchronisation status and number of beads dispensed can be communicated to a computer monitor. Beads containing IP cores are crosslinked once collected in a crosslinking solution positioned underneath the mount.

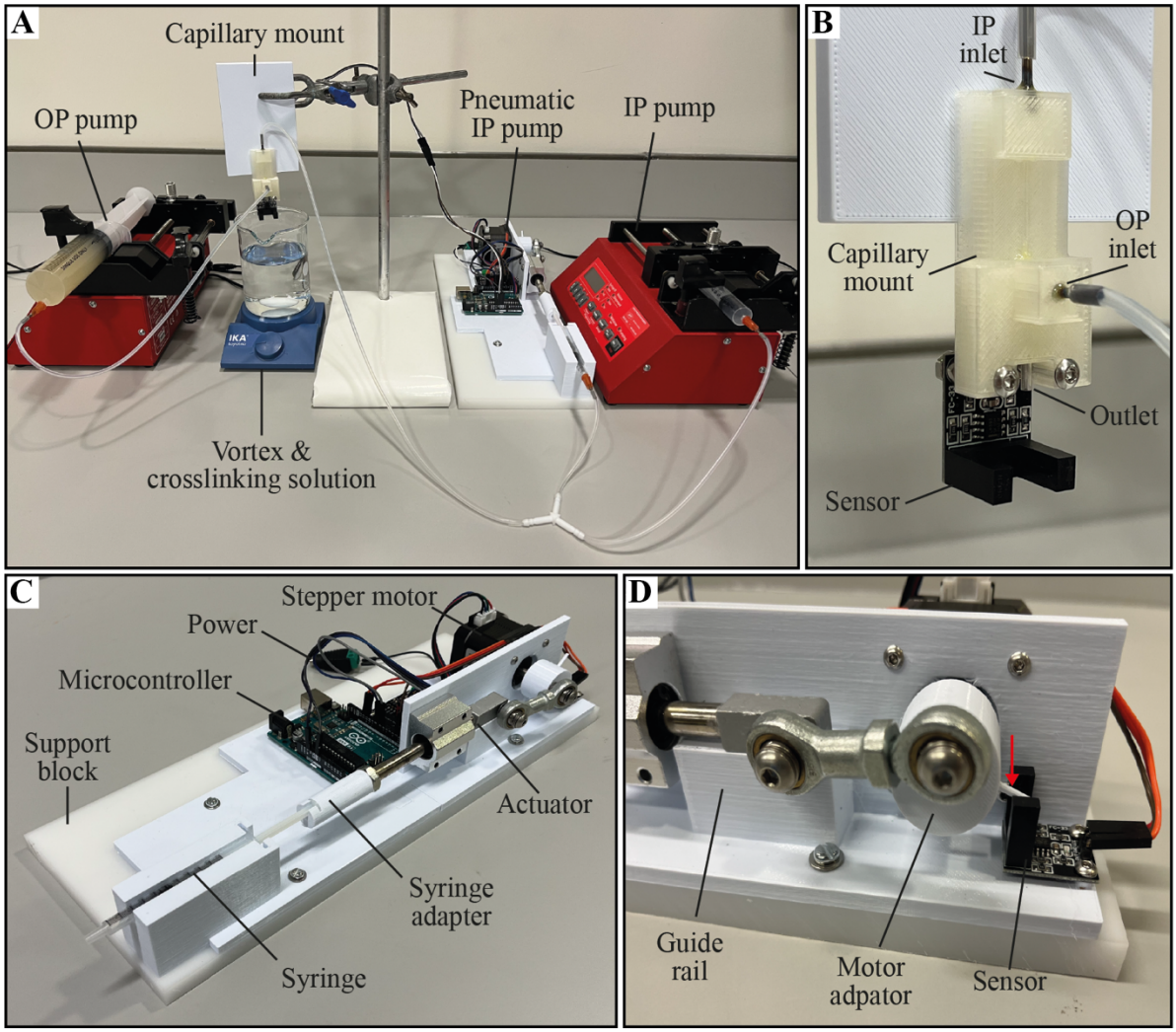

Figure 3.9: Apparatus with automated phase synchronisation and microinjection system. (**A**) Apparatus for microinjection and encapsulation of cells within alginate beads. OP and IP are delivered to the capillary mount at a constant flow rate via connected silicone tubing. The pneumatic IP pump oscillates the IP pressure synchronous with each OP drip to achieve encapsulation. Formed beads are collected in a vortexing crosslinking solution. (**B**) Zoom of capillary mount displaying IP and OP inlets leading to the capillary outlet positioned above a photointerrupter sensor that detects falling beads. (**C**) The pneumatic pump comprises a 3D printed frame housing a 1 ml syringe connected to the linear actuator via a syringe adapter. The speed of the stepper motor and actuator is controlled by a microcontroller with input from sensor readings of drip and pump timings. The system frame is anchored to a support block of white Delrin. (**D**) Zoom of actuator showing the stepper motor adaptor which possess a fixed trigger pin (red arrow) that activates the pump sensor at specific actuation position. A guide rail aids in maintaining stability of the actuator.

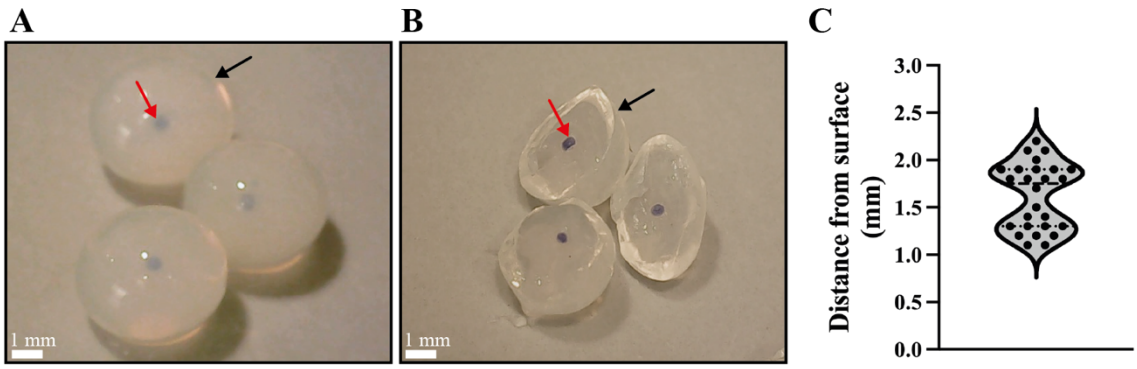

Figure 3.10: Positioning of IP within alginate beads.
(**A**) Crosslinked alginate beads with microinjected IP (red arrow, blue dye) contained within alginate OP (black arrow). (**B**) Sectioned beads highlighting centralised IP positioning. (**C**) Violin plot of IP distance from bead surfaces (n=26). Median shown in dashed line and upper/lower quartiles in dotted lines.

The permeability of alginate was then evaluated to ensure efficient diffusion of nutrients for *in situ* cultivation within the beads. Alginate beads were immersed in fluorescein dye, and samples were collected at various time intervals for quantification of dye absorption. Alginate concentrations ranging from 1% to 5% were compared. The dye was observed to rapidly diffuse into all percentages of alginate beads, reaching 80% diffusion within the first 3 hours and reaching a plateau thereafter (Figure 3.11).

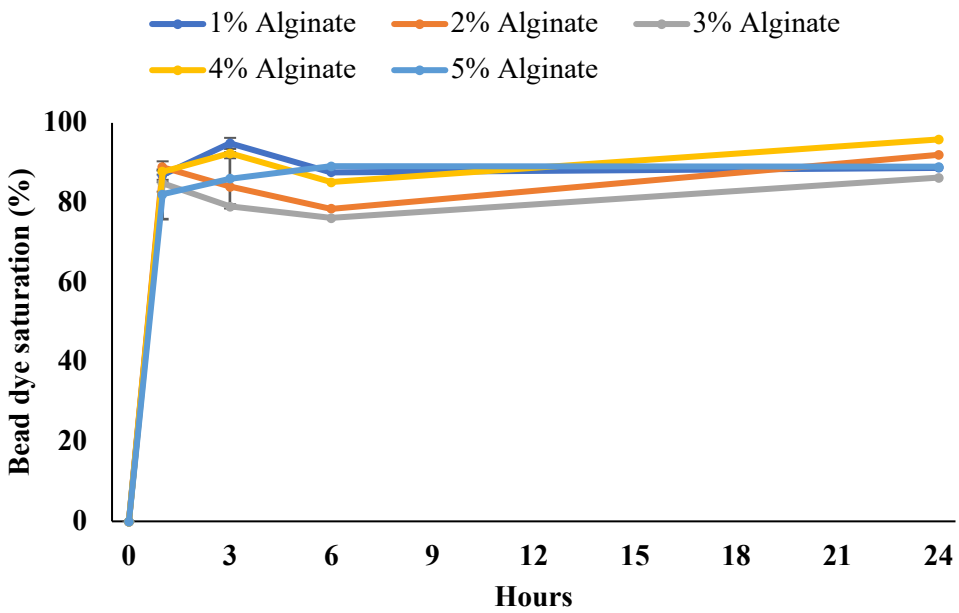

Figure 3.11: Diffusion of fluorescein into alginate beads.
Alginate beads comprising 4% PEG and varying alginate concentrations were compared for diffusion and absorption of the dye fluorescein.

3.3.6 Biocompatibility of alginate encapsulation

The biocompatibility of buffers used in the encapsulation process was assessed with the model species *B. subtilis*, *E. coli*, *S. coelicolor*, and pond water microbial communities. Exposure for one hour to $CaCl_2$ or $SrCl_2$, tween 20 as well as dextran were well tolerated without any significant decreases in CFU, except for *E. coli* to 0.1 M $SrCl_2$ ($p= 0.0234$, $F (9, 20) = 20.96$) (Figure 3.12A-D). Significant increases in CFU were seen in *B. subtilis* exposure to some buffers containing R2A media and *E. coli* to 10% dextran (Figure 3.12A-B). Although significant changes in CFU were not observed in pond water communities ($p=0.3176$ $F (9, 20) = 1.258$), the effects of the buffers on uncultivable species were unknown (Figure 3.12D). Therefore, cell viability upon exposure to buffers was additionally measured for pond communities using CFDA-SE staining. Significant decreases in cell viability were observed in

buffers containing 0.1% tween (Figure 3.13). However, there was a lack of overall effect correlation between cell type viability and buffer components (Figure 3.13).

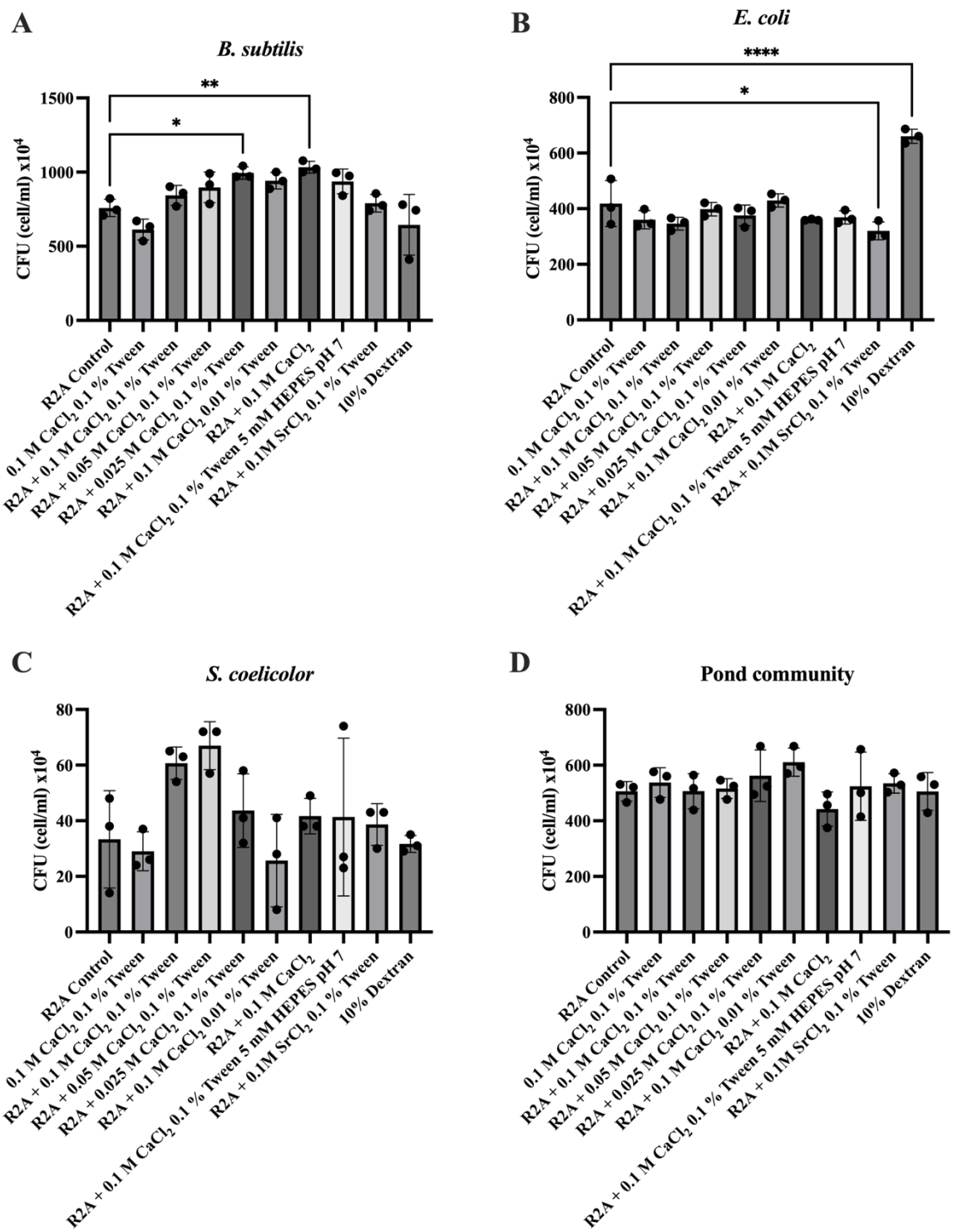

Figure 3.12: Biocompatibility of crosslinking buffers and media.
The biocompatibility of media and crosslinking components were compared with the CFU of (**A**) *B. subtilis*, (**B**) *E. coli*, (**C**) *S. coelicolor* and, (**D**) pond sediment microorganism communities. After one hour exposure. Results of one-way ANOVA and Tukey's multiple comparison test with only significant differences shown, * = $p < 0.05$, ** = $p < 0.01$, *** = $p < 0.001$, **** = $p < 0.0001$.

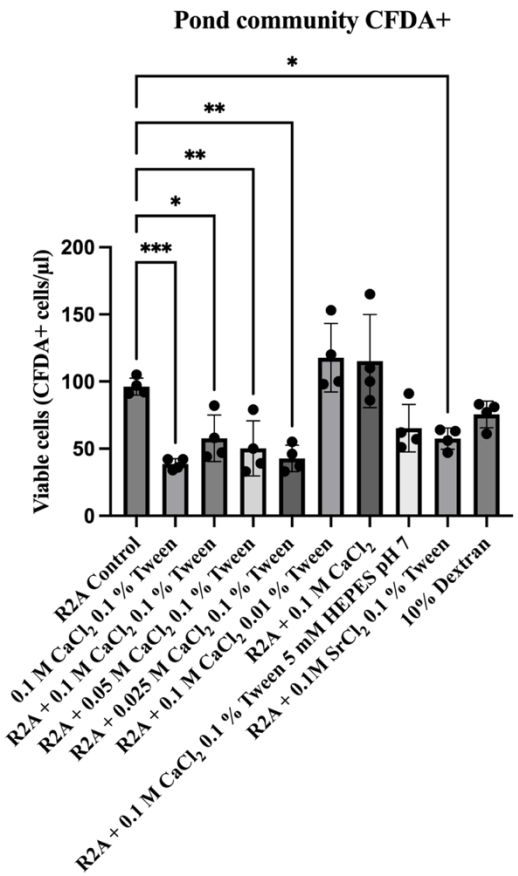

Figure 3.13: Biocompatibility of crosslinking buffers and media on viable pond community cells.
The biocompatibility of media and crosslinking components were compared with the viability of pond water microbial communities using CFDA SE staining. Results of one-way ANOVA and Tukey's multiple comparison test with only significant differences shown, * = $p < 0.05$, ** = $p < 0.01$, *** = $p < 0.001$.

3.3.7 Alginate encapsulation cell containment

Cell containment was next evaluated with centralised encapsulation of *B. subtilis*, *E. coli* and *S. coelicolor*. For comparison, the same bacteria were mixed in the alginate solution and thus encapsulated in random positions within the bead. ~100 beads encapsulating approximately 1-10 cells of each species were placed in separate 50 ml falcons containing R2A medium and monitored for outgrowth. 100% of beads had observable microcolonies by day 3. Cells randomly dispersed within alginate beads were found to rapidly outgrow capsules (mean 5 days containment, SD± 2). However, all centralised bacteria were contained for at least 2 weeks without detectable outgrowth into the surrounding medium, with a third of replicates reaching at least 21 days (mean containment 17 days, SD± 3) (Figure 3.14A). A comparison using a Kaplan-Meier estimator and log-rank test revealed the increased containment probability was

significant (χ^2 = 19.57, df = 1, p = <0.0001) (Figure 3.14B). Thus, the containment of microcolonies using the BEAD method was deemed suitable for the 14 days required for *in situ* cultivation.

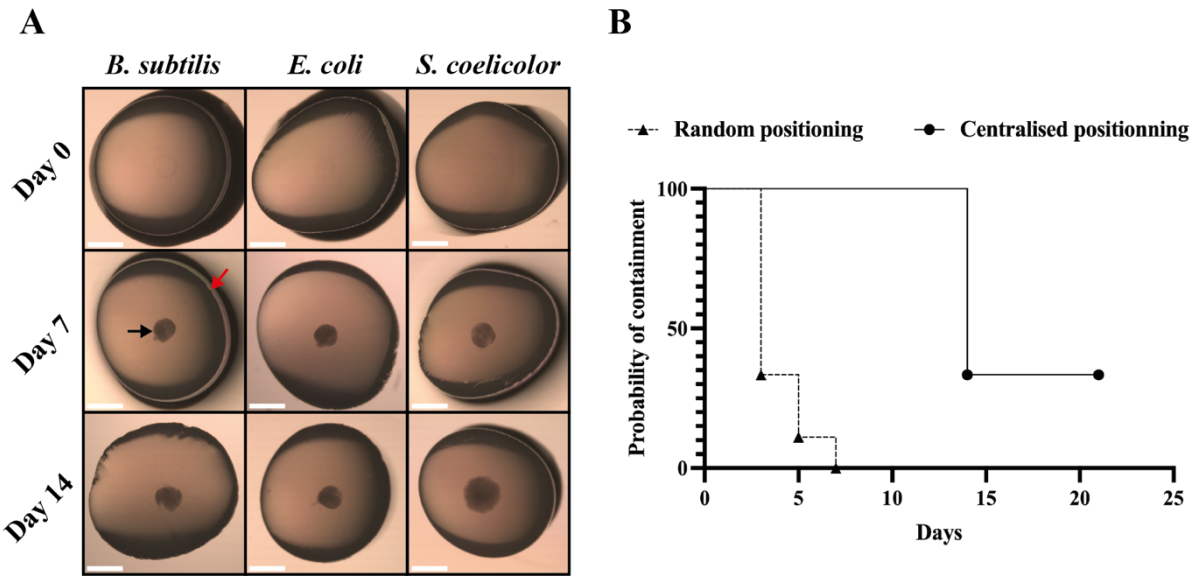

Figure 3.14: Contained cultivation of microcolonies within alginate beads.
(**A**) Cells of *B. subtilis*, *E. coli* and *S. coelicolor* were encapsulated within the cores of alginate beads by microinjection with containment for up to 14 days. Cultivated microcolonies (black arrow) were contained within the alginate beads (n=100) (red arrow). Scale bar 1 mm. (**B**) Kaplan-Meier survival analysis and log-rank test of containment comparison between cells that were randomly positioned in alginate beads and those centralised by microinjection (centralised positioning). Centralised positioning of microcolonies resulted in significantly greater duration of containment before detectable outgrowth. Results of 3 independent replicates.

3.3.8 Optimisation of cell decapsulation

The decapsulation of alginate-encapsulated cells can be achieved by enzymatic digestion using alginate lyase. Nevertheless, the precise duration and the optimal enzyme units needed for the complete removal of cross-linked alginate remained unclear. To maintain throughput, each alginate bead was placed on 60 mm R2A agar petri dishes, partially submerged in an enzyme solution. This allowed for simultaneous bead digestion and colony cultivation. Conditions were tested to ensure complete alginate digestion before the enzyme solutions evaporated (Table 3.1). The optimal conditions found were 26 °C with 3 ml of 1U/ml alginate lyase at 90 rpm, allowing for bead digestion and media drying overnight.

Temperature	Volume (ml)	Enzyme (U/ml)	Media dried?	Bead digestion?

26 ˚C	3	5	Y	Y
	2	5	Y	Y
	1	5	Y	N
	3	2.5	Y	Y
	2	2.5	Y	N
	1	2.5	Y	N
	3	1	Y	Y
	2	1	Y	N
	1	1	Y	N
RT (23˚C)	3	5	N	Y
	2	5	N	Y
	1	5	Y	N
	3	2.5	N	Y
	2	2.5	N	N
	1	2.5	Y	N
	3	1	N	Y
	2	1	N	N
	1	1	Y	N

Table 3.1: Optimal conditions for digesting alginate beads on agar petri dishes with alginate lyase.
Comparison of digestion of alginate beads on agar petri dishes with alginate lyase. Single beads were placed on agar petri dishes with varying volumes of media and concentrations of alginate lyase. Optimal conditions for both bead digestion and media evaporation were explored.

Although convenient for small-scale cultivations, larger-scale cultivations involving >500 beads would require microwell-compatible formatting and minimisation of enzyme usage to be cost-effective. Furthermore, digestion at RT with minimal exposure to the enzyme would be advantageous. Thus, bead digestion was optimised for a 96-well deep block at RT. Individual alginate beads were placed in the well with the enzyme, along with 5-10 1 mm glass beads, and agitated at 1000 rpm. Bead digestion was achievable with as little as 0.1 U of alginate lyase in a 0.1 ml volume, however, 0.25 ml volumes were optimal for ease of pipetting (Table 3.2).

Temperature	Volume (ml)	Enzyme (U/ml)	Digestion time (mins)
RT (23˚C)	1	5	210

	0.5	5	210
	0.25	5	210
	0.1	5	270
	1	2.5	270
	0.5	2.5	270
	0.25	2.5	270
	0.1	2.5	330
	1	1	390
	0.5	1	390
	0.25	1	390
	0.1	1	420

Table 3.2: Digestion time of alginate beads within 96 deep well blocks with alginate lyase. Comparison of digestion of alginate beads on agar petri dishes. Single beads were placed within 96 deep well blocks with glass beads and varying alginate lyase media volume and concentration. The time taken for beads to digest was compared.

3.3.9 Development of cultivation cassettes for *in situ* cultivation of encapsulated bacteria

Diffusible chambers were next assessed for accommodating encapsulated bacteria for *in situ* cultivation. Custom cultivation cassettes were built using a combination of autoclavable Delrin plastic, PC membrane, and silicone gaskets (Figure 3.15). The cassette size was 10 x 8 x 1.5 cm, allowing ~120 ml volume (Figure 3.15). These were sealed together using custom-designed 3D-printed PLA frames and 316L stainless-steel screws, washers, and nuts (Figure 3.15). A sealable opening in the cassette top was left to allow liquid filling or removal after assembly and recovery, respectively (Figure 3.15). The sterility of the cassettes was confirmed by submerging cassettes in collected pond water for two weeks and plating cassette contents on R2A medium. Contamination was occasionally observed (3/8 cassettes contaminated) during disassembly, likely due to residual liquid in the cassettes bridging the non-sterile exterior once tension was released from the gaskets. This could be mitigated but not completely resolved by sterilising the external surfaces of cassettes with 70% ethanol upon retrieval (1/8 cassettes contaminated).

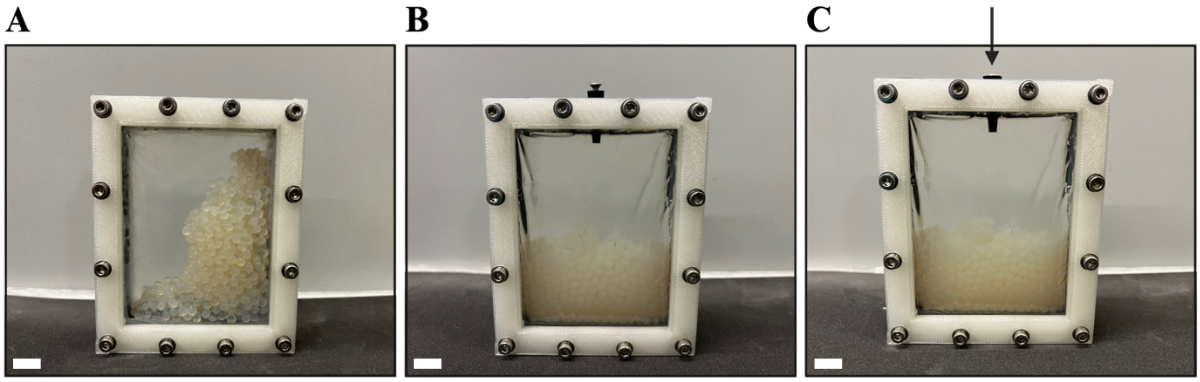

Figure 3.15: Loading of beads into cultivation cassettes.
(**A**) Pond water microorganisms encapsulated within cores of alginate beads were loaded and sealed within cultivation cassettes without liquid. (**B**) Next, native SFPW liquid is pipetted into the cassette chamber with beads via an access port at the top of the cassette. (**C**) The access port is then sealed with a silicone bung and a screw is inserted to maximise tightness (arrow) before covered with waterproof tape. Scale bar 1 cm.

3.3.10 *In situ* cultivation of encapsulated bacteria within cultivation cassettes

To investigate if *in situ* cultivation of encapsulated bacteria improves cultivation efficiency, environmental samples were collected from a pond sediment in Imperial College London Silwood Park campus. Extracted pond water bacteria were encapsulated using the BEAD method at approximately single viable cell/bead concentrations. Approximately 500 beads were then sealed within sterile cultivation cassettes filled with SFPW. These filled cassettes were then immersed in 10 L buckets of pond water containing sediment collected from Silwood Park. To compare with R2A cultivation, bead drippings from the capillary mount were directly collected onto individual R2A plates and cultivated at 23 ˚C. After 14 days incubation, cassettes were retrieved, and alginate beads were digested with alginate lyase before plating contents on R2A agar media (Figure 3.16A-E).

The proportions of colonies obtained by direct R2A cultivation and *in situ* cultivation were not statistically significant, although a considerable standard deviation in cultivation efficiency was observed (means 10.58 % SD ± 11.18 and 18.94% SD ± 25.83, respectively) ($t=0.5145$, $df=4$, $p=0.6340$) (Figure 3.16B). Cassettes without bacteria inoculated remained sterile, however, 5/18 of biological replicates (cassettes) showed contamination and therefore were excluded. 41 Isolated colonies on R2A plates were randomly selected from either *in situ* or standard R2A cultivation methods and identified by Sanger 16S rRNA sequencing and assignment of provisional taxa through Silva SINA classification (215). 11 bacterial orders were observed with approximately two-thirds overlapped in each condition (Figure 3.16D). R2A-only cultivation favoured the cultivation of Burkholderiales, whereas *in situ* BEAD

cultivation favoured greater Rhizobiales (Figure 3.16A). The average 16S rRNA identity (98.50% and 98.85% in R2A and BEAD *in situ*, respectively) as well as number of likely uncultivated species were comparable between the two methods (Figure 3.16 C-E).

It was hypothesised cultivation efficiency could be improved if incubation was extended to 21 days or greater. However, the extraction of beads at this time revealed clear signs of alginate biodegradation, with most beads becoming too fragile to manipulate or extract. Furthermore, levels of contamination in cassettes were unacceptable (16/18 cassettes).

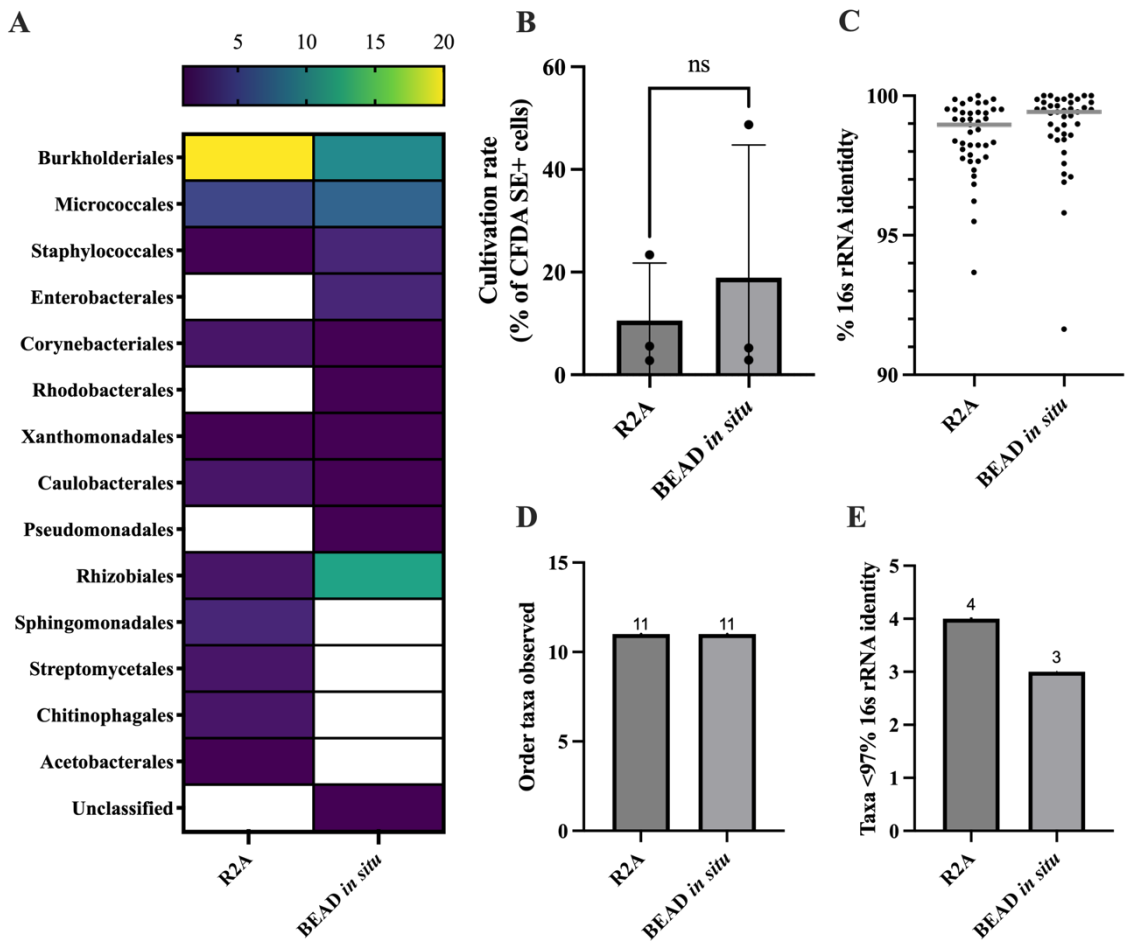

Figure 3.16: Isolate cultivation comparison of plate R2A and BEAD *in situ* methods.
Pond water microorganisms encapsulated within alginate beads were loaded into cultivation cassette for *in situ* cultivation prior to R2A cultivation. For comparison, bead drippings from the capillary mount were collected and cultivated on individual R2A agar plates. (**A**) Heatmap of cultivated isolates at the bacterial order taxonomic level. (**B**) Colony cultivation rate of independent experimental replicates. Results of t-test. ns=non-significant. (**C**) Scatter plot of isolate percentage identity to Silva reference LCA. Mean is shown in grey bar. (**D**) Number of distinct bacterial orders observed from isolates. (**E**) Number of isolate taxa that are likely uncultivated (<97% 16S rRNA sequence identity to Silva reference LCA). Results of n=41 isolates.

3.4 Discussion

3.4.1 Microfluidic approaches for encapsulation and *in situ cultivation* of microorganisms

Since the introduction of *in situ* cultivation methods, efforts have been made to integrate them with high-throughput cultivation or screening technologies (49,50,54,256). The encapsulation of bacteria through microfluidics or microencapsulation would not only provide significantly greater throughput for isolated cultivation and analysis but also preserve the diffusible interaction of encapsulated cells in 3D environments (49,50,54).

Consistent with previous reports, the use of agarose microcapsules for *in situ* cultivation was hindered by insufficient containment of microbial proliferation for the required incubation time (22,49,50) (Figure 3.2B). The consequences of outgrowth are contamination of the surrounding media by fast-growing cultivated species, thus limiting the efficacy in isolating rare or recalcitrant species. Previous authors had limited incubation durations to 7 days (50). While this may reduce potential outgrowth, cultivation of slow-growing or recalcitrant species may be affected (35,50). An optimal encapsulation methodology would therefore enable prolonged cell containment while remaining diffusible with external environments and have biocompatible cell encapsulation and release.

Attempts were made here to improve the cell containment of agarose microbeads with coatings of polydopamine, ZIF-8, or Fe(III)-tannic acid (78,253,257) (Figure 3.3). However, it was found that after bead coating cell division was abrogated. Previously, polydopamine has been shown to self-polymerise on cell surfaces to confer protection against environmental stresses, but also on hydrogel capsules to restrict cell outgrowth (78,257). Thus, the previous claims of using polydopamine for cell containment may be reflective of the restriction of cell division rather than the restriction of growing cells out of a capsule shell, due to soluble precursors diffusing through the hydrogel bead and coating cells directly (78,101). This is evidenced here by the restoration of cell growth through the interfacial layering approach of Fe(III)-tannic acid that would have mitigated potential cell-polymer coating (Figure 3.4). However, the reported ~24 nm film was still not sufficient in preventing *B. subtilis* outgrowth (103) (Figure 3.4). Future work could investigate more robust coating polymers, for example PDMS nano-culture capsules (53,54,101).

3.4.2 BEAD method performance

The BEAD method offers a cell-contained alternative for cell encapsulation and cultivation. Both cultivable model organisms and environmental cells well tolerated the buffer components and media (Figure 3.12-13). Encapsulation of bacterial cells localised within the core of the alginate beads offered over 3-fold longer containment of cells compared to randomly distributed cell beads (Figure 3.14). Thus, with the use of spatially controlled confinement within larger and stronger beads, BEAD presents an alternative tool for high-throughput cultivation, allowing for contained cell culture in a 3D vessel maintaining cellular communication between neighbouring beads and the native environment. Contained cultivation could increase the longevity of *in situ* cultivation without the potential for cross-contamination from fast-growing species. Here using model bacteria of *B. subtilis*, *E. coli* and *S. coelicolor*, BEADs could contain bacterial growth for at least two weeks, greater than previous reports utilising randomly-cell dispersed multi-layered capsules (Figure 3.14) (258). However, in field tests using environmental microorganisms, outgrowth was detected in a third of cassettes. Although the exact cause of the contamination was not confirmed, the BEAD cultivation method may not be compatible with species proficient in penetrating hydrogels or possessing degradative enzymes (75). Additional work should therefore investigate containment efficiency with a wider diversity of microbes or hydrogels.

Additionally, as with other gravity-assisted encapsulation devices, control of airflow is required to prevent disturbance in liquid flow and contamination of collection solutions (114). Moreover, throughput was limited to 30 beads/min to prevent jetting of fluid and instabilities with phase injection. However, the BEAD device is advantageous in providing high spatial control of phase positioning within alginate beads using ATPS with the novel automated pump system. The BEAD containment efficiency may be improved by selecting phases with matched density or by applying additional supporting coating layers (97,100).

In situ cultivation was found to result in a higher average cultivation yield than the R2A-only cultivation method, albeit differences were not significant likely due to large variances in replicates (Figure 3.16B). Such variances could be attributed to differences in weather season or sample complexity (15). Moreover, there was a lack of appreciable difference in isolate diversity or novelty (Figure 3.16BA-E). Although there were differences in taxa enrichment between the R2A-only and *in situ* cultivation methods, it is unclear how much is attributed to the encapsulation process or *in situ* cultivation, which could be elucidated in future with encapsulated bacteria incubated in R2A. Due to a lack of sample size, diversity comparison of the 3 independent cultivation runs was pooled in a single analysis. Greater sample sizes and replicates would provide sufficient data for a more robust statistical analysis.

Concurrently with experiments of this thesis, Pope et al. attempted *in situ* cultivation of marine bacteria within agarose microcapsules and Slide-A-Lyzer cassettes (50). Compared to plating on marine agar the cultivation yield was higher after *in situ* cultivation, although this was not statistically compared (50). The CFU of encapsulated cells were statistically lower than non-encapsulated after *in situ* incubation (50). Moreover, *in situ* incubation was found to negatively affect taxonomic diversity and novelty of isolates (50). In contrast to the results observed here, there was lower overlap between *in situ* and non-*in situ* cultivation methods (50).

However, both data described here and by Pope et al. share limitations in that taxa presence/absence relationships are clouded by insufficient sample sizes (50). Additionally noteworthy in comparison is the use of Slide-a-Lyzer cassettes by Pope et al. for *in situ* incubation, which contain a biodegradable cellulose membrane which may explain sterility issues with cassettes (50). The results here, as well as from Pope et al., contrast with previous reports demonstrating *in situ* cultivation use with the iChip, whereby improvements in colony yield and diversity were observed (11,216). Such discrepancies could be explained by the microfluidic format, however, the encapsulation process was demonstrated to be tolerated by environmental organisms (49,50,69). Greater work should explore the mechanisms or requirements for effective *in situ* cultivation use.

Additionally noteworthy was the degradation of alginate beads alongside prolonged *in situ* incubation in cultivation cassettes > 2 weeks. As stored beads were found to be intact after several months in 50 ml Falcon tubes (data not shown), degradation of the *in situ* incubated beads could be consequential of secreted enzymes or chelating agents present in the native pond water (75,90). Therefore, future work should explore non-biodegradable matrixes for encapsulation such as PDMS or polysulfone, although new challenges would emerge in biocompatible options for encapsulation and recovery (53,54).

3.4.3 BEAD method applications

The BEAD methodology could offer additional applications beyond *in situ* cultivation. For example, recent work demonstrated the potential for delivery of therapeutic agents by synthetic bacteria within immune-privileged cores of tumour spheroids, however, such research is hindered by bacterial growth in the surrounding medium of assays (259). The BEAD method therefore could allow high throughput contained co-cultivation of bacteria and tumour cells for screening of antitumoral activity (259). Additionally, contained cultivation within capsules is

important for preventing the environmental release of genetically modified biosensors. Thus, spatial control of bacteria positioning alongside additional capsule coatings may provide high containment efficiencies necessary for such applications (53,105).

3.5 Conclusion

In conclusion, this chapter introduces a novel method for cell encapsulation and cultivation. The BEAD method, equipped with a novel automated pneumatic phase injection system and capillary mount, demonstrated the capability for nanolitre-precision injection of bacteria into the core of alginate beads. Contained cultivation of model bacteria within beads for at least two weeks was successfully demonstrated. Moreover, the method employs biocompatible encapsulation and recovery techniques, enabling the exploration of high-throughput cell cultivation in 3D environments. The development of the cultivation cassette allowed for high-throughput *in situ* cultivation of encapsulated bacteria, however, this was found not to significantly improve cultivation yield or isolate diversity and novelty, although differences in taxa presence were observed. Future work may focus on optimising BEAD performance and exploring applications within in situ cultivation, tissue culture, and drug screening. The findings provide further insights into in situ cultivation and present a versatile new cultivation methodology.

References

1. Louca S, Mazel F, Doebeli M, Parfrey LW. A census-based estimate of Earth's bacterial and archaeal diversity. *PLOS Biology*. 2019;17(2): e3000106. https://doi.org/10.1371/journal.pbio.3000106.
2. Reimer LC, Sardà Carbasse J, Koblitz J, Ebeling C, Podstawka A, Overmann J. BacDive in 2022: the knowledge base for standardized bacterial and archaeal data. *Nucleic Acids Research*. 2022;50(D1): D741–D746. https://doi.org/10.1093/nar/gkab961.
3. Razumov AS. The direct method of calculation of bacteria in water: comparison with the Koch method. *Mikrobiologija*. 1932;1: 131–146.
4. Winterberg H. Zur Methodik der Bakterienzählung. *Zeitschrift für Hygiene und Infektionskrankheiten*. 1898;29(1): 75–93. https://doi.org/10.1007/BF02217377.
5. Staley JT, Konopka A. Measurement of in situ activities of nonphotosynthetic microorganisms in aquatic and terrestrial habitats. *Annual review of microbiology*. 1985;39: 321–346. https://doi.org/10.1146/annurev.mi.39.100185.001541.
6. Overmann J, Abt B, Sikorski J. Present and Future of Culturing Bacteria. *Annual Review of Microbiology*. 2017;71(1): 711–730. https://doi.org/10.1146/annurev-micro-090816-093449.
7. Rappé MS, Connon SA, Vergin KL, Giovannoni SJ. Cultivation of the ubiquitous SAR11 marine bacterioplankton clade. *Nature*. 2002;418(6898): 630–633. https://doi.org/10.1038/nature00917.
8. Dewi Puspita I, Kamagata Y, Tanaka M, Asano K, Nakatsu CH. Are Uncultivated Bacteria Really Uncultivable? *Microbes and Environments*. 2012;27(4): 356–366. https://doi.org/10.1264/jsme2.ME12092.
9. Steen AD, Crits-Christoph A, Carini P, DeAngelis KM, Fierer N, Lloyd KG, et al. High proportions of bacteria and archaea across most biomes remain uncultured. *The ISME Journal*. 2019;13(12): 3126–3130. https://doi.org/10.1038/s41396-019-0484-y.
10. Joseph SJ, Hugenholtz P, Sangwan P, Osborne CA, Janssen PH. Laboratory Cultivation of Widespread and PreviouslyUncultured SoilBacteria. *Applied and Environmental Microbiology*. 2003;69(12): 7210–7215. https://doi.org/10.1128/AEM.69.12.7210-7215.2003.
11. Nichols D, Cahoon N, Trakhtenberg EM, Pham L, Mehta A, Belanger A, et al. Use of Ichip for High-Throughput In Situ Cultivation of "Uncultivable" Microbial Species. *Applied and Environmental Microbiology*. 2010;76(8): 2445–2450. https://doi.org/10.1128/AEM.01754-09.
12. Amann RI, Ludwig W, Schleifer KH. Phylogenetic identification and in situ detection of individual microbial cells without cultivation. *Microbiological Reviews*. 1995;59(1): 143–169. https://doi.org/10.1128/mr.59.1.143-169.1995.
13. Ling LL, Schneider T, Peoples AJ, Spoering AL, Engels I, Conlon BP, et al. A new antibiotic kills pathogens without detectable resistance. *Nature*. 2015;517(7535): 455–459. https://doi.org/10.1038/nature14098.
14. Ferrari BC, Binnerup SJ, Gillings M. Microcolony Cultivation on a Soil Substrate Membrane System Selects for Previously Uncultured Soil Bacteria. *Applied and Environmental Microbiology*. 2005;71(12): 8714–8720. https://doi.org/10.1128/AEM.71.12.8714-8720.2005.
15. Chaudhary DK, Khulan A, Kim J. Development of a novel cultivation technique for uncultured soil bacteria. *Scientific Reports*. 2019;9(1): 6666. https://doi.org/10.1038/s41598-019-43182-x.

16. Takahiro M, Koichi W, Junji F, Yukiko M, Toshihiko T, Kazumasa M, et al. Development of 16S rRNA-Gene-Targeted Group-Specific Primers for the Detection and Identification of Predominant Bacteria in Human Feces. *Applied and Environmental Microbiology*. 2002;68(11): 5445–5451. https://doi.org/10.1128/AEM.68.11.5445-5451.2002.
17. Lester ED, Satomi M, Ponce A. Microflora of extreme arid Atacama Desert soils. *Soil Biology and Biochemistry*. 2007;39(2): 704–708. https://doi.org/https://doi.org/10.1016/j.soilbio.2006.09.020.
18. Martiny AC. High proportions of bacteria are culturable across major biomes. *The ISME Journal*. 2019;13(8): 2125–2128. https://doi.org/10.1038/s41396-019-0410-3.
19. Schloss PD, Girard RA, Martin T, Edwards J, Thrash JC. Status of the Archaeal and Bacterial Census: an Update. *mBio*. 2016;7(3). https://doi.org/10.1128/mBio.00201-16.
20. Blevins SM, Bronze MS. Robert Koch and the 'golden age' of bacteriology. *International Journal of Infectious Diseases*. 2010;14(9): e744–e751. https://doi.org/10.1016/j.ijid.2009.12.003.
21. Reasoner DJ, Geldreich EE. A new medium for the enumeration and subculture of bacteria from potable water. *Applied and Environmental Microbiology*. 1985;49(1): 1–7. https://doi.org/10.1128/aem.49.1.1-7.1985.
22. Connon S, Giovannoni S. High-Throughput Methods for Culturing Microorganisms in Very-Low-Nutrient Media Yield Diverse New Marine Isolates. *Applied and Environmental Microbiology*. 2002;68(8): 3878–3885. https://doi.org/10.1128/AEM.68.8.3878-3885.2002.
23. Bonnet M, Lagier JC, Raoult D, Khelaifia S. Bacterial culture through selective and non-selective conditions: the evolution of culture media in clinical microbiology. *New Microbes and New Infections*. 2020;34: 100622. https://doi.org/10.1016/j.nmni.2019.100622.
24. Nichols D, Lewis K, Orjala J, Mo S, Ortenberg R, O'Connor P, et al. Short Peptide Induces an "Uncultivable" Microorganism To Grow In Vitro. *Applied and Environmental Microbiology*. 2008;74(15): 4889–4897. https://doi.org/10.1128/AEM.00393-08.
25. Bruns A, Cypionka H, Overmann J. Cyclic AMP and Acyl Homoserine Lactones Increase the Cultivation Efficiency of Heterotrophic Bacteria from the Central Baltic Sea. *Applied and Environmental Microbiology*. 2002;68(8): 3978–3987. https://doi.org/10.1128/AEM.68.8.3978-3987.2002.
26. Davis KER, Joseph SJ, Janssen PH. Effects of Growth Medium, Inoculum Size, and Incubation Time on Culturability and Isolation of Soil Bacteria. *Applied and Environmental Microbiology*. 2005;71(2): 826–834. https://doi.org/10.1128/AEM.71.2.826-834.2005.
27. Browne HP, Forster SC, Anonye BO, Kumar N, Neville BA, Stares MD, et al. Culturing of 'unculturable' human microbiota reveals novel taxa and extensive sporulation. *Nature*. 2016;533(7604): 543–546. https://doi.org/10.1038/nature17645.
28. Connon SA, Giovannoni SJ. High-Throughput Methods for Culturing Microorganisms in Very-Low-Nutrient Media Yield Diverse New Marine Isolates. *Applied and Environmental Microbiology*. 2002;68(8): 3878–3885. https://doi.org/10.1128/AEM.68.8.3878-3885.2002.
29. Nguyen TM, Seo C, Ji M, Paik MJ, Myung SW, Kim J. Effective Soil Extraction Method for Cultivating Previously Uncultured Soil Bacteria. *Applied and Environmental Microbiology*. 2018;84(24). https://doi.org/10.1128/AEM.01145-18.

30. Liebeke M, Brözel VS, Hecker M, Lalk M. Chemical characterization of soil extract as growth media for the ecophysiological study of bacteria. *Applied Microbiology and Biotechnology*. 2009;83(1): 161–173. https://doi.org/10.1007/s00253-009-1965-0.
31. Nakamura K, Tamaki H, Kang MS, Mochimaru H, Lee ST, Nakamura K, et al. A Six-well Plate Method: Less Laborious and Effective Method for Cultivation of Obligate Anaerobic Microorganisms. *Microbes and Environments*. 2011;26(4): 301–306. https://doi.org/10.1264/jsme2.ME11120.
32. Eilers H, Pernthaler J, Glöckner FO, Amann R. Culturability and In Situ Abundance of Pelagic Bacteria from the North Sea. *Applied and Environmental Microbiology*. 2000;66(7): 3044–3051. https://doi.org/10.1128/AEM.66.7.3044-3051.2000.
33. Roesch LFW, Fulthorpe RR, Riva A, Casella G, Hadwin AKM, Kent AD, et al. Pyrosequencing enumerates and contrasts soil microbial diversity. *The ISME Journal*. 2007;1(4): 283–290. https://doi.org/10.1038/ismej.2007.53.
34. Button DK, Schut F, Quang P, Martin R, Robertson BR. Viability and Isolation of Marine Bacteria by Dilution Culture: Theory, Procedures, and Initial Results. *Applied and Environmental Microbiology*. 1993;59(3): 881–891. https://doi.org/10.1128/aem.59.3.881-891.1993.
35. Song J, Oh HM, Cho JC. Improved culturability of SAR11 strains in dilution-to-extinction culturing from the East Sea, West Pacific Ocean. *FEMS Microbiology Letters*. 2009;295(2): 141–147. https://doi.org/10.1111/j.1574-6968.2009.01623.x.
36. Ma L, Kim J, Hatzenpichler R, Karymov MA, Hubert N, Hanan IM, et al. Gene-targeted microfluidic cultivation validated by isolation of a gut bacterium listed in Human Microbiome Project's Most Wanted taxa. *Proceedings of the National Academy of Sciences*. 2014;111(27): 9768–9773. https://doi.org/10.1073/pnas.1404753111.
37. Mahler L, Niehs SP, Martin K, Weber T, Scherlach K, Hertweck C, et al. Highly parallelized droplet cultivation and prioritization of antibiotic producers from natural microbial communities. Kana BD, Dhar N, Sclavi B (eds.) *eLife*. 2021;10: e64774. https://doi.org/10.7554/eLife.64774.
38. Akselband Y, Cabral C, Castor TP, Chikarmane HM, McGrath P. Enrichment of slow-growing marine microorganisms from mixed cultures using gel microdrop (GMD) growth assay and fluorescence-activated cell sorting. *Journal of Experimental Marine Biology and Ecology*. 2006;329(2): 196–205. https://doi.org/https://doi.org/10.1016/j.jembe.2005.08.018.
39. Alke B, Ulrich N, Heribert C, Jörg O. Effect of Signal Compounds and Incubation Conditions on the Culturability of Freshwater Bacterioplankton. *Applied and Environmental Microbiology*. 2003;69(4): 1980–1989. https://doi.org/10.1128/AEM.69.4.1980-1989.2003.
40. Nichols D, Lewis K, Orjala J, Mo S, Ortenberg R, O'Connor P, et al. Short Peptide Induces an "Uncultivable" Microorganism To Grow In Vitro. *Applied and Environmental Microbiology*. 2008;74(15): 4889–4897. https://doi.org/10.1128/AEM.00393-08.
41. OHNO M, OKANO I, WATSUJI T o, KAKINUMA T, UEDA K, BEPPU T. Establishing the Independent Culture of a Strictly Symbiotic Bacterium Symbiobacterium thermophilum from Its Supporting Bacillus Strain. *Bioscience, Biotechnology, and Biochemistry*. 1999;63(6): 1083–1090. https://doi.org/10.1271/bbb.63.1083.
42. Foster KR, Bell T. Competition, Not Cooperation, Dominates Interactions among Culturable Microbial Species. *Current Biology*. 2012;22(19): 1845–1850. https://doi.org/10.1016/j.cub.2012.08.005.

43. Coyte KZ, Schluter J, Foster KR. The ecology of the microbiome: Networks, competition, and stability. *Science*. 2015;350(6261): 663–666. https://doi.org/10.1126/science.aad2602.
44. Jackson R, Monnin D, Patapiou PA, Golding G, Helanterä H, Oettler J, et al. Convergent evolution of a labile nutritional symbiosis in ants. *The ISME Journal*. 2022;16(9): 2114–2122. https://doi.org/10.1038/s41396-022-01256-1.
45. Marmann A, Aly A, Lin W, Wang B, Proksch P. Co-Cultivation—A Powerful Emerging Tool for Enhancing the Chemical Diversity of Microorganisms. *Marine Drugs*. 2014;12(2): 1043–1065. https://doi.org/10.3390/md12021043.
46. Kaeberlein T, Lewis K, Epstein SS. Isolating 'Uncultivable' Microorganisms in Pure Culture in a Simulated Natural Environment. *Science*. 2002;296(5570): 1127–1129. https://doi.org/10.1126/science.1070633.
47. Ledford H. Promising antibiotic discovered in microbial 'dark matter'. *Nature*. 2015; https://doi.org/10.1038/nature.2015.16675.
48. Aoi Y, Kinoshita T, Hata T, Ohta H, Obokata H, Tsuneda S. Hollow-Fiber Membrane Chamber as a Device for In Situ Environmental Cultivation. *Applied and Environmental Microbiology*. 2009;75(11): 3826–3833. https://doi.org/10.1128/AEM.02542-08.
49. Alkayyali T, Pope E, Wheatley SK, Cartmell C, Haltli B, Kerr RG, et al. Development of a microbe domestication pod (MD Pod) for in situ cultivation of micro-encapsulated marine bacteria. *Biotechnology and Bioengineering*. 2021;118(3): 1166–1176. https://doi.org/10.1002/bit.27633.
50. Pope E, Cartmell C, Haltli B, Ahmadi A, Kerr RG. Microencapsulation and in situ incubation methodology for the cultivation of marine bacteria. *Frontiers in Microbiology*. 2022;13. https://doi.org/10.3389/fmicb.2022.958660.
51. Pope E, Cartmell C, Haltli B, Ahmadi A, Kerr RG. Microencapsulation and in situ incubation methodology for the cultivation of marine bacteria. *Frontiers in Microbiology*. 2022;13. https://doi.org/10.3389/fmicb.2022.958660.
52. Zengler K, Toledo G, Rappé M, Elkins J, Mathur EJ, Short JM, et al. Cultivating the uncultured. *Proceedings of the National Academy of Sciences*. 2002;99(24): 15681–15686. https://doi.org/10.1073/pnas.252630999.
53. Ben-Dov E, Kramarsky-Winter E, Kushmaro A. An in situ method for cultivating microorganisms using a double encapsulation technique. *FEMS Microbiology Ecology*. 2009;68(3): 363–371. https://doi.org/10.1111/j.1574-6941.2009.00682.x.
54. Usman H, Davidson SL, Manimaran NH, Nguyen JT, Bah A, Seth R, et al. Design of a well-defined poly(dimethylsiloxane)-based microbial nanoculture system. *Materials Today Communications*. 2021;27: 102185. https://doi.org/10.1016/j.mtcomm.2021.102185.
55. Davidson SL, Niepa THR. Controlling Microbial Dynamics through Selective Solute Transport across Functional Nanocultures. *ACS Applied Polymer Materials*. 2022;4(5): 2999–3012. https://doi.org/10.1021/acsapm.1c01422.
56. Ben-Dov E, Kramarsky-Winter E, Kushmaro A. An in situ method for cultivating microorganisms using a double encapsulation technique. *FEMS Microbiology Ecology*. 2009;68(3): 363–371. https://doi.org/10.1111/j.1574-6941.2009.00682.x.
57. Usman H, Davidson SL, Manimaran NH, Nguyen JT, Bah A, Seth R, et al. Design of a well-defined poly(dimethylsiloxane)-based microbial nanoculture system. *Materials Today Communications*. 2021;27: 102185. https://doi.org/10.1016/j.mtcomm.2021.102185.

58. Murray CJ, Ikuta KS, Sharara F, Swetschinski L, Robles Aguilar G, Gray A, et al. Global burden of bacterial antimicrobial resistance in 2019: a systematic analysis. *The Lancet*. 2022;399(10325): 629–655. https://doi.org/10.1016/S0140-6736(21)02724-0.
59. Miethke M, Pieroni M, Weber T, Brönstrup M, Hammann P, Halby L, et al. Towards the sustainable discovery and development of new antibiotics. *Nature Reviews Chemistry*. 2021;5(10): 726–749. https://doi.org/10.1038/s41570-021-00313-1.
60. Crits-Christoph A, Diamond S, Butterfield CN, Thomas BC, Banfield JF. Novel soil bacteria possess diverse genes for secondary metabolite biosynthesis. *Nature*. 2018;558(7710): 440–444. https://doi.org/10.1038/s41586-018-0207-y.
61. Lewis K, Epstein S, D'Onofrio A, Ling LL. Uncultured microorganisms as a source of secondary metabolites. *The Journal of Antibiotics*. 2010;63(8): 468–476. https://doi.org/10.1038/ja.2010.87.
62. Hover BM, Kim SH, Katz M, Charlop-Powers Z, Owen JG, Ternei MA, et al. Culture-independent discovery of the malacidins as calcium-dependent antibiotics with activity against multidrug-resistant Gram-positive pathogens. *Nature Microbiology*. 2018;3(4): 415–422. https://doi.org/10.1038/s41564-018-0110-1.
63. Bódalo A, Bastida J, Gómez JL, Gómez E, Alcaraz I, Asanza ML. Stabilization studies of l-aminoacylase-producing Pseudomonas sp. BA2 immobilized in calcium alginate gel. *Enzyme and Microbial Technology*. 1997;21(1): 64–69. https://doi.org/https://doi.org/10.1016/S0141-0229(96)00227-X.
64. Qin L, Li C, Li X, Zhang X, Shen C, Meng Q, et al. Confined encapsulation of living cells in self-assembled fiber macrospheres with micro/nanoporous polymer shells for the transformation of contaminants to green energy. *Journal of Materials Chemistry A*. 2020;8(4): 1929–1938. https://doi.org/10.1039/C9TA11252A.
65. Wu S, Wang L, Fang Y, Huang H, You X, Wu J. Advances in Encapsulation and Delivery Strategies for Islet Transplantation. *Advanced Healthcare Materials*. 2021;10(20): 2100965. https://doi.org/https://doi.org/10.1002/adhm.202100965.
66. Alkayyali T, Cameron T, Haltli B, Kerr RG, Ahmadi A. Microfluidic and cross-linking methods for encapsulation of living cells and bacteria - A review. *Analytica Chimica Acta*. 2019;1053: 1–21. https://doi.org/10.1016/j.aca.2018.12.056.
67. Gasperini L, Mano JF, Reis RL. Natural polymers for the microencapsulation of cells. *Journal of The Royal Society Interface*. 2014;11(100): 20140817. https://doi.org/10.1098/rsif.2014.0817.
68. Ekerdt BL, Fuentes CM, Lei Y, Adil MM, Ramasubramanian A, Segalman RA, et al. Thermoreversible Hyaluronic Acid-PNIPAAm Hydrogel Systems for 3D Stem Cell Culture. *Advanced Healthcare Materials*. 2018;7(12): 1800225. https://doi.org/https://doi.org/10.1002/adhm.201800225.
69. Pope E, Haltli B, Kerr RG, Ahmadi A. Effects of Matrix Composition and Temperature on Viability and Metabolic Activity of Microencapsulated Marine Bacteria. *Microorganisms*. 2022;10(5): 996. https://doi.org/10.3390/microorganisms10050996.
70. Duarte JM, Barbier I, Schaerli Y. Bacterial Microcolonies in Gel Beads for High-Throughput Screening of Libraries in Synthetic Biology. *ACS Synthetic Biology*. 2017;6(11): 1988–1995. https://doi.org/10.1021/acssynbio.7b00111.
71. Buffi N, Merulla D, Beutier J, Barbaud F, Beggah S, van Lintel H, et al. Development of a microfluidics biosensor for agarose-bead immobilized Escherichia coli bioreporter cells for arsenite detection in aqueous samples. *Lab on a Chip*. 2011;11(14): 2369–2377. https://doi.org/10.1039/C1LC20274J.

72. Mørch ÝA, Donati I, Strand BL, Skjåk-Bræk G. Effect of Ca2+, Ba2+, and Sr2+ on Alginate Microbeads. *Biomacromolecules*. 2006;7(5): 1471–1480. https://doi.org/10.1021/bm060010d.
73. Simó G, Fernández-Fernández E, Vila-Crespo J, Ruipérez V, Rodríguez-Nogales JM. Research progress in coating techniques of alginate gel polymer for cell encapsulation. *Carbohydrate Polymers*. 2017;170: 1–14. https://doi.org/https://doi.org/10.1016/j.carbpol.2017.04.013.
74. Lee KY, Mooney DJ. Alginate: Properties and biomedical applications. *Progress in Polymer Science*. 2012;37(1): 106–126. https://doi.org/10.1016/j.progpolymsci.2011.06.003.
75. Wong TY, Preston LA, Schiller NL. Alginate Lyase: Review of Major Sources and Enzyme Characteristics, Structure-Function Analysis, Biological Roles, and Applications. *Annual Review of Microbiology*. 2000;54(1): 289–340. https://doi.org/10.1146/annurev.micro.54.1.289.
76. Gadziński P, Froelich A, Jadach B, Wojtyłko M, Tatarek A, Białek A, et al. Ionotropic Gelation and Chemical Crosslinking as Methods for Fabrication of Modified-Release Gellan Gum-Based Drug Delivery Systems. *Pharmaceutics*. 2022;15(1): 108. https://doi.org/10.3390/pharmaceutics15010108.
77. Zhu K, Yu Y, Cheng Y, Tian C, Zhao G, Zhao Y. All-Aqueous-Phase Microfluidics for Cell Encapsulation. *ACS Applied Materials & Interfaces*. 2019;11(5): 4826–4832. https://doi.org/10.1021/acsami.8b19234.
78. Kim BJ, Park T, Moon HC, Park SY, Hong D, Ko EH, et al. Cytoprotective Alginate/Polydopamine Core/Shell Microcapsules in Microbial Encapsulation. *Angewandte Chemie International Edition*. 2014;53(52): 14443–14446. https://doi.org/10.1002/anie.201408454.
79. Baruch L, Machluf M. Alginate–chitosan complex coacervation for cell encapsulation: Effect on mechanical properties and on long-term viability. *Biopolymers*. 2006;82(6): 570–579. https://doi.org/https://doi.org/10.1002/bip.20509.
80. Choi JR, Yong KW, Choi JY, Cowie AC. Recent advances in photo-crosslinkable hydrogels for biomedical applications. *BioTechniques*. 2019;66(1): 40–53. https://doi.org/10.2144/btn-2018-0083.
81. Ma Y, Thiele J, Abdelmohsen L, Xu J, Huck WTS. Biocompatible macro-initiators controlling radical retention in microfluidic on-chip photo-polymerization of water-in-oil emulsions. *Chem. Commun.* 2014;50(1): 112–114. https://doi.org/10.1039/C3CC46733C.
82. Smeds KA, Pfister-Serres A, Miki D, Dastgheib K, Inoue M, Hatchell DL, et al. Photocrosslinkable polysaccharides for in situ hydrogel formation. *Journal of Biomedical Materials Research*. 2001;55(2): 254–255. https://doi.org/https://doi.org/10.1002/1097-4636(200105)55:2<254::AID-JBM1012>3.0.CO;2-5.
83. Al Rashid A, Ahmed W, Khalid MY, Koç M. Vat photopolymerization of polymers and polymer composites: Processes and applications. *Additive Manufacturing*. 2021;47: 102279. https://doi.org/https://doi.org/10.1016/j.addma.2021.102279.
84. Panda P, Ali S, Lo E, Chung BG, Hatton TA, Khademhosseini A, et al. Stop-flow lithography to generate cell-laden microgel particles. *Lab on a Chip*. 2008;8(7): 1056. https://doi.org/10.1039/b804234a.
85. Liu VA, Bhatia SN. Three-Dimensional Photopatterning of Hydrogels Containing Living Cells. *Biomedical Microdevices*. 2002;4(4): 257–266. https://doi.org/10.1023/A:1020932105236.

86. Xia B, Jiang Z, Debroy D, Li D, Oakey J. Cytocompatible cell encapsulation via hydrogel photopolymerization in microfluidic emulsion droplets. *Biomicrofluidics*. 2017;11(4): 044102. https://doi.org/10.1063/1.4993122.
87. Steinacher M, Cont A, Du H, Persat A, Amstad E. Monodisperse Selectively Permeable Hydrogel Capsules Made from Single Emulsion Drops. *ACS Applied Materials & Interfaces*. 2021;13(13): 15601–15609. https://doi.org/10.1021/acsami.1c00230.
88. Li P, Müller M, Chang MW, Frettlöh M, Schönherr H. Encapsulation of Autoinducer Sensing Reporter Bacteria in Reinforced Alginate-Based Microbeads. *ACS Applied Materials & Interfaces*. 2017;9(27): 22321–22331. https://doi.org/10.1021/acsami.7b07166.
89. Jiang Z, Xia B, McBride R, Oakey J. A microfluidic-based cell encapsulation platform to achieve high long-term cell viability in photopolymerized PEGNB hydrogel microspheres. *Journal of Materials Chemistry B*. 2017;5(1): 173–180. https://doi.org/10.1039/C6TB02551J.
90. Chi WJ, Chang YK, Hong SK. Agar degradation by microorganisms and agar-degrading enzymes. *Applied Microbiology and Biotechnology*. 2012;94(4): 917–930. https://doi.org/10.1007/s00253-012-4023-2.
91. Teh SY, Lin R, Hung LH, Lee AP. Droplet microfluidics. *Lab on a Chip*. 2008;8(2): 198. https://doi.org/10.1039/b715524g.
92. Durst CA, Cuchiara MP, Mansfield EG, West JL, Grande-Allen KJ. Flexural characterization of cell encapsulated PEGDA hydrogels with applications for tissue engineered heart valves. *Acta Biomaterialia*. 2011;7(6): 2467–2476. https://doi.org/https://doi.org/10.1016/j.actbio.2011.02.018.
93. Lee KG, Park TJ, Soo SY, Wang KW, Kim BII, Park JH, et al. Synthesis and utilization of E. coli-encapsulated PEG-based microdroplet using a microfluidic chip for biological application. *Biotechnology and Bioengineering*. 2010;107(4): 747–751. https://doi.org/https://doi.org/10.1002/bit.22861.
94. WISEMAN H, HALLIWELL B. Damage to DNA by reactive oxygen and nitrogen species: role in inflammatory disease and progression to cancer. *Biochemical Journal*. 1996;313(1): 17–29. https://doi.org/10.1042/bj3130017.
95. Lin CC, Raza A, Shih H. PEG hydrogels formed by thiol-ene photo-click chemistry and their effect on the formation and recovery of insulin-secreting cell spheroids. *Biomaterials*. 2011;32(36): 9685–9695. https://doi.org/https://doi.org/10.1016/j.biomaterials.2011.08.083.
96. Alkayyali T, Pope E, Wheatley SK, Cartmell C, Haltli B, Kerr RG, et al. Development of a microbe domestication pod (MD Pod) for in situ cultivation of micro-encapsulated marine bacteria. *Biotechnology and Bioengineering*. 2021;118(3): 1166–1176. https://doi.org/10.1002/bit.27633.
97. Liu T, Wang Y, Zhong W, Li B, Mequanint K, Luo G, et al. Biomedical Applications of Layer-by-Layer Self-Assembly for Cell Encapsulation: Current Status and Future Perspectives. *Advanced Healthcare Materials*. 2019;8(1): 1800939. https://doi.org/https://doi.org/10.1002/adhm.201800939.
98. Li W, Lei X, Feng H, Li B, Kong J, Xing M. Layer-by-Layer Cell Encapsulation for Drug Delivery: The History, Technique Basis, and Applications. *Pharmaceutics*. 2022;14(2): 297. https://doi.org/10.3390/pharmaceutics14020297.
99. Galogahi FM, Zhu Y, An H, Nguyen NT. Core-shell microparticles: Generation approaches and applications. *Journal of Science: Advanced Materials and Devices*. 2020;5(4): 417–435. https://doi.org/10.1016/j.jsamd.2020.09.001.

100. Coradin T, Nassif N, Livage J. Silica–alginate composites for microencapsulation. *Applied Microbiology and Biotechnology*. 2003;61(5): 429–434. https://doi.org/10.1007/s00253-003-1308-5.
101. Coradin T, Mercey E, Lisnard L, Livage J. Design of silica-coated microcapsules for bioencapsulation. *Chemical Communications*. 2001;(23): 2496–2497. https://doi.org/10.1039/B108324B.
102. Desmet J, Meunier CF, Danloy EP, Duprez ME, Hantson AL, Thomas D, et al. Green and sustainable production of high value compounds via a microalgae encapsulation technology that relies on CO_2 as a principle reactant. *J. Mater. Chem. A*. 2014;2(48): 20560–20569. https://doi.org/10.1039/C4TA04659E.
103. Kim BJ, Han S, Lee KB, Choi IS. Biphasic Supramolecular Self-Assembly of Ferric Ions and Tannic Acid across Interfaces for Nanofilm Formation. *Advanced Materials*. 2017;29(28): 1700784. https://doi.org/10.1002/adma.201700784.
104. Kim BJ, Park T, Moon HC, Park SY, Hong D, Ko EH, et al. Cytoprotective Alginate/Polydopamine Core/Shell Microcapsules in Microbial Encapsulation. *Angewandte Chemie International Edition*. 2014;53(52): 14443–14446. https://doi.org/https://doi.org/10.1002/anie.201408454.
105. Tang TC, Tham E, Liu X, Yehl K, Rovner AJ, Yuk H, et al. Hydrogel-based biocontainment of bacteria for continuous sensing and computation. *Nature Chemical Biology*. 2021;17(6): 724–731. https://doi.org/10.1038/s41589-021-00779-6.
106. Raj M K, Chakraborty S. PDMS microfluidics: A mini review. *Journal of Applied Polymer Science*. 2020;137(27): 48958. https://doi.org/10.1002/app.48958.
107. Christopher GF, Anna SL. Microfluidic methods for generating continuous droplet streams. *Journal of Physics D: Applied Physics*. 2007;40(19): R319–R336. https://doi.org/10.1088/0022-3727/40/19/R01.
108. Hardt S, Hahn T. Microfluidics with aqueous two-phase systems. *Lab Chip*. 2012;12(3): 434–442. https://doi.org/10.1039/C1LC20569B.
109. Mahler L, Tovar M, Weber T, Brandes S, Rudolph MM, Ehgartner J, et al. Enhanced and homogeneous oxygen availability during incubation of microfluidic droplets. *RSC Advances*. 2015;5(123): 101871–101878. https://doi.org/10.1039/C5RA20118G.
110. Nabavi SA, Vladisavljević GT, Gu S, Ekanem EE. Double emulsion production in glass capillary microfluidic device: Parametric investigation of droplet generation behaviour. *Chemical Engineering Science*. 2015;130: 183–196. https://doi.org/https://doi.org/10.1016/j.ces.2015.03.004.
111. Utada AS, Lorenceau E, Link DR, Kaplan PD, Stone HA, Weitz DA. Monodisperse Double Emulsions Generated from a Microcapillary Device. *Science*. 2005;308(5721): 537–541. https://doi.org/10.1126/science.1109164.
112. Mohamed M, Kumar H, Wang Z, Martin N, Mills B, Kim K. Rapid and Inexpensive Fabrication of Multi-Depth Microfluidic Device using High-Resolution LCD Stereolithographic 3D Printing. *Journal of Manufacturing and Materials Processing*. 2019;3(1): 26. https://doi.org/10.3390/jmmp3010026.
113. Morgan AJL, Hidalgo San Jose L, Jamieson WD, Wymant JM, Song B, Stephens P, et al. Simple and Versatile 3D Printed Microfluidics Using Fused Filament Fabrication. *PLOS ONE*. 2016;11(4): e0152023. https://doi.org/10.1371/journal.pone.0152023.
114. Rathore S, Desai PM, Liew CV, Chan LW, Heng PWS. Microencapsulation of microbial cells. *Journal of Food Engineering*. 2013;116(2): 369–381. https://doi.org/https://doi.org/10.1016/j.jfoodeng.2012.12.022.
115. Enayati M, Chang MW, Bragman F, Edirisinghe M, Stride E. Electrohydrodynamic preparation of particles, capsules and bubbles for biomedical engineering applications.

Colloids and Surfaces A: Physicochemical and Engineering Aspects. 2011;382(1): 154–164. https://doi.org/https://doi.org/10.1016/j.colsurfa.2010.11.038.
116. Prüße U, Bruske F, Breford J, Vorlop KD. Improvement of the Jet Cutting Method for the Preparation of Spherical Particles from Viscous Polymer Solutions. *Chemical Engineering & Technology*. 1998;21(2): 153–157. https://doi.org/https://doi.org/10.1002/(SICI)1521-4125(199802)21:2<153::AID-CEAT153>3.0.CO;2-8.
117. Huang SB, Wu MH, Lee GB. Microfluidic device utilizing pneumatic micro-vibrators to generate alginate microbeads for microencapsulation of cells. *Sensors and Actuators B: Chemical*. 2010;147(2): 755–764. https://doi.org/https://doi.org/10.1016/j.snb.2010.04.021.
118. Barron C, He JQ. Alginate-based microcapsules generated with the coaxial electrospray method for clinical application. *Journal of Biomaterials Science, Polymer Edition*. 2017;28(13): 1245–1255. https://doi.org/10.1080/09205063.2017.1318030.
119. Capel AJ, Rimington RP, Lewis MP, Christie SDR. 3D printing for chemical, pharmaceutical and biological applications. *Nature Reviews Chemistry*. 2018;2(12): 422–436. https://doi.org/10.1038/s41570-018-0058-y.
120. Dave HK, Patel ST. Introduction to Fused Deposition Modeling Based 3D Printing Process. In: Dave HK, Davim JP (eds.) *Fused Deposition Modeling Based 3D Printing*. Cham: Springer International Publishing; 2021. p. 1–21. https://doi.org/10.1007/978-3-030-68024-4_1.
121. Li F, Macdonald NP, Guijt RM, Breadmore MC. Increasing the functionalities of 3D printed microchemical devices by single material, multimaterial, and print-pause-print 3D printing. *Lab on a Chip*. 2019;19(1): 35–49. https://doi.org/10.1039/C8LC00826D.
122. Rajan K, Samykano M, Kadirgama K, Harun WSW, Rahman MdM. Fused deposition modeling: process, materials, parameters, properties, and applications. *The International Journal of Advanced Manufacturing Technology*. 2022;120(3): 1531–1570. https://doi.org/10.1007/s00170-022-08860-7.
123. Li F, Smejkal P, Macdonald NP, Guijt RM, Breadmore MC. One-Step Fabrication of a Microfluidic Device with an Integrated Membrane and Embedded Reagents by Multimaterial 3D Printing. *Analytical Chemistry*. 2017;89(8): 4701–4707. https://doi.org/10.1021/acs.analchem.7b00409.
124. DeStefano V, Khan S, Tabada A. Applications of PLA in modern medicine. *Engineered Regeneration*. 2020;1: 76–87. https://doi.org/https://doi.org/10.1016/j.engreg.2020.08.002.
125. Shilov SY, Rozhkova YA, Markova LN, Tashkinov MA, Vindokurov I V., Silberschmidt V V. Biocompatibility of 3D-Printed PLA, PEEK and PETG: Adhesion of Bone Marrow and Peritoneal Lavage Cells. *Polymers*. 2022;14(19): 3958. https://doi.org/10.3390/polym14193958.
126. Perez DB, Celik E, Karkkainen RL. Investigation of Interlayer Interface Strength and Print Morphology Effects in Fused Deposition Modeling 3D-Printed PLA. *3D Printing and Additive Manufacturing*. 2021;8(1): 23–32. https://doi.org/10.1089/3dp.2020.0109.
127. Raj SA, Muthukumaran E, Jayakrishna K. A Case Study of 3D Printed PLA and Its Mechanical Properties. *Materials Today: Proceedings*. 2018;5(5, Part 2): 11219–11226. https://doi.org/https://doi.org/10.1016/j.matpr.2018.01.146.
128. Suder J, Bobovsky Z, Mlotek J, Vocetka M, Zeman Z, Safar M. Experimental Analysis of Temperature Resistance Of 3d Printed PLA Components. *MM Science Journal*. 2021;2021(1): 4322–4327. https://doi.org/10.17973/MMSJ.2021_03_2021004.

129. Holcomb G, Caldona EB, Cheng X, Advincula RC. On the optimized 3D printing and post-processing of PETG materials. *MRS Communications*. 2022;12(3): 381–387. https://doi.org/10.1557/s43579-022-00188-3.
130. Coba Salcedo MF, Penaloza CA, Gomez GG. Experimental characterization of the mechanical properties of PETG and PA6 thermoplastics. *Contemporary Engineering Sciences*. 2018;11(76): 3771–3779. https://doi.org/10.12988/ces.2018.88369.
131. Petrov P, Agzamova D, Pustovalov V, Zhikhareva E, Saprykin B, Chmutin I, et al. Research into the effect of the 3D-printing mode on changing the properties of PETG transparent plastic. *ESAFORM 2021*. 2021; https://doi.org/10.25518/esaform21.3763.
132. Ramírez-Revilla S, Camacho-Valencia D, Gonzales-Condori EG, Márquez G. Evaluation and comparison of the degradability and compressive and tensile properties of 3D printing polymeric materials: PLA, PETG, PC, and ASA. *MRS Communications*. 2023;13(1): 55–62. https://doi.org/10.1557/s43579-022-00311-4.
133. Bertolino M, Battegazzore D, Arrigo R, Frache A. Designing 3D printable polypropylene: Material and process optimisation through rheology. *Additive Manufacturing*. 2021;40: 101944. https://doi.org/https://doi.org/10.1016/j.addma.2021.101944.
134. van Midwoud PM, Janse A, Merema MT, Groothuis GMM, Verpoorte E. Comparison of Biocompatibility and Adsorption Properties of Different Plastics for Advanced Microfluidic Cell and Tissue Culture Models. *Analytical Chemistry*. 2012;84(9): 3938–3944. https://doi.org/10.1021/ac300771z.
135. Dautzenberg P, Volk HA, Huels N, Cieciora L, Dohmen K, Lüpke M, et al. The effect of steam sterilization on different 3D printable materials for surgical use in veterinary medicine. *BMC Veterinary Research*. 2021;17(1): 389. https://doi.org/10.1186/s12917-021-03065-8.
136. Fischer KM, Howell AP. Reusability of autoclaved 3D printed polypropylene compared to a glass filled polypropylene composite. *3D Printing in Medicine*. 2021;7(1): 20. https://doi.org/10.1186/s41205-021-00111-x.
137. Diep TT, Ray PP, Edwards AD. Methods for rapid prototyping novel labware: using CAD and desktop 3D printing in the microbiology laboratory. *Letters in Applied Microbiology*. 2022;74(2): 247–257. https://doi.org/10.1111/lam.13615.
138. Amini A, Guijt RM, Themelis T, De Vos J, Eeltink S. Recent developments in digital light processing 3D-printing techniques for microfluidic analytical devices. *Journal of Chromatography A*. 2023;1692: 463842. https://doi.org/https://doi.org/10.1016/j.chroma.2023.463842.
139. Weiss I, Marom DM. Direct 3D nano-printing on optical fiber tip. In: *2015 International Conference on Optical MEMS and Nanophotonics (OMN)*. IEEE; 2015. p. 1–2. https://doi.org/10.1109/OMN.2015.7288865.
140. Lin Y, Gao C, Gritsenko D, Zhou R, Xu J. Soft lithography based on photolithography and two-photon polymerization. *Microfluidics and Nanofluidics*. 2018;22(9): 97. https://doi.org/10.1007/s10404-018-2118-5.
141. Ligon SC, Liska R, Stampfl J, Gurr M, Mülhaupt R. Polymers for 3D Printing and Customized Additive Manufacturing. *Chemical Reviews*. 2017;117(15): 10212–10290. https://doi.org/10.1021/acs.chemrev.7b00074.
142. Wang M, Li W, Hao J, Gonzales A, Zhao Z, Flores RS, et al. Molecularly cleavable bioinks facilitate high-performance digital light processing-based bioprinting of functional volumetric soft tissues. *Nature Communications*. 2022;13(1): 3317. https://doi.org/10.1038/s41467-022-31002-2.
143. Mao Q, Wang Y, Li Y, Juengpanich S, Li W, Chen M, et al. Fabrication of liver microtissue with liver decellularized extracellular matrix (dECM) bioink by digital

light processing (DLP) bioprinting. *Materials Science and Engineering: C*. 2020;109: 110625. https://doi.org/10.1016/j.msec.2020.110625.
144. Shen Y, Tang H, Huang X, Hang R, Zhang X, Wang Y, et al. DLP printing photocurable chitosan to build bio-constructs for tissue engineering. *Carbohydrate Polymers*. 2020;235: 115970. https://doi.org/https://doi.org/10.1016/j.carbpol.2020.115970.
145. Kadry H, Wadnap S, Xu C, Ahsan F. Digital light processing (DLP) 3D-printing technology and photoreactive polymers in fabrication of modified-release tablets. *European Journal of Pharmaceutical Sciences*. 2019;135: 60–67. https://doi.org/https://doi.org/10.1016/j.ejps.2019.05.008.
146. Knowlton S, Yu CH, Ersoy F, Emadi S, Khademhosseini A, Tasoglu S. 3D-printed microfluidic chips with patterned, cell-laden hydrogel constructs. *Biofabrication*. 2016;8(2): 025019. https://doi.org/10.1088/1758-5090/8/2/025019.
147. Bodenberger N, Paul P, Kubiczek D, Walther P, Gottschalk KE, Rosenau F. A Novel Cheap and Easy to Handle Protein Hydrogel for 3D Cell Culture Applications: A High Stability Matrix with Tunable Elasticity and Cell Adhesion Properties. *ChemistrySelect*. 2016;1(7): 1353–1360. https://doi.org/https://doi.org/10.1002/slct.201600206.
148. Schwartz JJ. Additive manufacturing: Frameworks for chemical understanding and advancement in vat photopolymerization. *MRS Bulletin*. 2022;47(6): 628–641. https://doi.org/10.1557/s43577-022-00343-0.
149. González G, Baruffaldi D, Martinengo C, Angelini A, Chiappone A, Roppolo I, et al. Materials Testing for the Development of Biocompatible Devices through Vat-Polymerization 3D Printing. *Nanomaterials*. 2020;10(9): 1788. https://doi.org/10.3390/nano10091788.
150. Urrios A, Parra-Cabrera C, Bhattacharjee N, Gonzalez-Suarez AM, Rigat-Brugarolas LG, Nallapatti U, et al. 3D-printing of transparent bio-microfluidic devices in PEG-DA. *Lab on a Chip*. 2016;16(12): 2287–2294. https://doi.org/10.1039/C6LC00153J.
151. Guttridge C, Shannon A, O'Sullivan A, O'Sullivan KJ, O'Sullivan LW. Biocompatible 3D printing resins for medical applications: A review of marketed intended use, biocompatibility certification, and post-processing guidance. *Annals of 3D Printed Medicine*. 2022;5: 100044. https://doi.org/https://doi.org/10.1016/j.stlm.2021.100044.
152. Rengarajan V, Clyde A, Pontsler J, Valiente J, Peel A, Huang Y. Assessing Leachable Cytotoxicity of 3D-Printed Polymers and Facile Detoxification Methods. *3D Printing and Additive Manufacturing*. 2022; https://doi.org/10.1089/3dp.2021.0216.
153. Zhu F, Friedrich T, Nugegoda D, Kaslin J, Wlodkowic D. Assessment of the biocompatibility of three-dimensional-printed polymers using multispecies toxicity tests. *Biomicrofluidics*. 2015;9(6): 061103. https://doi.org/10.1063/1.4939031.
154. Goh CBS, Goh CHP, Wong LW, Cheng WT, Yule CM, Ong KS, et al. A three-dimensional (3D) printing approach to fabricate an isolation chip for high throughput in situ cultivation of environmental microbes. *Lab on a Chip*. 2022;22(2): 387–402. https://doi.org/10.1039/D1LC00723H.
155. Dupard SJ, Garcia AG, Bourgine PE. Customizable 3D printed perfusion bioreactor for the engineering of stem cell microenvironments. *Frontiers in Bioengineering and Biotechnology*. 2023;10. https://doi.org/10.3389/fbioe.2022.1081145.
156. Subbarao C V, Srinivasa Reddy Y, Inturi V, Indra Reddy M. Dynamic Mechanical Analysis of 3D Printed PETG Material. *IOP Conference Series: Materials Science and Engineering*. 2021;1057(1): 012031. https://doi.org/10.1088/1757-899X/1057/1/012031.

157. Shumeiko V, Hidas G, Nowogrodski C, Pinto Y, Gofrit O, Duvdevani M, et al. BactoSpin: Novel Technology for Rapid Bacteria Detection and Antibiotic Susceptibility Testing. *Sensors*. 2021;21(17): 5902. https://doi.org/10.3390/s21175902.
158. Romanov V, Samuel R, Chaharlang M, Jafek AR, Frost A, Gale BK. FDM 3D Printing of High-Pressure, Heat-Resistant, Transparent Microfluidic Devices. *Analytical Chemistry*. 2018;90(17): 10450–10456. https://doi.org/10.1021/acs.analchem.8b02356.
159. Peterson AM. Review of acrylonitrile butadiene styrene in fused filament fabrication: A plastics engineering-focused perspective. *Additive Manufacturing*. 2019;27: 363–371. https://doi.org/https://doi.org/10.1016/j.addma.2019.03.030.
160. Li D, Wang S. Acrylonitrile–Butadiene–Styrene (ABS) Polymers. In: *Kirk-Othmer Encyclopedia of Chemical Technology*. Wiley; 2021. p. 1–27. https://doi.org/10.1002/0471238961.01021911211209.a01.pub3.
161. Tiganis BE, Burn LS, Davis P, Hill AJ. Thermal degradation of acrylonitrile–butadiene–styrene (ABS) blends. *Polymer Degradation and Stability*. 2002;76(3): 425–434. https://doi.org/https://doi.org/10.1016/S0141-3910(02)00045-9.
162. Ramian J, Ramian J, Dziob D. Thermal Deformations of Thermoplast during 3D Printing: Warping in the Case of ABS. *Materials*. 2021;14(22): 7070. https://doi.org/10.3390/ma14227070.
163. Costa PF, Hutmacher DW, Theodoropoulos C, Gomes ME, Reis RL, Vaquette C. Additively Manufactured Device for Dynamic Culture of Large Arrays of 3D Tissue Engineered Constructs. *Advanced Healthcare Materials*. 2015;4(6): 864–873. https://doi.org/https://doi.org/10.1002/adhm.201400591.
164. Dogan SK, Boyacioglu S, Kodal M, Gokce O, Ozkoc G. Thermally induced shape memory behavior, enzymatic degradation and biocompatibility of PLA/TPU blends: "Effects of compatibilization". *Journal of the Mechanical Behavior of Biomedical Materials*. 2017;71: 349–361. https://doi.org/https://doi.org/10.1016/j.jmbbm.2017.04.001.
165. Nelson MD, Ramkumar N, Gale BK. Flexible, transparent, sub-100 µm microfluidic channels with fused deposition modeling 3D-printed thermoplastic polyurethane. *Journal of Micromechanics and Microengineering*. 2019;29(9): 095010. https://doi.org/10.1088/1361-6439/ab2f26.
166. Luchini K, Sloan SNB, Mauro R, Sargsyan A, Newman A, Persaud P, et al. Sterilization and sanitizing of 3D-printed personal protective equipment using polypropylene and a Single Wall design. *3D Printing in Medicine*. 2021;7(1): 16. https://doi.org/10.1186/s41205-021-00106-8.
167. Woishnis W, Ebnesajjad S. *Chemical Resistance of Thermoplastics*. Elsevier; 2012. https://doi.org/10.1016/C2010-1-68838-4.
168. Riester O, Laufer S, Deigner HP. Direct 3D printed biocompatible microfluidics: assessment of human mesenchymal stem cell differentiation and cytotoxic drug screening in a dynamic culture system. *Journal of Nanobiotechnology*. 2022;20(1): 540. https://doi.org/10.1186/s12951-022-01737-7.
169. Ilyas RA, Sapuan SM, Harussani MM, Hakimi MYAY, Haziq MZM, Atikah MSN, et al. Polylactic Acid (PLA) Biocomposite: Processing, Additive Manufacturing and Advanced Applications. *Polymers*. 2021;13(8). https://doi.org/10.3390/polym13081326.
170. You J, Preen RJ, Bull L, Greenman J, Ieropoulos I. 3D printed components of microbial fuel cells: Towards monolithic microbial fuel cell fabrication using additive layer manufacturing. *Sustainable Energy Technologies and Assessments*. 2017;19: 94–101. https://doi.org/https://doi.org/10.1016/j.seta.2016.11.006.

171. Balakrishnan HK, Doeven EH, Merenda A, Dumée LF, Guijt RM. 3D printing for the integration of porous materials into miniaturised fluidic devices: A review. *Analytica Chimica Acta*. 2021;1185: 338796. https://doi.org/https://doi.org/10.1016/j.aca.2021.338796.
172. Oberoi G, Nitsch S, Janjić K, Shokoohi-Tabrizi H, Moritz A, Moscato F, et al. The impact of 3D-printed LAY-FOMM 40 and LAY-FOMM 60 on L929 cells and human oral fibroblasts. *Clinical Oral Investigations*. 2021;25(4): 1869–1877. https://doi.org/10.1007/s00784-020-03491-2.
173. Beauchamp MJ, Nordin GP, Woolley AT. Moving from millifluidic to truly microfluidic sub-100-µm cross-section 3D printed devices. *Analytical and Bioanalytical Chemistry*. 2017;409(18): 4311–4319. https://doi.org/10.1007/s00216-017-0398-3.
174. Kreß S, Schaller-Ammann R, Feiel J, Priedl J, Kasper C, Egger D. 3D Printing of Cell Culture Devices: Assessment and Prevention of the Cytotoxicity of Photopolymers for Stereolithography. *Materials*. 2020;13(13). https://doi.org/10.3390/ma13133011.
175. Oskui SM, Diamante G, Liao C, Shi W, Gan J, Schlenk D, et al. Assessing and Reducing the Toxicity of 3D-Printed Parts. *Environmental Science & Technology Letters*. 2016;3(1): 1–6. https://doi.org/10.1021/acs.estlett.5b00249.
176. Männel MJ, Fischer C, Thiele J. A Non-Cytotoxic Resin for Micro-Stereolithography for Cell Cultures of HUVECs. *Micromachines*. 2020;11(3). https://doi.org/10.3390/mi11030246.
177. Fu J, Shi L, Yuan S, Zhong Q, Zhang D, Chen Y, et al. Morphology, toughness mechanism, and thermal properties of hyperbranched epoxy modified diglycidyl ether of bisphenol A (DGEBA) interpenetrating polymer networks. *Polymers for Advanced Technologies*. 2008;19(11): 1597–1607. https://doi.org/10.1002/pat.1175.
178. Yang Y, He X, Shi J, Hickel R, Reichl FX, Högg C. Effects of antioxidants on DNA double-strand breaks in human gingival fibroblasts exposed to dental resin co-monomer epoxy metabolites. *Dental Materials*. 2017;33(4): 418–426. https://doi.org/https://doi.org/10.1016/j.dental.2017.01.005.
179. Peerzada M, Abbasi S, Lau KT, Hameed N. Additive Manufacturing of Epoxy Resins: Materials, Methods, and Latest Trends. *Industrial & Engineering Chemistry Research*. 2020;59(14): 6375–6390. https://doi.org/10.1021/acs.iecr.9b06870.
180. Wilhelm E, Neumann C, Sachsenheimer K, Schmitt T, Länge K, Rapp BE. Rapid bonding of polydimethylsiloxane to stereolithographically manufactured epoxy components using a photogenerated intermediary layer. *Lab on a Chip*. 2013;13(12): 2268. https://doi.org/10.1039/c3lc50341k.
181. Kim Y, Castro K, Bhattacharjee N, Folch A. Digital Manufacturing of Selective Porous Barriers in Microchannels Using Multi-Material Stereolithography. *Micromachines*. 2018;9(3): 125. https://doi.org/10.3390/mi9030125.
182. Kang K, Oh S, Yi H, Han S, Hwang Y. Fabrication of truly 3D microfluidic channel using 3D-printed soluble mold. *Biomicrofluidics*. 2018;12(1): 014105. https://doi.org/10.1063/1.5012548.
183. Gong H, Woolley AT, Nordin GP. High density 3D printed microfluidic valves, pumps, and multiplexers. *Lab on a Chip*. 2016;16(13): 2450–2458. https://doi.org/10.1039/C6LC00565A.
184. Wang Z, Martin N, Hini D, Mills B, Kim K. Rapid Fabrication of Multilayer Microfluidic Devices Using the Liquid Crystal Display-Based Stereolithography 3D Printing System. *3D Printing and Additive Manufacturing*. 2017;4(3): 156–164. https://doi.org/10.1089/3dp.2017.0028.

185. Wilson L, Iqbal KM, Simmons-Ehrhardt T, Bertino MF, Shah MR, Yadavalli VK, et al. Customizable 3D printed diffusion chambers for studies of bacterial pathogen phenotypes in complex environments. *Journal of Microbiological Methods*. 2019;162: 8–15. https://doi.org/https://doi.org/10.1016/j.mimet.2019.05.002.
186. Dogan AA, Dufva M. Customized 3D-printed stackable cell culture inserts tailored with bioactive membranes. *Scientific Reports*. 2022;12(1): 3694. https://doi.org/10.1038/s41598-022-07739-7.
187. Yuen PK. Embedding objects during 3D printing to add new functionalities. *Biomicrofluidics*. 2016;10(4): 044104. https://doi.org/10.1063/1.4958909.
188. Neches RY, Flynn KJ, Zaman L, Tung E, Pudlo N. On the intrinsic sterility of 3D printing. *PeerJ*. 2016;4: e2661. https://doi.org/10.7717/peerj.2661.
189. Durkan R, Gürbüz A, Yilmaz B, Özel MB, Bağış B. Effect of Autoclave Postpolymerization Treatments on the Fracture Toughness of Autopolymerizing Dental Acrylic Resins. *Journal of Applied Biomaterials & Functional Materials*. 2012;10(1): 37–42. https://doi.org/10.5301/JABFM.2012.9271.
190. Sharma N, Cao S, Msallem B, Kunz C, Brantner P, Honigmann P, et al. Effects of Steam Sterilization on 3D Printed Biocompatible Resin Materials for Surgical Guides—An Accuracy Assessment Study. *Journal of Clinical Medicine*. 2020;9(5): 1506. https://doi.org/10.3390/jcm9051506.
191. Told R, Ujfalusi Z, Pentek A, Kerenyi M, Banfai K, Vizi A, et al. A state-of-the-art guide to the sterilization of thermoplastic polymers and resin materials used in the additive manufacturing of medical devices. *Materials & Design*. 2022;223: 111119. https://doi.org/https://doi.org/10.1016/j.matdes.2022.111119.
192. Azevedo NF, Bragança SM, Simões LC, Cerqueira L, Almeida C, Keevil CW, et al. Proposal for a method to estimate nutrient shock effects in bacteria. *BMC Research Notes*. 2012;5(1): 422. https://doi.org/10.1186/1756-0500-5-422.
193. Hahn MW, Stadler P, Wu QL, Pöckl M. The filtration–acclimatization method for isolation of an important fraction of the not readily cultivable bacteria. *Journal of Microbiological Methods*. 2004;57(3): 379–390. https://doi.org/10.1016/j.mimet.2004.02.004.
194. Olsen RA, Bakken LR. Viability of Soil Bacteria: Optimization of Plate-Counting Technique and Comparison between Total Counts and Plate Counts within Different Size Groups. *Microbial Ecology*. 1987;13(1): 59–74. http://www.jstor.org/stable/4250906
195. Chaudhary DK, Khulan A, Kim J. Development of a novel cultivation technique for uncultured soil bacteria. *Scientific Reports*. 2019;9(1): 6666. https://doi.org/10.1038/s41598-019-43182-x.
196. Jung D, Aoi Y, Epstein SS. In Situ Cultivation Allows for Recovery of Bacterial Types Competitive in Their Natural Environment. *Microbes and environments*. 2016;31(4): 456–459. https://doi.org/10.1264/jsme2.ME16079.
197. Köpke B, Wilms R, Engelen B, Cypionka H, Sass H. Microbial Diversity in Coastal Subsurface Sediments: a Cultivation Approach Using Various Electron Acceptors and Substrate Gradients. *Applied and Environmental Microbiology*. 2005;71(12): 7819–7830. https://doi.org/10.1128/AEM.71.12.7819-7830.2005.
198. Alke B, Heribert C, Jörg O. Cyclic AMP and Acyl Homoserine Lactones Increase the Cultivation Efficiency of Heterotrophic Bacteria from the Central Baltic Sea. *Applied and Environmental Microbiology*. 2002;68(8): 3978–3987. https://doi.org/10.1128/AEM.68.8.3978-3987.2002.

199. Koblitz J, Halama P, Spring S, Thiel V, Baschien C, Hahnke RL, et al. MediaDive: the expert-curated cultivation media database. *Nucleic Acids Research*. 2022; https://doi.org/10.1093/nar/gkac803.
200. Reimer LC, Sardà Carbasse J, Koblitz J, Ebeling C, Podstawka A, Overmann J. BacDive in 2022: the knowledge base for standardized bacterial and archaeal data. *Nucleic Acids Research*. 2022;50(D1): D741–D746. https://doi.org/10.1093/nar/gkab961.
201. Ashino K, Sugano K, Amagasa T, Ying BW. Predicting the decision making chemicals used for bacterial growth. *Scientific Reports*. 2019;9(1): 7251. https://doi.org/10.1038/s41598-019-43587-8.
202. Straškrabová V. The effect of substrate shock on populations of starving aquatic bacteria. *Journal of Applied Bacteriology*. 1983;54(2): 217–224. https://doi.org/10.1111/j.1365-2672.1983.tb02610.x.
203. Bartscht K, Cypionka H, Overmann J. Evaluation of cell activity and of methods for the cultivation of bacteria from a natural lake community. *FEMS Microbiology Ecology*. 1999;28(3): 249–259. https://doi.org/10.1111/j.1574-6941.1999.tb00580.x.
204. Baym M, Lieberman TD, Kelsic ED, Chait R, Gross R, Yelin I, et al. Spatiotemporal microbial evolution on antibiotic landscapes. *Science*. 2016;353(6304): 1147–1151. https://doi.org/10.1126/science.aag0822.
205. Ultimaker B.V. *Ultimaker Cura*. 2023.
206. Turner S, Pryer KM, Miao VPW, Palmer JD. Investigating Deep Phylogenetic Relationships among Cyanobacteria and Plastids by Small Subunit rRNA Sequence Analysis1. *Journal of Eukaryotic Microbiology*. 1999;46(4): 327–338. https://doi.org/https://doi.org/10.1111/j.1550-7408.1999.tb04612.x.
207. Kisand V, Cuadros R, Wikner J. Phylogeny of Culturable Estuarine Bacteria Catabolizing Riverine Organic Matter in the Northern Baltic Sea. *Applied and Environmental Microbiology*. 2002;68(1): 379–388. https://doi.org/10.1128/AEM.68.1.379-388.2002.
208. Straub D, Blackwell N, Langarica-Fuentes A, Peltzer A, Nahnsen S, Kleindienst S. Interpretations of Environmental Microbial Community Studies Are Biased by the Selected 16S rRNA (Gene) Amplicon Sequencing Pipeline. *Frontiers in Microbiology*. 2020;11. https://doi.org/10.3389/fmicb.2020.550420.
209. Andrews Simon. FastQC: a quality control tool for high throughput sequence data. 2010;
210. Martin M. Cutadapt removes adapter sequences from high-throughput sequencing reads. *EMBnet.journal*. 2011;17(1): 10. https://doi.org/10.14806/ej.17.1.200.
211. Callahan BJ, McMurdie PJ, Rosen MJ, Han AW, Johnson AJA, Holmes SP. DADA2: High-resolution sample inference from Illumina amplicon data. *Nature Methods*. 2016;13(7): 581–583. https://doi.org/10.1038/nmeth.3869.
212. Quast C, Pruesse E, Yilmaz P, Gerken J, Schweer T, Yarza P, et al. The SILVA ribosomal RNA gene database project: improved data processing and web-based tools. *Nucleic Acids Research*. 2013;41(D1): D590–D596. https://doi.org/10.1093/nar/gks1219.
213. Dixon P. VEGAN, a package of R functions for community ecology. *Journal of Vegetation Science*. 2003;14(6): 927–930. https://doi.org/https://doi.org/10.1111/j.1654-1103.2003.tb02228.x.
214. Klindworth A, Pruesse E, Schweer T, Peplies J, Quast C, Horn M, et al. Evaluation of general 16S ribosomal RNA gene PCR primers for classical and next-generation sequencing-based diversity studies. *Nucleic Acids Research*. 2013;41(1): e1–e1. https://doi.org/10.1093/nar/gks808.

215. Pruesse E, Peplies J, Glöckner FO. SINA: Accurate high-throughput multiple sequence alignment of ribosomal RNA genes. *Bioinformatics*. 2012;28(14): 1823–1829. https://doi.org/10.1093/bioinformatics/bts252.
216. Berdy B, Spoering AL, Ling LL, Epstein SS. In situ cultivation of previously uncultivable microorganisms using the ichip. *Nature Protocols*. 2017;12(10): 2232–2242. https://doi.org/10.1038/nprot.2017.074.
217. Prusa Research. *PrusaSlicer*. 2023.
218. Pham VHT, Kim J. Cultivation of unculturable soil bacteria. *Trends in Biotechnology*. 2012;30(9): 475–484. https://doi.org/https://doi.org/10.1016/j.tibtech.2012.05.007.
219. Miyanaga K, Takano S, Morono Y, Hori K, Unno H, Tanji Y. Optimization of distinction between viable and dead cells by fluorescent staining method and its application to bacterial consortia. *Biochemical Engineering Journal*. 2007;37(1): 56–61. https://doi.org/https://doi.org/10.1016/j.bej.2007.03.007.
220. Hahn MW, Koll U, Schmidt J. Isolation and Cultivation of Bacteria. In: Hurst CJ (ed.) *The Structure and Function of Aquatic Microbial Communities*. Cham: Springer International Publishing; 2019. p. 313–351. https://doi.org/10.1007/978-3-030-16775-2_10.
221. Molina-Menor E, Gimeno-Valero H, Pascual J, Peretó J, Porcar M. High Culturable Bacterial Diversity From a European Desert: The Tabernas Desert. *Frontiers in Microbiology*. 2021;11. https://doi.org/10.3389/fmicb.2020.583120.
222. Duda VI, Suzina NE, Polivtseva VN, Boronin AM. Ultramicrobacteria: Formation of the concept and contribution of ultramicrobacteria to biology. *Microbiology*. 2012;81(4): 379–390. https://doi.org/10.1134/S0026261712040054.
223. Stoddard SF, Smith BJ, Hein R, Roller BRK, Schmidt TM. rrnDB: improved tools for interpreting rRNA gene abundance in bacteria and archaea and a new foundation for future development. *Nucleic Acids Research*. 2015;43(D1): D593–D598. https://doi.org/10.1093/nar/gku1201.
224. Bodilis J, Nsigue-Meilo S, Besaury L, Quillet L. Variable Copy Number, Intra-Genomic Heterogeneities and Lateral Transfers of the 16S rRNA Gene in Pseudomonas. *PLOS ONE*. 2012;7(4): e35647-. https://doi.org/10.1371/journal.pone.0035647
225. Stämmler F, Gläsner J, Hiergeist A, Holler E, Weber D, Oefner PJ, et al. Adjusting microbiome profiles for differences in microbial load by spike-in bacteria. *Microbiome*. 2016;4(1): 28. https://doi.org/10.1186/s40168-016-0175-0.
226. Moon K, Xu F, Zhang C, Seyedsayamdost MR. Bioactivity-HiTES Unveils Cryptic Antibiotics Encoded in Actinomycete Bacteria. *ACS Chemical Biology*. 2019;14(4): 767–774. https://doi.org/10.1021/acschembio.9b00049.
227. Xu F, Wu Y, Zhang C, Davis KM, Moon K, Bushin LB, et al. A genetics-free method for high-throughput discovery of cryptic microbial metabolites. *Nature Chemical Biology*. 2019;15(2): 161–168. https://doi.org/10.1038/s41589-018-0193-2.
228. Depoorter E, Bull MJ, Peeters C, Coenye T, Vandamme P, Mahenthiralingam E. Burkholderia: an update on taxonomy and biotechnological potential as antibiotic producers. *Applied Microbiology and Biotechnology*. 2016;100(12): 5215–5229. https://doi.org/10.1007/s00253-016-7520-x.
229. Benjamin H, A AGG, R SCR, Qiyun Z, M GD, B BK, et al. Evaluating the Information Content of Shallow Shotgun Metagenomics. *mSystems*. 2018;3(6): 10.1128/msystems.00069-18. https://doi.org/10.1128/msystems.00069-18.
230. Rappé MS, Giovannoni SJ. The Uncultured Microbial Majority. *Annual Review of Microbiology*. 2003;57(1): 369–394. https://doi.org/10.1146/annurev.micro.57.030502.090759.

231. Mujakić I, Piwosz K, Koblížek M. Phylum Gemmatimonadota and Its Role in the Environment. *Microorganisms*. 2022;10(1): 151. https://doi.org/10.3390/microorganisms10010151.
232. Pascual J, García-López M, Bills GF, Genilloud O. Longimicrobium terrae gen. nov., sp. nov., an oligotrophic bacterium of the under-represented phylum Gemmatimonadetes isolated through a system of miniaturized diffusion chambers. *International Journal of Systematic and Evolutionary Microbiology*. 2016;66(5): 1976–1985. https://doi.org/https://doi.org/10.1099/ijsem.0.000974.
233. Kawecki TJ, Lenski RE, Ebert D, Hollis B, Olivieri I, Whitlock MC. Experimental evolution. *Trends in Ecology & Evolution*. 2012;27(10): 547–560. https://doi.org/10.1016/j.tree.2012.06.001.
234. Lindsey HA, Gallie J, Taylor S, Kerr B. Evolutionary rescue from extinction is contingent on a lower rate of environmental change. *Nature*. 2013;494(7438): 463–467. https://doi.org/10.1038/nature11879.
235. Wistrand-Yuen E, Knopp M, Hjort K, Koskiniemi S, Berg OG, Andersson DI. Evolution of high-level resistance during low-level antibiotic exposure. *Nature Communications*. 2018;9(1): 1599. https://doi.org/10.1038/s41467-018-04059-1.
236. Spagnolo F, Rinaldi C, Sajorda DR, Dykhuizen DE. Evolution of Resistance to Continuously Increasing Streptomycin Concentrations in Populations of Escherichia coli. *Antimicrobial Agents and Chemotherapy*. 2016;60(3): 1336–1342. https://doi.org/10.1128/AAC.01359-15.
237. Klironomos JN, Allen MF, Rillig MC, Piotrowski J, Makvandi-Nejad S, Wolfe BE, et al. Abrupt rise in atmospheric CO2 overestimates community response in a model plant–soil system. *Nature*. 2005;433(7026): 621–624. https://doi.org/10.1038/nature03268.
238. Eydallin G, Ryall B, Maharjan R, Ferenci T. The nature of laboratory domestication changes in freshly isolated Escherichia coli strains. *Environmental Microbiology*. 2014;16(3): 813–828. https://doi.org/https://doi.org/10.1111/1462-2920.12208.
239. Ramamurthy T, Ghosh A, Pazhani GP, Shinoda S. Current Perspectives on Viable but Non-Culturable (VBNC) Pathogenic Bacteria. *Frontiers in Public Health*. 2014;2. https://doi.org/10.3389/fpubh.2014.00103.
240. Oliver JD. Formation of Viable but Nonculturable Cells. In: Kjelleberg S (ed.) *Starvation in Bacteria*. Boston, MA: Springer US; 1993. p. 239–272. https://doi.org/10.1007/978-1-4899-2439-1_11.
241. Bodor A, Bounedjoum N, Vincze GE, Erdeiné Kis Á, Laczi K, Bende G, et al. Challenges of unculturable bacteria: environmental perspectives. *Reviews in Environmental Science and Bio/Technology*. 2020;19(1): 1–22. https://doi.org/10.1007/s11157-020-09522-4.
242. Pinto D, Almeida V, Almeida Santos M, Chambel L. Resuscitation of Escherichia coli VBNC cells depends on a variety of environmental or chemical stimuli. *Journal of Applied Microbiology*. 2011;110(6): 1601–1611. https://doi.org/10.1111/j.1365-2672.2011.05016.x.
243. Arseny S. Kaprelyants, Douglas B. Kell. Dormancy in Stationary-Phase Cultures of Micrococcus luteus: Flow Cytometric Analysis of Starvation and Resuscitation. *Applied and Environmental Microbiology*. 1993;59(10): 3187–3196. https://doi.org/10.1128/aem.59.10.3187-3196.1993.
244. Mukamolova G V., Turapov O, Malkin J, Woltmann G, Barer MR. Resuscitation-promoting Factors Reveal an Occult Population of Tubercle Bacilli in Sputum. *American Journal of Respiratory and Critical Care Medicine*. 2010;181(2): 174–180. https://doi.org/10.1164/rccm.200905-0661OC.

245. Epstein SS. Microbial awakenings. *Nature*. 2009;457(7233): 1083–1083. https://doi.org/10.1038/4571083a.
246. Saxer G, Krepps MD, Merkley ED, Ansong C, Deatherage Kaiser BL, Valovska MT, et al. Mutations in Global Regulators Lead to Metabolic Selection during Adaptation to Complex Environments. *PLoS Genetics*. 2014;10(12): e1004872. https://doi.org/10.1371/journal.pgen.1004872.
247. Hannes H, Ulrike M, Andreas O, Florian B, Leif S, Erhard B, et al. A Comprehensive Proteomics and Transcriptomics Analysis of Bacillus subtilis Salt Stress Adaptation. *Journal of Bacteriology*. 2010;192(3): 870–882. https://doi.org/10.1128/jb.01106-09.
248. Postgate JR, Hunter JR. Accelerated Death of Aerobacter aerogenes Starved in the Presence of Growth-Limiting Substrates. *Microbiology*. 1964;34(3): 459–473. https://doi.org/https://doi.org/10.1099/00221287-34-3-459.
249. Blin K, Shaw S, Augustijn HE, Reitz ZL, Biermann F, Alanjary M, et al. antiSMASH 7.0: new and improved predictions for detection, regulation, chemical structures and visualisation. *Nucleic Acids Research*. 2023;51(W1): W46–W50. https://doi.org/10.1093/nar/gkad344.
250. Guiziou S, Sauveplane V, Chang HJ, Clerté C, Declerck N, Jules M, et al. A part toolbox to tune genetic expression in Bacillus subtilis. *Nucleic Acids Research*. 2016; https://doi.org/10.1093/nar/gkw624.
251. Harwood CR, Cutting SM. *Molecular Biological Methods for Bacillus*. Wiley; 1990.
252. Perret E, Leung A, Morel A, Feracci H, Nassoy P. Versatile Decoration of Glass Surfaces To Probe Individual Protein−Protein Interactions and Cellular Adhesion. *Langmuir*. 2002;18(3): 846–854. https://doi.org/10.1021/la015601y.
253. Liang K, Richardson JJ, Cui J, Caruso F, Doonan CJ, Falcaro P. Metal-Organic Framework Coatings as Cytoprotective Exoskeletons for Living Cells. *Advanced Materials*. 2016;28(36): 7910–7914. https://doi.org/10.1002/adma.201602335.
254. Tang R, Shen L, Yang L, You K, Li Z, Wei X, et al. Killing Two Birds with One Stone: Biomineralized Bacteria Tolerate Adverse Environments and Absorb Hexavalent Chromium. *ACS Omega*. 2022;7(18): 15385–15395. https://doi.org/10.1021/acsomega.1c06877.
255. Kim BJ, Han S, Lee KB, Choi IS. Biphasic Supramolecular Self-Assembly of Ferric Ions and Tannic Acid across Interfaces for Nanofilm Formation. *Advanced Materials*. 2017;29(28): 1700784. https://doi.org/10.1002/adma.201700784.
256. Ma L, Datta SS, Karymov MA, Pan Q, Begolo S, Ismagilov RF. Individually addressable arrays of replica microbial cultures enabled by splitting SlipChips. *Integr. Biol.* 2014;6(8): 796–805. https://doi.org/10.1039/C4IB00109E.
257. Yang SH, Kang SM, Lee KB, Chung TD, Lee H, Choi IS. Mussel-Inspired Encapsulation and Functionalization of Individual Yeast Cells. *Journal of the American Chemical Society*. 2011;133(9): 2795–2797. https://doi.org/10.1021/ja1100189.
258. Jeong Y, Irudayaraj J. Hierarchical encapsulation of bacteria in functional hydrogel beads for inter- and intra- species communication. *Acta Biomaterialia*. 2023;158: 203–215. https://doi.org/https://doi.org/10.1016/j.actbio.2023.01.003.
259. Harimoto T, Deb D, Danino T. A rapid screening platform to coculture bacteria within tumor spheroids. *Nature Protocols*. 2022;17(10): 2216–2239. https://doi.org/10.1038/s41596-022-00723-5.
260. Kampker A, Triebs J, Kawollek S, Ayvaz P, Hohenstein S. Review on Machine Designs of Material Extrusion based Additive Manufacturing (AM) Systems - Status-Quo and Potential Analysis for Future AM Systems. *Procedia CIRP*. 2019;81: 815–819. https://doi.org/https://doi.org/10.1016/j.procir.2019.03.205.

261. Attarilar S, Ebrahimi M, Djavanroodi F, Fu Y, Wang L, Yang J. 3D Printing Technologies in Metallic Implants: A Thematic Review on the Techniques and Procedures. *IJB*. 7(1): 306.